

3710347

LIBRARY
Michigan State
University

This is to certify that the
thesis entitled

**Scattering from a Coated Curved Surface of Varying
Thickness with Application to Nondestructive Evaluation**

presented by

Jonathan Wierzba

has been accepted towards fulfillment
of the requirements for the

 M. S. degree in Electrical Engineering

Edward J. Rothwell
Major Professor's Signature

May 11, 2005
Date

PLACE IN RETURN BOX to remove this checkout from your record.
TO AVOID FINES return on or before date due.
MAY BE RECALLED with earlier due date if requested.

<u>DATE DUE</u>	<u>DATE DUE</u>	<u>DATE DUE</u>

**Scattering from a Coated Curved Surface of Varying
Thickness with Application to Nondestructive Evaluation**

By

Jonathan F. Wierzba

A THESIS

Submitted to
Michigan State University
in partial fulfillment of the requirements
for the degree of

MASTER OF SCIENCE

Department of Electrical and Computer Engineering

2005

ABSTRACT

Scattering from a Coated Curved Surface of Varying Thickness with Application to Nondestructive Evaluation

By

Jonathan F. Wierzba

The extinction pulse (E-pulse) has been used to diagnose changes in the electromagnetic parameters of a coated surface. The E-pulse technique has been successfully applied to a flat surface and constant curve surface with a constant thickness. An important extension is to apply the E-pulse technique to a surface with a varying thickness and curvature.

The coated surface investigated in this thesis is an elliptical metallic cylinder with a circular dielectric coating. An incident plane wave with TE_z and TM_z polarization is reflected off the coated cylinder having either a vertical or a horizontal major axis. The monostatic results generated in the frequency domain are transformed using an FFT, providing the time domain data for convolution with the E-pulse.

The E-pulse for a planar coated surface is applied to the data obtain for the elliptical metallic core with a circular dielectric coating. The placement of the major axis and the type of polarization chosen has a greater impact on the E-pulse Discrimination Number (EDN) as the radius decreases in size.

Copyright © by
Jonathan F. Wierzba
2005

To my parents, Gregory and Joan

ACKNOWLEDGMENTS

I would like to thank my family for the support during the thesis.
Also, I would like to thank Dr. Ed Rothwell for his help on the thesis.

TABLE OF CONTENTS

LIST OF TABLES	viii
LIST OF FIGURES	ix
1 Introduction	1
2 Background	3
3 Equations for Scattering	5
3.1 TMz Case	5
3.2 TMz Case Comparison	15
3.3 TEz Case	17
3.4 TEz Case Comparison	29
4 Computational Considerations	31
4.1 Computation Method	31
4.2 Flat Case	34
4.3 Circular Case	38
4.4 Echo Width of Elliptical Metallic Core	39
5 Results for the Elliptical Case	43
5.1 Frequency Response	43
5.2 Time Domain Results	63
6 E-pulse Results	93
7 Conclusion	115
APPENDICES	118
A TMz Case Source Code	118
B TEz Case Source Code	133

C Flat Case Source Code	148
BIBLIOGRAPHY	151

LIST OF TABLES

6.1 EDN values calculated for flat case and for cylinders of various radii in meters	114
--	-----

LIST OF FIGURES

3.1	Orientation of the elliptical metallic core with the x-axis being the major axis.	6
3.2	Orientation of the elliptical metallic core with the y-axis being the major axis.	6
4.1	Flat case normalized field magnitude vs. frequency with $d = .1$ m, $\epsilon_r = 9$, $\mu_r = 1$	35
4.2	Flat case phase vs. frequency with $d = .1$ m, $\epsilon_r = 9$, $\mu_r = 1$	36
4.3	Flat case normalized amplitude vs. time with $d = .1$ m, $\epsilon_r = 9$, $\mu_r = 1$	37
4.4	Echo width vs wave number, x as major axis, $a_1 = 1.4$ m, $a_2 = 1.3$ m.	41
4.5	Echo width vs wave number, y as major axis, $a_1 = 1.4$ m, $a_2 = 1.45$ m.	42
5.1	TMz normalized field magnitude vs. frequency, $a = .9$ m, $a_1 = .8$ m, $a_2 = .7$ m, with x as the major axis.	46
5.2	TMz normalized field magnitude vs. frequency, $a = 1.5$ m, $a_1 = 1.4$ m, $a_2 = 1.3$ m, with x as the major axis.	47
5.3	TMz normalized field magnitude vs. frequency, $a = 2$ m, $a_1 = 1.9$ m, $a_2 = 1.8$ m, with x as the major axis.	48
5.4	TMz normalized field magnitude vs. frequency, $a = .9$ m, $a_1 = .8$ m, $a_2 = .85$ m, with y as the major axis.	49
5.5	TMz normalized field magnitude vs. frequency, $a = 1.5$ m, $a_1 = 1.4$ m, $a_2 = 1.45$ m, with y as the major axis.	50
5.6	TMz normalized field magnitude vs. frequency, $a = 2$ m, $a_1 = 1.9$ m, $a_2 = 1.95$ m, with y as the major axis.	51
5.7	TEz normalized field magnitude vs. frequency, $a = .9$ m, $a_1 = .8$ m, $a_2 = .7$ m, with x as the major axis.	52
5.8	TEz normalized field magnitude vs. frequency, $a = 1.5$ m, $a_1 = 1.4$ m, $a_2 = 1.3$ m, with x as the major axis.	53
5.9	TEz normalized field magnitude vs. frequency, $a = 2$ m, $a_1 = 1.9$ m, $a_2 = 1.8$ m, with x as the major axis.	54

5.10 TEz normalized field magnitude vs. frequency, $a = .9$ m, $a_1 = .8$ m, $a_2 = .85$ m, with y as the major axis.	55
5.11 TEz normalized field magnitude vs. frequency, $a = 1.5$ m, $a_1 = 1.4$ m, $a_2 = 1.45$ m, with y as the major axis.	56
5.12 TEz normalized field magnitude vs. frequency, $a = 2$ m, $a_1 = 1.9$ m, $a_2 = 1.95$ m, with y as the major axis.	57
5.13 TEz normalized field magnitude metallic elliptical cylinder	58
5.14 TEz normalized field magnitude difference	59
5.15 TMz normalized field magnitude metallic elliptical cylinder	60
5.16 TMz normalized field magnitude difference	61
5.17 TMz phase vs. frequency, $a = 1.5$ m, $a_1 = 1.4$ m, $a_2 = 1.45$ m, with y as the major axis.	62
5.18 The electromagnetic pulse multiple reflections, x is the major axis of the ellipse.	66
5.19 The electromagnetic pulse multiple reflection, y is the major axis of the ellipse.	66
5.20 TMz normalized amplitude vs. time, $a = 1.5$ m, $a_1 = 1.4$ m, $a_2 = 1.3$ m, with x as the major axis.	67
5.21 TMz normalized amplitude vs. time, $a = 1.5$ m, $a_1 = 1.4$ m, $a_2 = 1.45$ m, with y as the major axis.	68
5.22 TEz normalized amplitude vs. time, $a = 1.5$ m, $a_1 = 1.4$ m, $a_2 = 1.3$ m, with x as the major axis.	69
5.23 TEz normalized amplitude vs. time, $a = 1.5$ m, $a_1 = 1.4$ m, $a_2 = 1.45$ m, and with y as the major axis.	70
5.24 TMz normalized amplitude vs. time with $a = .9$ m, 1.5 m, 2 m and with x as the major axis.	71
5.25 TMz normalized amplitude vs. time with $a = .9$ m, 1.5 m, 2 m and with y as the major axis.	72
5.26 TEz normalized amplitude vs. time with $a = .9$ m, 1.5 m, 2 m and with x as the major axis.	73
5.27 TEz normalized amplitude vs. time with $a = .9$ m, 1.5 m, 2 m and with y as the major axis.	74
5.28 TMz normalized amplitude vs. time comparison of flat with $a = .9$ m and with x as the major axis.	75
5.29 TMz normalized amplitude vs. time comparison of flat with $a = 1.5$ m and with x as the major axis.	76

5.30	TMz normalized amplitude vs. time comparison of flat with $a = 2.0$ m and with x as the major axis.	77
5.31	TMz normalized amplitude vs. time comparison of flat with $a = .9$ m and with y as the major axis.	78
5.32	TMz normalized amplitude vs. time comparison of flat with $a = 1.5$ m and with y as the major axis.	79
5.33	TMz normalized amplitude vs. time comparison of flat with $a = 2.0$ m and with y as the major axis.	80
5.34	TEz normalized amplitude vs. time comparison of flat with $a = .9$ m and with x as the major axis.	81
5.35	TEz normalized amplitude vs. time comparison of flat with $a = 1.5$ m and with x as the major axis.	82
5.36	TEz normalized amplitude vs. time comparison of flat with $a = 2.0$ m and with x as the major axis.	83
5.37	TEz normalized amplitude vs. time comparison of flat with $a = .9$ m and with y as the major axis.	84
5.38	TEz normalized amplitude vs. time comparison of flat with $a = 1.5$ m and with y as the major axis.	85
5.39	TEz normalized amplitude vs. time comparison of flat with $a = 2.0$ m and with y as the major axis.	86
5.40	TMz normalized amplitude vs. time comparison of x vs y as the major axis, $a = 1.5$ m.	87
5.41	TEz normalized amplitude vs. time comparison of x vs y as the major axis, $a = 1.5$ m.	88
5.42	TMz normalized amplitude vs. time comparison of standard cylinder response with subtracted metallic core response with $a = 1.5$ m and x as the major axis.	89
5.43	TMz normalized amplitude vs. time comparison of standard cylinder response with subtracted metallic core response with $a = 1.5$ m and y as the major axis.	90
5.44	TEz normalized amplitude vs. time comparison of standard cylinder response with subtracted metallic core response with $a = 1.5$ m and x as the major axis.	91
5.45	TEz normalized amplitude vs. time comparison of standard cylinder response with subtracted metallic core response with $a = 1.5$ m and y as the major axis.	92
6.1	E-pulse for the planar coated conductor vs time.	96

6.2	Convulated E-pulse vs. time, flat case.	97
6.3	TMz convolved E-pulse vs. time, $a = .9$ m, $a_1 = .8$ m, $a_2 = .7$ m, with x as the major axis.	98
6.4	TMz convolved E-pulse vs. time, $a = 1.5$ m, $a_1 = 1.4$ m, $a_2 = 1.3$ m, with x as the major axis.	99
6.5	TMz convolved E-pulse vs. time, $a = 2$ m, $a_1 = 1.9$ m, $a_2 = 1.8$ m, with x as the major axis.	100
6.6	TMz convolved E-pulse vs. time, $a = .9$ m, $a_1 = .8$ m, $a_2 = .7$ m, with y as the major axis.	101
6.7	TMz convolved E-pulse vs. time, $a = 1.5$ m, $a_1 = 1.4$ m, $a_2 = 1.3$ m, with y as the major axis.	102
6.8	TMz convolved E-pulse vs. time, $a = 2$ m, $a_1 = 1.9$ m, $a_2 = 1.8$ m, with y as the major axis.	103
6.9	TEz convolved E-pulse vs. time, $a = .9$ m, $a_1 = .8$ m, $a_2 = .7$ m, with x as the major axis.	104
6.10	TEz convolved E-pulse vs. time, $a = 1.5$ m, $a_1 = 1.4$ m, $a_2 = 1.3$ m, with x as the major axis.	105
6.11	TEz convolved E-pulse vs. time, $a = 2$ m, $a_1 = 1.9$ m, $a_2 = 1.8$ m, with x as the major axis.	106
6.12	TEz convolved E-pulse vs. time, $a = .9$ m, $a_1 = .8$ m, $a_2 = .7$ m, with y as the major axis.	107
6.13	TEz convolved E-pulse vs. time, $a = 1.5$ m, $a_1 = 1.4$ m, $a_2 = 1.3$ m, with y as the major axis.	108
6.14	TEz convolved E-pulse vs. time, $a = 2$ m, $a_1 = 1.9$ m, $a_2 = 1.8$ m, with y as the major axis.	109
6.15	TMz subtracted convolved E-pulse vs. time, $a = .9$ m, $a_1 = .8$ m, a_2 $= .7$ m, with y as the major axis.	110
6.16	TEz subtracted convolved E-pulse vs. time, $a = .9$ m, $a_1 = .8$ m, a_2 $= .7$ m, with x as the major axis.	111
6.17	EDN vs outer radii, subtracted vs non-subtracted, x as major axis. XD indicates that it is the subtracted case with x as the major axis. X indicates that it is the non-subtracted case with x as the major axis.	112
6.18	EDN vs outer radii, subtracted vs non-subtracted, y as major axis. YD indicates that it is the subtracted case with y as the major axis. Y indicates that it is the non-subtracted case with y as the major axis.	113

CHAPTER 1

Introduction

In this thesis the field scattered from an elliptic cylinder coated with a circular dielectric material is computed. This provides a test case for the E-pulse technique, which can be used to diagnose changes to the coating parameters (thickness and dielectric constant). The coated elliptical presents a case with a varying surface curvature and thickness, which approaches the planar case studied in detail in [9], when the radius becomes large. The goal is to determine whether the E-pulse technique remains valid when the surface curvature and coating thickness is varying.

The background of this thesis is covered in Chapter two. The E-pulse technique origins show how the technique was first applied to coated surfaces. Also, the origins of the equations that are used to derive the scattered electric field equation and the calculation of the echo width of the elliptical cylinder are covered.

The equations for the scattered field are derived in Chapter three for both transverse electric and transverse magnetic incident plane-wave fields. The derivations for the two polarizations start by describing the incident, scattered, and dielectric region electromagnetic fields and then apply the boundary conditions at the conductor and dielectric interfaces to determine the scattered electric field. Use of the point-matching method leads to a matrix equation for the expansion coefficients used to compute the scattered field. These coefficients are compared

against the coefficients for the circular case derived in [10].

Chapter four contains the computation method for the computer code and the results of the flat case, circular case, and the calculation of the echo width of the uncoated elliptical cylinder. In the computation section, the logic and layout that is used in writing the computer code is shown. For the flat case, the results are shown for the standard that will be used against the elliptical case. The circular case shows a matching of the data when the ellipse becomes a circle. The echo width of the elliptical cylinder is calculated as a check to see if the equations are derived correctly.

In Chapter five, the scattered field data is plotted in the frequency and time domains. The frequency domain plots show the effects of the various size of the radii and the polarization on the scattered electric field. The time domain plots, which are obtained using the FFT show the amplitude of the reflections of the electromagnetic wave from the various cylinder configurations. Also, the time domain plots are used to compare and contrast the effects of different geometries and polarizations on the multiple reflections of the waves trapped within the dielectric layer.

In Chapter six, the E-pulse for the planar coated surface is convolved with the time domain scattered field waveforms, to determine the effectiveness of the E-pulse technique on a coated surface with varying curvature and thickness. The various shapes of the convolution are shown and compared to the flat case. The E-pulse Discrimination Number (EDN) is calculated and compared for different sized radii of the coated cylinder.

Finally, Chapter seven provides a summary and some concluding remarks.

CHAPTER 2

Background

The E-pulse technique was first developed to identify radar targets based on their temporal scattered-field responses [6]. When a radar target is illuminated by a short electromagnetic pulse, the induced currents will oscillate in the natural resonance of the target. Since the resonant frequencies are unique to the target, the time-domain scattered field set up by the induced currents can be used for identification. An E-pulse is a time domain waveform that is constructed based on a specific set of natural frequencies. When the E-pulse is convolved with a natural mode series containing these same natural frequencies a zero late-time waveform is produced. When the same E-pulse is convolved with a natural mode series consisting of different natural frequencies, a non-zero late-time response is produced, allowing an identification decision to be made. The decision is quantified using the E-pulse discrimination number (EDN) [3].

Recently, the E-pulse technique has been applied to layered media. When an electromagnetic pulse is reflected by a layered medium, the time domain response consists of a number of peaks produced by the multiple reflections within the layers. This response may be written as a natural mode series, with resonant frequencies dependent on the electromagnetic properties and thickness of the layers. Thus the E-pulse technique may be used to determine when layer properties have changed [9].

For any given surface, there is a unique E-pulse that is created and if the surface parameters change in anyway, the E-pulse will no longer match the reference and a change is detected. The greater the difference in surface parameters, the larger EDN value from the application E-pulse technique.

An important extension of the E-pulse technique is to apply it to a coated curved surface with a constant thickness and curvature. This was investigated in [11], where it was shown that under certain circumstances, the E-pulse technique may be used successfully with curved layered surfaces.

In this thesis, the E-pulse technique is applied to a curved coated surface with a varying curvature and thickness, by examining the time-domain response of an elliptic cylinder coated with circular dielectric. The equations that describe the scattered electric field with a circular outer region with arbitrary metallic core cross-section were derived by Yee using the point-matching method in the 1960's [13]. To provide a varying thickness and curvature of the coating, an elliptical cross-section was chosen. The varying thickness is chosen since it provides a more realistic model of a curved coated surface where a constant coating thickness is not always possible.

The point-matching method has also been used to compute the field scattered by an uncoated elliptical cylinder [5]. There, the echo width of an elliptical cylinder was computed for various illumination conditions. In this thesis, the echo width of the elliptical metallic cylinder is used as a check to see if the equations are derived correctly, since high-frequency the limit of the echo width is merely π times the radius of curvature at the contact contract point of the incident wave.

CHAPTER 3

Equations for Scattering

3.1 TMz Case

The electric field scattering equation is needed for finding the frequency response. With the frequency response, applying the Fast Fourier Transform to the data, a time domain plot can be obtained to see how the electromagnetic wave is scattered off the cylinder. The plane electromagnetic excitation wave is chosen to be incident on the cylinder along the -x axis for the derivations. With the elliptical shape of the metallic core there are two choices for the major axis, the x-axis or the y-axis. Figure 3.1 shows the cross section of the circular dielectric layer around the elliptical metallic core with the x-axis being the major axis. In Figure 3.2, the y-axis is the major axis. The placement of the major axis has no impact on the derivation of the electric scattered field equation. However, the major axis placement greatly affects the numerical calculations as shown later.

The incident plane electric field in region 2 is represented using the last expression in the sequence from [2, eq. 11-81b]:

$$E_z^i = E_0 e^{jk_0 x} = E_0 e^{jk_0 r \cos \phi} = E_0 \sum_{n=-\infty}^{\infty} j^n J_n(k_0 r) e^{jn\phi}. \quad (3.1)$$

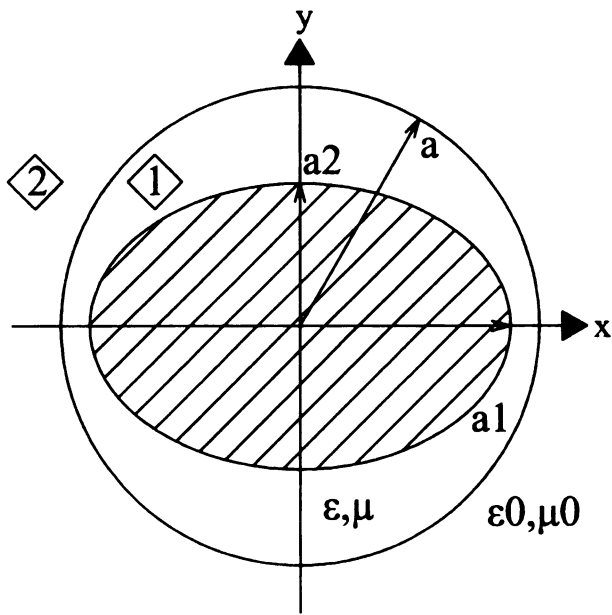


Figure 3.1. Orientation of the elliptical metallic core with the x-axis being the major axis.

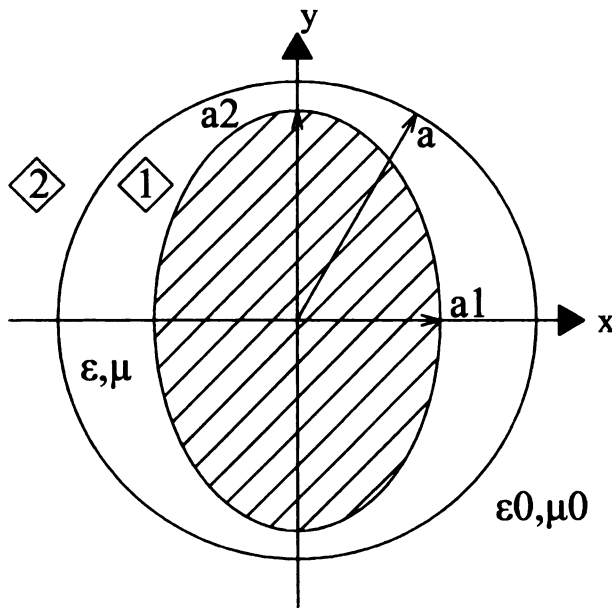


Figure 3.2. Orientation of the elliptical metallic core with the y-axis being the major axis.

Since the electric field will be calculated in a numerical form, breaking up the equation into summation of terms is the next step. The desired end result for this equation is to combine the positive and negative indexed terms in order to reduce the size of resulting the matrix by half. So the next equation shown is the breaking of the summation into positive, zero, and negative terms:

$$E_z^i = E_0 \left[\sum_{n=-\infty}^{-1} j^n J_n(k_0 r) e^{jn\phi} + J_0(k_0 r) + \sum_{n=1}^{\infty} j^n J_n(k_0 r) e^{jn\phi} \right]. \quad (3.2)$$

The following equation has the modification to the summation that contains the negative terms by replacing "n" with "-n". Also, the J_{-n} is replaced by $(-1)^n J_n$ as found in [2, eq. IV-8]:

$$E_z^i = E_0 \left[\sum_{n=1}^{\infty} j^{-n} (-1)^n J_n(k_0 r) e^{-jn\phi} + J_0(k_0 r) + \sum_{n=1}^{\infty} j^n J_n(k_0 r) e^{jn\phi} \right]. \quad (3.3)$$

The $j^{-n} (-1)^n$ product is equal to j^n . The next step is to combine the two positive summations:

$$E_z^i = E_0 \left[J_0(k_0 r) + \sum_{n=1}^{\infty} j^n J_n(k_0 r) (e^{jn\phi} + e^{-jn\phi}) \right]. \quad (3.4)$$

The final equation below is created by combining the exponentials into a cosine function:

$$E_z^i = E_0 \sum_{n=0}^{\infty} j^n \varepsilon_n J_n(k_0 r) \cos(n\phi) \quad \varepsilon_n = \begin{cases} 1 & n = 0 \\ 2 & n \neq 0 \end{cases}. \quad (3.5)$$

The incident magnetic field is calculated by taking the curl of the electric field:

$$H^i = -\frac{1}{j\omega\mu_0} \nabla \times E_z^i = -\frac{1}{j\omega\mu_0} (\hat{r} \partial_\phi \frac{E_z^i}{r} - \hat{\phi} \partial_r E_z^i). \quad (3.6)$$

Substituting the derivatives of the electric field (3.5) gives:

$$H^i = -\frac{1}{j\omega\mu_0} \left[\hat{r} \frac{E_0}{r} \sum_{n=0}^{\infty} j^n \varepsilon_n J_n(k_0 r) n \sin(n\phi) - \hat{\phi} E_0 k_0 \sum_{n=0}^{\infty} j^n \varepsilon_n J'_n(k_0 r) \cos(n\phi) \right]. \quad (3.7)$$

The \hat{r} term is not needed when the boundary conditions are applied, leaving only the $\hat{\phi}$ term. Also, k_0 and $1/(j\omega\mu_0)$ combine to form $1/\eta_0$:

$$H_{\phi}^i = -\frac{jE_0}{\eta_0} \sum_{n=0}^{\infty} \varepsilon_n j^n J_n'(k_0 r) \cos(n\phi). \quad (3.8)$$

The scattered electric field in region 2 is given by:

$$E_z^s = E_0 \sum_{n=0}^{\infty} C_n H_n^{(2)}(k_0 r) \cos(n\phi) \quad (3.9)$$

To find the scattered magnetic field in region 2, the curl of electric field needs to be calculated. As before, only the $\hat{\phi}$ component of the magnetic field needs to be calculated:

$$H_{\phi}^s = \frac{1}{j\omega\mu_0} \partial_r E_z^s = \frac{E_0}{j\omega\mu_0} \sum_{n=0}^{\infty} \partial_r (C_n H_n^{(2)}(k_0 r) \cos(n\phi)). \quad (3.10)$$

After taking the curl of the electric field, the scattered magnetic field is:

$$H_{\phi}^s = -\frac{jE_0}{\eta_0} \sum_{n=0}^{\infty} C_n H_n^{(2)'}(k_0 r) \cos(n\phi). \quad (3.11)$$

The electric field in region 1 (dielectric region) is given by:

$$E_z^d = E_0 \sum_{n=0}^{\infty} [A_n J_n(kr) + B_n Y_n(kr)] \cos(n\phi). \quad (3.12)$$

The magnetic field in this region is calculated by taking the curl of the electric field.

As above, only the $\hat{\phi}$ component is needed:

$$H_{\phi}^d = \frac{1}{j\omega\mu} \partial_r E_z^d = \frac{E_0}{j\omega\mu} \sum_{n=0}^{\infty} \partial_r ([A_n J_n(kr) + B_n Y_n(kr)] \cos(n\phi)). \quad (3.13)$$

The magnetic field $\hat{\phi}$ component is:

$$H_{\phi}^d = -\frac{jE_0}{\eta} \sum_{n=0}^{\infty} [A_n J_n'(kr) + B_n Y_n'(kr)] \cos(n\phi). \quad (3.14)$$

Now that the electric and magnetic fields have been calculated in the various regions, the next step is to apply the boundary conditions on the tangent electric field which is continuous at $r = a$:

$$E_0 \sum_{n=0}^{\infty} j^n \varepsilon_n J_n(k_0 a) \cos(n\phi) + E_0 \sum_{n=0}^{\infty} C_n H_n^{(2)}(k_0 a) \cos(n\phi) = E_0 \sum_{n=0}^{\infty} [A_n J_n(ka) + B_n Y_n(ka)] \cos(n\phi). \quad (3.15)$$

By multiplying the equation by $\cos m\phi$ and integrating the result is eliminating the summations to isolate A_n , B_n , and C_n terms through the orthogonality relation:

$$\int \cos(n\phi) \cos(m\phi) d\phi = \pi \bar{\varepsilon}_m \delta_{mn}. \quad (3.16)$$

The $\bar{\varepsilon}_m$ term is created when the integral is evaluated, with the result of two when m equals zero and one when m is not equal to zero. The δ_{mn} term is the Kronicker delta given by:

$$\bar{\varepsilon}_m = \begin{cases} 2 & m = 0 \\ 1 & m \neq 0 \end{cases} \quad \delta_{mn} = \begin{cases} 1 & m = n \\ 0 & m \neq n \end{cases}. \quad (3.17)$$

Multiplying (3.15) by $\cos(m\phi)$ and applying the integral gives:

$$\int (E_0 \sum_{n=0}^{\infty} j^n \varepsilon_n J_n(k_0 a) \cos(n\phi) \cos(m\phi) + E_0 \sum_{n=0}^{\infty} C_n H_n^{(2)}(k_0 a) \cos(n\phi) \cos(m\phi)) d\phi = \int (E_0 \sum_{n=0}^{\infty} [A_n J_n(ka) + B_n Y_n(ka)] \cos(n\phi) \cos(m\phi)) d\phi. \quad (3.18)$$

After evaluating the integral, the summations drop out, leaving the following equation:

$$j^n \varepsilon_n J_n(k_0 a) + C_n H_n^{(2)}(k_0 a) = A_n J_n(ka) + B_n Y_n(ka). \quad (3.19)$$

To create another equation to use to eliminate a variable, the boundary condition for the tangent magnetic field being continuous at $r = a$ is applied, giving:

$$\begin{aligned}
-\frac{jE_0}{\eta_0} \sum_{n=0}^{\infty} \varepsilon_n j^n J'_n(k_0 a) \cos(n\phi) - \frac{jE_0}{\eta_0} \sum_{n=0}^{\infty} C_n H_n^{(2)'}(k_0 a) \cos(n\phi) = \\
-\frac{jE_0}{\eta} \sum_{n=0}^{\infty} [A_n J'_n(ka) + B_n Y'_n(ka)] \cos(n\phi). \quad (3.20)
\end{aligned}$$

Repeating the same process above that eliminated the summation results in:

$$\varepsilon_n j^n J'_n(k_0 a) + C_n H_n^{(2)'}(k_0 a) = \frac{\eta_0}{\eta} [A_n J'_n(ka) + B_n Y'_n(ka)]. \quad (3.21)$$

With the two equations above, (3.19) and (3.21), the next step is to solve for A_n and B_n in terms of C_n . The first step is to find A_n in terms of B_n and C_n using (3.21):

$$A_n J'_n(ka) = \frac{\eta}{\eta_0} \left[\varepsilon_n j^n J'_n(k_0 a) + C_n H_n^{(2)'}(k_0 a) \right] - B_n Y'_n(ka). \quad (3.22)$$

After solving for A_n , the next step is to solve the other equation, (3.19) for B_n in terms of A_n and C_n :

$$B_n = \frac{1}{Y_n(ka)} \left[j^n \varepsilon_n J_n(k_0 a) + C_n H_n^{(2)}(k_0 a) - A_n J_n(ka) \right]. \quad (3.23)$$

After having A_n and B_n isolated, substituting B_n into (3.22) gives A_n in terms of just C_n :

$$\begin{aligned}
A_n J'_n(ka) = \frac{\eta}{\eta_0} \left[\varepsilon_n j^n J'_n(k_0 a) + C_n H_n^{(2)'}(k_0 a) \right] - \\
\frac{Y'_n(ka)}{Y_n(ka)} \left[j^n \varepsilon_n J_n(k_0 a) + C_n H_n^{(2)}(k_0 a) - A_n J_n(ka) \right]. \quad (3.24)
\end{aligned}$$

The next step is to combine all the like terms and factor out A_n :

$$\begin{aligned}
A_n [Y_n(ka) J'_n(ka) - Y'_n(ka) J_n(ka)] = \varepsilon_n j^n \left[\frac{\eta}{\eta_0} Y_n(ka) J'_n(k_0 a) - Y'_n(ka) J_n(k_0 a) \right] \\
+ C_n \left[\frac{\eta}{\eta_0} Y_n(ka) H_n^{(2)'}(k_0 a) - Y'_n(ka) H_n^{(2)}(k_0 a) \right]. \quad (3.25)
\end{aligned}$$

The following equation from [2, eq. 11-95], reduces the expression multiplying A_n to a constant:

$$Y_n(ka)J'_n(ka) - Y'_n(ka)J_n(ka) = -\frac{2}{\pi ka}. \quad (3.26)$$

Thus A_n is now in terms of just C_n :

$$A_n = -\frac{\pi ka}{2} \left[\varepsilon_n j^n \left[\frac{\eta}{\eta_0} Y_n(ka) J'_n(k_0a) - Y'_n(ka) J_n(k_0a) \right] + C_n \left[\frac{\eta}{\eta_0} Y_n(ka) H_n^{(2)'}(k_0a) - Y'_n(ka) H_n^{(2)'}(k_0a) \right] \right]. \quad (3.27)$$

After solving for A_n , the same equation can be solved for B_n :

$$B_n Y_n(ka) = j^n \varepsilon_n J_n(k_0a) + C_n H_n^{(2)'}(k_0a) - \frac{J_n(ka)}{J'_n(ka)} \left[\frac{\eta}{\eta_0} \left[\varepsilon_n j^n J'_n(k_0a) + C_n H_n^{(2)'}(k_0a) \right] - B_n Y'_n(ka) \right]. \quad (3.28)$$

Combining like terms gives:

$$B_n [Y_n(ka) J'_n(ka) - J_n(ka) Y'_n(ka)] = j^n \varepsilon_n \left[J'_n(ka) J_n(k_0a) - \frac{\eta}{\eta_0} J_n(ka) J'_n(k_0a) \right] + C_n \left[J'_n(ka) H_n^{(2)'}(k_0a) - \frac{\eta}{\eta_0} J_n(ka) H_n^{(2)'}(k_0a) \right]. \quad (3.29)$$

Replacing the Bessel function expression with the constant from [2, eq. 11-95] gives

B_n :

$$B_n = \frac{\pi ka}{2} \left[j^n \varepsilon_n \left[\frac{\eta}{\eta_0} J_n(ka) J'_n(k_0a) - J'_n(ka) J_n(k_0a) \right] + C_n \left[\frac{\eta}{\eta_0} J_n(ka) H_n^{(2)'}(k_0a) - J'_n(ka) H_n^{(2)'}(k_0a) \right] \right]. \quad (3.30)$$

Since there are three unknowns and two equations so far, another equation is needed to solve for C_n . The last equation comes from setting the tangent electric field equal to zero where the dielectric material interfaces with the metallic core:

$$E_z^d = E_0 \sum_{n=0}^{\infty} [A_n J_n(kr) + B_n Y_n(kr)] \cos(n\phi) = 0. \quad (3.31)$$

Define the expressions f_n , \bar{f}_n , g_n , and \bar{g}_n to represent parts of the equations that describe A_n and B_n :

$$f_n = - \left[\frac{\eta}{\eta_0} Y_n(ka) H_n^{(2)'}(k_0 a) - Y_n'(ka) H_n^{(2)}(k_0 a) \right] \quad (3.32)$$

$$\bar{f}_n = \frac{\eta}{\eta_0} J_n(ka) H_n^{(2)'}(k_0 a) - J_n'(ka) H_n^{(2)}(k_0 a) \quad (3.33)$$

$$g_n = -\varepsilon_n j^n \left[\frac{\eta}{\eta_0} Y_n(ka) J_n'(k_0 a) - Y_n'(ka) J_n(k_0 a) \right] \quad (3.34)$$

$$\bar{g}_n = \varepsilon_n j^n \left[\frac{\eta}{\eta_0} J_n(ka) J_n'(k_0 a) - J_n'(ka) J_n(k_0 a) \right] \quad (3.35)$$

Then A_n and B_n can be simplified using the f_n , \bar{f}_n , g_n , and \bar{g}_n expressions.

$$A_n = [f_n C_n + g_n] \frac{\pi ka}{2} \quad B_n = [\bar{f}_n C_n + \bar{g}_n] \frac{\pi ka}{2} \quad (3.36)$$

Substituting these into (3.31) gives:

$$E_z^d = E_0 \frac{\pi ka}{2} \sum_{n=0}^{\infty} [[C_n f_n + g_n] J_n(kr) + [C_n \bar{f}_n + \bar{g}_n] Y_n(kr)] \cos(n\phi) = 0. \quad (3.37)$$

The boundary condition on the conducting cylinder is satisfied at a finite number of points (r_m, ϕ_m) with $m = 0, 1, 2, \dots, M$ (point matching)

$$E_z^d = E_0 \frac{\pi ka}{2} \sum_{n=0}^{\infty} [[C_n f_n + g_n] J_n(kr_m) + [C_n \bar{f}_n + \bar{g}_n] Y_n(kr_m)] \cos(n\phi_m) = 0 \quad (3.38)$$

The next step is to combine like terms, starting with f_n and \bar{f}_n .

$$\begin{aligned}
f_n J_n(kr_m) + \bar{f}_n Y_n(kr_m) &= -\frac{\eta}{\eta_0} H_n^{(2)'}(k_0 a) Y_n(ka) J_n(kr_m) + \\
H_n^{(2)}(k_0 a) Y_n'(ka) J_n(kr_m) - H_n^{(2)}(k_0 a) J_n'(ka) Y_n(kr_m) &+ \frac{\eta}{\eta_0} J_n(ka) H_n^{(2)'}(k_0 a)
\end{aligned} \tag{3.39}$$

Factoring the Hankel functions out of the equations gives:

$$\begin{aligned}
f_n J_n(kr_m) + \bar{f}_n Y_n(kr_m) &= \frac{\eta}{\eta_0} H_n^{(2)'}(k_0 a) [J_n(ka) Y_n(kr_m) - Y_n(ka) J_n(kr_m)] - \\
H_n^{(2)}(k_0 a) [J_n'(ka) Y_n(kr_m) - Y_n'(ka) J_n(kr_m)]. & \tag{3.40}
\end{aligned}$$

Define F_{mn} and \bar{F}_{mn} to simplify the equations:

$$F_{mn} = J_n(ka) Y_n(kr_m) - Y_n(ka) J_n(kr_m) \tag{3.41}$$

$$\bar{F}_{mn} = J_n'(ka) Y_n(kr_m) - Y_n'(ka) J_n(kr_m) \tag{3.42}$$

$$f_n J_n(kr_m) + \bar{f}_n Y_n(kr_m) = \frac{\eta}{\eta_0} H_n^{(2)'}(k_0 a) F_{mn} - H_n^{(2)}(k_0 a) \bar{F}_{mn}. \tag{3.43}$$

After finishing the rearrangement of the f_n and \bar{f}_n expressions, the next step is to combine the g_n and \bar{g}_n expressions:

$$\begin{aligned}
g_n J_n(kr_m) + \bar{g}_n Y_n(kr_m) &= \varepsilon_n j^n \left[-\frac{\eta}{\eta_0} Y_n(ka) J_n(kr_m) J_n'(k_0 a) + \right. \\
Y_n'(ka) J_n(kr_m) J_n(k_0 a) + \frac{\eta}{\eta_0} J_n(ka) Y_n(kr_m) J_n'(k_0 a) - J_n'(ka) Y_n(kr_m) J_n(k_0 a) &\left. \right].
\end{aligned} \tag{3.44}$$

Next factor out the terms from the Bessel functions with $k_0 a$ as the argument:

$$\begin{aligned}
g_n J_n(kr_m) + \bar{g}_n Y_n(kr_m) &= \varepsilon_n j^n \left[\frac{\eta}{\eta_0} [J_n(ka) Y_n(kr_m) - Y_n(ka) J_n(kr_m)] J_n'(k_0 a) - \right. \\
[Y_n'(ka) J_n(kr_m) - J_n'(ka) Y_n(kr_m)] J_n(k_0 a) &\left. \right]. \tag{3.45}
\end{aligned}$$

Replace the term that multiply $J_n(k_0a)$ and $J'_n(k_0a)$ with F_{mn} and \bar{F}_{mn} :

$$g_n J_n(kr_m) + \bar{g}_n Y_n(kr_m) = \varepsilon_n j^n \left[\frac{\eta}{\eta_0} F_{mn} J'_n(k_0a) - \bar{F}_{mn} J_n(k_0a) \right]. \quad (3.46)$$

Substitute in the expressions for f_n , \bar{f}_n , g_n , and \bar{g}_n with new expressions that have been simplified:

$$E_z^d = E_0 \frac{\pi k a}{2} \sum_{n=0}^{\infty} \left[C_n \left[\frac{\eta}{\eta_0} H_n^{(2)'}(k_0a) F_{mn} - \bar{F}_{mn} H_n^{(2)}(k_0a) \right] \cos(n\phi_m) + \varepsilon_n j^n \left[\frac{\eta}{\eta_0} J'_n(k_0a) F_{mn} - \bar{F}_{mn} J_n(k_0a) \right] \cos(n\phi_m) \right] = 0. \quad (3.47)$$

This can be written as:

$$\sum_{n=0}^{\infty} C_n \left[\frac{\eta}{\eta_0} H_n^{(2)'}(k_0a) F_{mn} - \bar{F}_{mn} H_n^{(2)}(k_0a) \right] \cos(n\phi_m) = - \sum_{n=0}^{\infty} \varepsilon_n j^n \left[\frac{\eta}{\eta_0} J'_n(k_0a) F_{mn} - \bar{F}_{mn} J_n(k_0a) \right] \cos(n\phi_m). \quad (3.48)$$

By truncating the sum at $n=N$, and choosing $M=N$ matching points, this can be written as a matrix equation of the form $\sum A_{mn} C_n = B_m$ which can be solved for C_n . Then C_n can be plugged into (3.9), to give the scattered field:

$$E_z^s = E_0 \sum_{n=0}^{\infty} C_n H_n^{(2)}(k_0r) \cos(n\phi). \quad (3.49)$$

For $k_0r \gg 1$ The Hankel function can be approximated using the following equation:

$$H_n^{(2)}(k_0r) = \sqrt{\frac{2}{\pi k_0r}} e^{-j(k_0r - \pi/4 - n\pi/2)} \quad (3.50)$$

Substituting this into (3.49) gives:

$$E_z^s = E_0 \sqrt{\frac{2}{\pi k_0r}} e^{-j(k_0r - \pi/4)} \sum_{n=0}^{\infty} C_n \cos(n\phi) e^{-jn\pi/2} \quad (3.51)$$

3.2 TMz Case Comparison

The TMz case comparison is to check the derivation for the elliptical case with the circular case that was derived in Heike Vollmer's thesis [10]. The comparison starts with the equation that describes the metallic core interfacing with the dielectric layer and then having tangential electrical field going to zero at the interface. To simplify the comparison, only the n th term in the summation is used. Also, kr_m is now a constant value, with $r_m = b$ forming a circle. Beginning with (3.48) and substituting for F_{mn} and \bar{F}_{mn} gives:

$$\begin{aligned} & \sum_{n=0}^{\infty} C_n \left[\frac{\eta}{\eta_0} [J_n(ka)Y_n(ka) - Y_n(ka)J_n(kr_m)] H_n^{(2)'}(k_0a) \right. \\ & \quad - [J_n'(ka)Y_n(kr_m) - Y_n'(ka)J_n(kr_m)] H_n^{(2)}(k_0a) \left. \right] \cos(n\phi_m) = \\ & \quad - \sum_{n=0}^{\infty} \varepsilon_n j^n \left[\frac{\eta}{\eta_0} [J_n(ka)Y_n(kr_m) - Y_n(ka)J_n(kr_m)] J_n'(k_0a) \right. \\ & \quad \left. - [J_n'(ka)Y_n(kr_m) - Y_n'(ka)J_n(kr_m)] J_n(k_0a) \right] \cos(n\phi_m). \quad (3.52) \end{aligned}$$

The orthogonality of the cosine functions can now be applied since $r_m = b$ is a constant. This gives:

$$\begin{aligned} & C_n \left[\frac{\eta}{\eta_0} [J_n(ka)Y_n(ka) - Y_n(ka)J_n(kr_m)] H_n^{(2)'}(k_0a) \right. \\ & \quad \left. - [J_n'(ka)Y_n(kr_m) - Y_n'(ka)J_n(kr_m)] H_n^{(2)}(k_0a) \right] \\ & = -\varepsilon_n j^n \left[\frac{\eta}{\eta_0} [J_n(ka)Y_n(kr_m) - Y_n(ka)J_n(kr_m)] J_n'(k_0a) \right. \\ & \quad \left. - [J_n'(ka)Y_n(kr_m) - Y_n'(ka)J_n(kr_m)] J_n(k_0a) \right]. \quad (3.53) \end{aligned}$$

Define D and L to simplify the fractions:

$$D = \frac{J_n(ka)}{J_n(k_0a)} - \frac{Y_n(ka)J_n(kr_m)}{Y_n(kr_m)J_n(k_0a)} \quad (3.54)$$

$$L = \frac{J'_n(ka)}{J'_n(k_0a)} - \frac{Y'_n(ka)J_n(kr_m)}{J'_n(k_0a)Y_n(kr_m)} \quad (3.55)$$

This expression matches with the expression for C_n from Heike Vollmer's thesis on [10, p. 21] with minor corrections, since radii are named by different methods.

Solving for C_n then gives:

$$C_n = \frac{\varepsilon_n j^n [D - \sqrt{\varepsilon_r} L] \frac{J_n(k_0a)}{H_n^{(2)}(k_0a)}}{D \frac{H_n^{(2)'}(k_0a)J_n(k_0a)}{H_n^{(2)}(k_0a)J'_n(k_0a)} - \sqrt{\varepsilon_r} L}. \quad (3.56)$$

3.3 TEz Case

Using the same figures in section 3.1, the incident magnetic field assumed to be z-directed and is incident on the cylinder along the -x axis. The incident magnetic field in region 2 is represented as a summation from negative infinity to positive infinity, so the magnetic field can be calculated numerically. Using the expression from [2, eq. 11-81b], the incident field can be written as:

$$H_z^i = \frac{E_0}{\eta_0} e^{jk_0 x} = \frac{E_0}{\eta_0} e^{jk_0 r \cos(\phi)} = \frac{E_0}{\eta_0} \sum_{n=-\infty}^{\infty} j^n J_n(k_0 r) e^{jn\phi} \quad (3.57)$$

The summation is broken up into negative and positive terms to simplify the summation:

$$H_z^i = \frac{E_0}{\eta_0} \left[\sum_{n=-\infty}^{-1} j^n J_n(k_0 r) e^{jn\phi} + J_0(k_0 r) + \sum_{n=1}^{\infty} j^n J_n(k_0 r) e^{jn\phi} \right]. \quad (3.58)$$

Now take the negative indexed terms and replace “n” with “-n” to gives:

$$H_z^i = \frac{E_0}{\eta_0} \left[\sum_{n=1}^{\infty} j^{-n} J_{-n}(k_0 r) e^{-jn\phi} + J_0(k_0 r) + \sum_{n=1}^{\infty} j^n J_n(k_0 r) e^{jn\phi} \right]. \quad (3.59)$$

The $J_{-n}(k_0 r)$ term is equivalent to $(-1)^n J_n(k_0 r)$ [2, eq. IV-8], giving:

$$H_z^i = \frac{E_0}{\eta_0} \left[\sum_{n=1}^{\infty} j^{-n} (-1)^n J_n(k_0 r) e^{-jn\phi} + J_0(k_0 r) + \sum_{n=1}^{\infty} j^n J_n(k_0 r) e^{jn\phi} \right]. \quad (3.60)$$

Combining the summations gives:

$$H_z^i = \frac{E_0}{\eta_0} \left[\sum_{n=1}^{\infty} j^n J_n(k_0 r) \left[e^{-jn\phi} + e^{jn\phi} \right] + J_0(k_0 r) \right]. \quad (3.61)$$

The exponentials can be combined into a cosine function and ε_n is needed since there is a two factored out of the exponentials for n greater than zero. For n equal to zero, there is only one exponential, so only one is factored out. This gives:

$$H_z^i = \frac{E_0}{\eta_0} \sum_{n=0}^{\infty} \varepsilon_n j^n J_n(k_0 r) \cos(n\phi) \quad \varepsilon_n = \begin{cases} 1 & n = 0 \\ 2 & n \neq 0 \end{cases}. \quad (3.62)$$

The electric field is calculated by taking the curl of the magnetic field:

$$\vec{E}^i = -\frac{1}{j\omega\varepsilon} [\hat{z} \times \nabla_t H_z^i] = -\frac{1}{j\omega\varepsilon} \left[\hat{r} \frac{1}{r} \partial_\phi H_z^i + \hat{\phi} \partial_r H_z^i \right] \quad (3.63)$$

Applying the derivatives gives:

$$\vec{E}^i = -\frac{1}{j\omega\varepsilon} \left[\left[\hat{r} \frac{E_0}{\eta_0 r} \sum_{n=0}^{\infty} \varepsilon_n j^n J_n(k_0 r) n \sin(n\phi) \right] + \hat{\phi} \frac{E_0}{\eta_0} \left[\sum_{n=0}^{\infty} \varepsilon_n j^n k_0 J_n'(k_0 r) \cos(n\phi) \right] \right] \quad (3.64)$$

The \hat{r} part of the electric field is not needed in the calculation for the tangential electrical field in the boundary conditions. Simplifying gives:

$$E_\phi^i = \frac{jE_0 k_0}{\eta_0 \omega \varepsilon} \sum_{n=0}^{\infty} \varepsilon_n j^n J_n'(k_0 r) \cos(n\phi) = jE_0 \sum_{n=0}^{\infty} \varepsilon_n j^n J_n'(k_0 r) \cos(n\phi) \quad (3.65)$$

The magnetic scattered field in region two is given by the equation:

$$H_z^s = \frac{E_0}{\eta_0} \sum_{n=0}^{\infty} C_n H_n^{(2)}(k_0 r) \cos(n\phi) \quad (3.66)$$

The electric scattered field is calculated by taking the curl of the magnetic scattered field. As before, only the $\hat{\phi}$ component is needed:

$$E_\phi^s = -\frac{1}{j\omega\varepsilon} \partial_r H_z^s = \frac{j}{\omega\varepsilon_0} \partial_r \left[\frac{E_0}{\eta_0} \sum_{n=0}^{\infty} C_n H_n^{(2)}(k_0 r) \cos(n\phi) \right]. \quad (3.67)$$

Taking the derivative and simplifying gives:

$$E_\phi^s = \frac{jkE_0}{\eta_0 \omega \varepsilon_0} \sum_{n=0}^{\infty} C_n H_n^{(2)'}(k_0 r) \cos(n\phi) = jE_0 \sum_{n=0}^{\infty} C_n H_n^{(2)'}(k_0 r) \cos(n\phi) \quad (3.68)$$

The magnetic field in region one (dielectric region) is given by the following equation:

$$H_z^d = \frac{E_0}{\eta} \sum_{n=0}^{\infty} [A_n J_n(kr) + B_n Y_n(kr)] \cos(n\phi). \quad (3.69)$$

The electric field in the dielectric region is calculated by taking the curl of the magnetic field equation in the dielectric material. As in the pervious cases, only the $\hat{\phi}$ component is needed:

$$E_\phi^d = -\frac{1}{j\omega\varepsilon} \partial_r H_z = -\frac{1}{j\omega\varepsilon} \partial_r \frac{E_0}{\eta} \sum_{n=0}^{\infty} [A_n J_n(kr) + B_n Y_n(kr)] \cos(n\phi). \quad (3.70)$$

Applying the derivative gives:

$$E_\phi^d = \frac{jkE_0}{\eta\omega\varepsilon} \sum_{n=0}^{\infty} [A_n J'_n(kr) + B_n Y'_n(kr)] \cos(n\phi) \quad (3.71)$$

After the derivative is applied, the constants in front of the summation are simplified to give:

$$E_\phi^d = jE_0 \sum_{n=0}^{\infty} [A_n J'_n(kr) + B_n Y'_n(kr)] \cos(n\phi). \quad (3.72)$$

After finding the electric and magnetic fields in the various regions, the next step is to apply the boundary conditions. The first boundary condition that is applied is that the tangential electric field is continuous at $r = a$.

$$jE_0 \sum_{n=0}^{\infty} \varepsilon_n j^n J'_n(k_0 a) \cos(n\phi) + jE_0 \sum_{n=0}^{\infty} C_n H_n^{(2)'}(k_0 a) \cos(n\phi) = jE_0 \sum_{n=0}^{\infty} [A_n J'_n(ka) + B_n Y'_n(ka)] \cos(n\phi) \quad (3.73)$$

Applying orthogonality of the $\cos(n\phi)$ functions gives:

$$\frac{\eta}{\eta_0} \varepsilon_n j^n J'_n(k_0 a) + \frac{\eta}{\eta_0} C_n H_n^{(2)'}(k_0 a) = [A_n J'_n(ka) + B_n Y'_n(ka)]. \quad (3.74)$$

The next boundary conditions that is applied is the continuity of tangent magnetic field being at $r = a$:

$$\frac{E_0}{\eta_0} \sum_{n=0}^{\infty} \varepsilon_n j^n J_n(k_0 a) \cos(n\phi) + \frac{E_0}{\eta_0} \sum_{n=0}^{\infty} C_n H_n^{(2)}(k_0 a) \cos(n\phi) = \frac{E_0}{\eta} \sum_{n=0}^{\infty} [A_n J_n(ka) + B_n Y_n(ka)] \cos(n\phi). \quad (3.75)$$

Using the same process described above, the summation is removed, leaving the A_n , B_n , and C_n terms:

$$\frac{\eta}{\eta_0} \varepsilon_n j^n J_n(k_0 a) + \frac{\eta}{\eta_0} C_n H_n^{(2)}(k_0 a) = A_n J_n(ka) + B_n Y_n(ka) \quad (3.76)$$

Since there are two equations, (3.74) and (3.76) two of the variables can be eliminated by solving for them in terms of the third variable. The first step is to solve for A_n from equation (3.76):

$$A_n = \frac{1}{J_n(ka)} \left[\frac{\eta}{\eta_0} \varepsilon_n j^n J_n(k_0 a) + \frac{\eta}{\eta_0} C_n H_n^{(2)}(k_0 a) \cos(n\phi) - B_n Y_n(ka) \right]. \quad (3.77)$$

Next, substitute in place A_n into (3.74) to give:

$$\varepsilon_n j^n J_n'(k_0 a) + C_n H_n^{(2)'}(k_0 a) = B_n Y_n'(ka) + \left[\frac{\eta}{\eta_0} E_0 \varepsilon_n j^n J_n(k_0 a) + \frac{\eta}{\eta_0} C_n H_n^{(2)}(k_0 a) - B_n Y_n(ka) \right] \frac{J_n'(ka)}{J_n(ka)}. \quad (3.78)$$

Next factor the common terms:

$$\varepsilon_n j^n \left[J_n'(k_0 a) J_n(ka) - \frac{\eta}{\eta_0} J_n'(ka) J_n(k_0 a) \right] + C_n \left[H_n^{(2)'}(k_0 a) J_n(ka) - \frac{\eta}{\eta_0} H_n^{(2)}(k_0 a) J_n'(ka) \right] = B_n [Y_n'(ka) J_n(ka) - Y_n(ka) J_n'(ka)]. \quad (3.79)$$

The term that multiplies B_n is equivalent to the following equation [2, eq. 11-95]:

$$Y_n'(ka) J_n(ka) - Y_n(ka) J_n'(ka) = \frac{2}{\pi ka}. \quad (3.80)$$

Finally, solving for B_n gives:

$$B_n = \frac{\pi ka}{2} \left[\varepsilon_n j^n \left[J'_n(k_0 a) J_n(ka) - \frac{\eta}{\eta_0} J_n(k_0 a) J'_n(ka) \right] + C_n \left[H_n^{(2)'}(k_0 a) J_n(ka) - \frac{\eta}{\eta_0} H_n^{(2)}(k_0 a) J'_n(ka) \right] \right]. \quad (3.81)$$

After solving for B_n , the next step is to solve for A_n in terms of C_n . First solve for B_n from equation (3.76):

$$B_n = \frac{1}{Y_n(ka)} \left[\frac{\eta}{\eta_0} \varepsilon_n j^n J_n(k_0 a) + \frac{\eta}{\eta_0} C_n H_n^{(2)}(k_0 a) \cos(n\phi) - A_n J_n(ka) \right]. \quad (3.82)$$

Equating this with the B_n in equation (3.74) gives:

$$\varepsilon_n j^n J'_n(k_0 a) + C_n H_n^{(2)'}(k_0 a) = A_n J'_n(ka) + \frac{Y'_n(ka)}{Y_n(ka)} \left[\frac{\eta}{\eta_0} \varepsilon_n j^n J_n(k_0 a) + \frac{\eta}{\eta_0} C_n H_n^{(2)}(k_0 a) - A_n J_n(ka) \right]. \quad (3.83)$$

Factoring out the common terms gives:

$$\varepsilon_n j^n \left[J'_n(k_0 a) Y_n(ka) - \frac{\eta}{\eta_0} J_n(k_0 a) Y'_n(ka) \right] + C_n \left[H_n^{(2)'}(k_0 a) Y_n(ka) - \frac{\eta}{\eta_0} H_n^{(2)}(k_0 a) Y'_n(ka) \right] = A_n [J'_n(ka) Y_n(ka) - Y'_n(ka) J_n(ka)]. \quad (3.84)$$

Using equation (3.80) to simplify the expression multiplying A_n gives:

$$A_n = \frac{-\pi ka}{2} \left[\varepsilon_n j^n \left[J'_n(k_0 a) Y_n(ka) - \frac{\eta}{\eta_0} J_n(k_0 a) Y'_n(ka) \right] + \left[H_n^{(2)'}(k_0 a) Y_n(ka) - \frac{\eta}{\eta_0} H_n^{(2)}(k_0 a) Y'_n(ka) \right] \right]. \quad (3.85)$$

The derivatives of the magnetic field are needed for various equations later in the derivation. The derivative of the magnetic field with respect to ϕ is:

$$\frac{1}{r} \partial_{\phi} H_z^d = \frac{1}{r} \partial_{\phi} \left[\frac{E_0}{\eta} \sum_{n=0}^{\infty} [A_n J_n(kr) + B_n Y_n(kr)] \cos(n\phi) \right] \quad (3.86)$$

or

$$\frac{1}{r} \partial_{\phi} H_z^d = -\frac{1}{r} \left[\frac{E_0}{\eta} \sum_{n=0}^{\infty} [A_n J_n(kr) + B_n Y_n(kr)] n \sin(n\phi) \right]. \quad (3.87)$$

Also needed is the derivative with respect to r :

$$\partial_r H_z^d = \partial_r \left[\frac{E_0}{\eta} \sum_{n=0}^{\infty} [A_n J_n(kr) + B_n Y_n(kr)] \cos(n\phi) \right] \quad (3.88)$$

or

$$\partial_r H_z^d = k \left[\frac{E_0}{\eta} \sum_{n=0}^{\infty} [A_n J'_n(kr) + B_n Y'_n(kr)] \cos(n\phi) \right]. \quad (3.89)$$

The last boundary condition to be applied is that of zero tangential electric field at the metallic surface. Finding the tangent to the ellipse is necessary because the tangential electric field is not the z component. The tangent vector is calculated by taking the derivative of the position vector describing the points on the ellipse divided by the magnitude of the same vector. Let $\vec{r}'(\phi)$ describe the position vector to points on the ellipse. Then the tangent vector is:

$$\vec{T}(\phi) = \frac{\vec{r}'(\phi)}{|\vec{r}'(\phi)|} \quad (3.90)$$

Where

$$\vec{r}(\phi) = \hat{x}a_1 \cos(\phi) + \hat{y}a_2 \sin(\phi) \quad (3.91)$$

and

$$\vec{r}'(\phi) = \frac{d\vec{r}(\phi)}{d\phi} \quad (3.92)$$

The derivative of the position vector and its magnitude are:

$$\vec{r}'(\phi) = -\hat{x}a_1 \sin(\phi) + \hat{y}a_2 \cos(\phi) \quad |\vec{r}'(\phi)| = \sqrt{a_1^2(\sin(\phi))^2 + a_2^2(\cos(\phi))^2} \quad (3.93)$$

Thus

$$\begin{aligned} \vec{T}(\phi) &= \hat{x} \frac{-a_1 \sin(\phi)}{\sqrt{a_1^2(\sin(\phi))^2 + a_2^2(\cos(\phi))^2}} + \hat{y} \frac{a_2 \cos(\phi)}{\sqrt{a_1^2(\sin(\phi))^2 + a_2^2(\cos(\phi))^2}} \\ &= t_x \hat{x} + t_y \hat{y}. \end{aligned} \quad (3.94)$$

By the boundary condition the dot product of the electric field vector and the tangent vector is equal to zero on surface of the conductor. Also, the electric field is equal to the curl of the magnetic field, so

$$\hat{i} \cdot \vec{E}^d = (t_x \hat{x} + t_y \hat{y}) \cdot \hat{r} \frac{1}{r} \partial_\phi H_z^d + (t_x \hat{x} + t_y \hat{y}) \cdot \hat{\phi} \partial_r H_z^d = 0. \quad (3.95)$$

Since the curl of the magnetic field is in cylindrical coordinates and the tangent vector is in rectangular coordinates, the cylindrical coordinate unit vectors need to be converted to rectangular coordinates [7, eqs. D.44, D.45]:

$$\begin{aligned} (t_x \hat{x} + t_y \hat{y}) \cdot (\hat{x} \cos(\phi) + \hat{y} \sin(\phi)) \frac{1}{r} \partial_\phi H_z^d + \\ (t_x \hat{x} + t_y \hat{y}) \cdot (-\hat{x} \sin(\phi) + \hat{y} \cos(\phi)) \partial_r H_z^d = 0. \end{aligned} \quad (3.96)$$

Multiplying out the unit vectors gives:

$$(t_x \cos(\phi) + t_y \sin(\phi)) \frac{1}{r} \partial_\phi H_z^d + (-t_x \sin(\phi) + t_y \cos(\phi)) \partial_r H_z^d = 0. \quad (3.97)$$

The derivatives of the magnetic field are inserted to the equation from equations (3.87) and (3.89) to give:

$$\frac{(a_2 - a_1) \sin(\phi) \cos(\phi)}{\sqrt{a_1^2(\sin(\phi))^2 + a_2^2(\cos(\phi))^2}} \frac{E_0}{\eta} \left[\frac{1}{r} \sum_{n=0}^{\infty} [A_n J_n(kr) + B_n Y_n(kr)] n \sin(n\phi) \right] +$$

$$\frac{a_1(\sin(\phi))^2 + a_2(\cos(\phi))^2}{\sqrt{a_1^2(\sin(n\phi))^2 + a_2^2(\cos(\phi))^2}} \frac{E_0}{\eta} \sum_{n=0}^{\infty} [A_n J'_n(kr) + B_n Y'_n(kr)] k \cos(n\phi) = 0.$$

(3.98)

Define $G(\phi)$ and $\bar{G}(\phi)$ to simplify the previous equation:

$$G(\phi) = \frac{(a_2 - a_1) \sin(\phi) \cos(\phi)}{\sqrt{a_1^2(\sin(\phi))^2 + a_2^2(\cos(\phi))^2}}. \quad (3.99)$$

$$\bar{G}(\phi) = \frac{a_1(\sin(\phi))^2 + a_2(\cos(\phi))^2}{\sqrt{a_1^2(\sin(n\phi))^2 + a_2^2(\cos(\phi))^2}} \quad (3.100)$$

Also define f_{n1} , \bar{f}_{n1} , g_{n1} , and \bar{g}_{n1} as:

$$f_{n1} = -H_n^{(2)'}(k_0 a) Y_n(k a) + \frac{\eta}{\eta_0} H_n^{(2)}(k_0 a) Y_n'(k a) \quad (3.101)$$

$$\bar{f}_{n1} = H_n^{(2)'}(k_0 a) J_n(k a) - \frac{\eta}{\eta_0} H_n^{(2)}(k_0 a) J_n'(k a) \quad (3.102)$$

$$g_{n1} = -\varepsilon_n j^n \left[J_n'(k_0 a) Y_n(k a) + \frac{\eta}{\eta_0} J_n(k_0 a) Y_n'(k a) \right] \quad (3.103)$$

$$\bar{g}_{n1} = \varepsilon_n j^n \left[J_n'(k_0 a) J_n(k a) + \frac{\eta}{\eta_0} J_n(k_0 a) J_n'(k a) \right]. \quad (3.104)$$

Using these, A_n and B_n can be written as:

$$A_n = \frac{\pi k a}{2} [C_n f_{n1} + g_{n1}] \quad B_n = \frac{\pi k a}{2} [C_n \bar{f}_{n1} + \bar{g}_{n1}]. \quad (3.105)$$

Equation (3.96) becomes

$$\begin{aligned}
G(\phi) \frac{\pi k a}{2r} \sum_{n=0}^{\infty} [(C_n f_{n1} + g_{n1}) J_n(kr) + (C_n \bar{f}_{n1} + \bar{g}_{n1}) Y_n(kr)] n \sin(n\phi) + \\
\bar{G}(\phi) \frac{\pi k a}{2} k \sum_{n=0}^{\infty} [(C_n f_{n1} + g_{n1}) J'_n(kr) + (C_n \bar{f}_{n1} + \bar{g}_{n1}) Y'_n(kr)] \cos(n\phi) = 0.
\end{aligned} \tag{3.106}$$

The common terms drop out and the point matching technique used in section 3.1 is used to give:

$$\begin{aligned}
G(\phi_m) \frac{1}{r} \sum_{n=0}^{\infty} [(C_n f_{n1} + g_{n1}) J_n(kr) + (C_n \bar{f}_{n1} + \bar{g}_{n1}) Y_n(kr)] n \sin(n\phi_m) + \\
\bar{G}(\phi_m) k \sum_{n=0}^{\infty} [(C_n f_{n1} + g_{n1}) J'_n(kr) + (C_n \bar{f}_{n1} + \bar{g}_{n1}) Y'_n(kr)] \cos(n\phi_m) = 0.
\end{aligned} \tag{3.107}$$

The terms of the f_{n1} , \bar{f}_{n1} , g_{n1} , and \bar{g}_{n1} are combined separate the C_n terms and non C_n terms. The first expression in the first summation can be written as:

$$\begin{aligned}
f_{n1} J_n(kr_m) + \bar{f}_{n1} Y_n(kr_m) = \\
- H_n^{(2)'}(k_0 a) Y_n(k a) J_n(kr_m) + \frac{\eta}{\eta_0} H_n^{(2)}(k_0 a) Y'_n(k a) J_n(kr_m) + \\
H_n^{(2)'}(k_0 a) Y_n(kr_m) J_n(k a) - \frac{\eta}{\eta_0} H_n^{(2)}(k_0 a) Y_n(kr_m) J'_n(k a). \tag{3.108}
\end{aligned}$$

Combining like terms gives:

$$\begin{aligned}
f_{n1} J_n(kr_m) + \bar{f}_{n1} Y_n(kr_m) = H_n^{(2)'}(k_0 a) [Y_n(kr_m) J_n(k a) - Y_n(k a) J_n(kr_m)] - \\
\frac{\eta}{\eta_0} H_n^{(2)}(k_0 a) [Y_n(kr_m) J'_n(k a) - Y'_n(k a) J_n(kr_m)]. \tag{3.109}
\end{aligned}$$

The last step is to simplify the equation by using F_{mn} and \bar{F}_{mn} defined in (3.41)

and (3.42), since the terms appear in multiple expressions allowing a simplification of the expression:

$$f_{n1}J_n(kr_m) + \bar{f}_{n1}Y_n(kr_m) = F_{mn}H_n^{(2)'}(k_0a) - \frac{\eta}{\eta_0}\bar{F}_{mn}H_n^{(2)}(k_0a) \quad (3.110)$$

Simplifying the second expression in first summation gives:

$$\begin{aligned} g_{n1}J_n(kr_m) + \bar{g}_{n1}Y_n(kr_m) = \\ \varepsilon_n j^n \left[-J_n'(k_0a)Y_n(ka)J_n(kr_m) + \frac{\eta}{\eta_0}J_n(k_0a)Y_n'(ka)J_n(kr_m) + \right. \\ \left. J_n'(k_0a)Y_n(kr_m)J_n(ka) - \frac{\eta}{\eta_0}J_n(k_0a)Y_n(kr_m)J_n'(ka) \right]. \quad (3.111) \end{aligned}$$

Combining like terms gives:

$$\begin{aligned} g_{n1}J_n(kr_m) + \bar{g}_{n1}Y_n(kr_m) = \\ \varepsilon_n j^n \left[J_n'(k_0a) [Y_n(kr_m)J_n(ka) - Y_n(ka)J_n(kr_m)] - \right. \\ \left. \frac{\eta}{\eta_0}J_n(k_0a) [Y_n(kr_m)J_n'(ka) - Y_n'(ka)J_n(kr_m)] \right]. \quad (3.112) \end{aligned}$$

The last step is to simplify the expression by using F_{mn} and \bar{F}_{mn} :

$$g_{n1}J_n(kr_m) + \bar{g}_{n1}Y_n(kr_m) = \varepsilon_n j^n \left[J_n'(k_0a)F_{mn} - \frac{\eta}{\eta_0}J_n(k_0a)\bar{F}_{mn} \right]. \quad (3.113)$$

The next expression to be simplified is the first expression of the second summation, giving

$$\begin{aligned} f_{n1}J_n'(kr_m) + \bar{f}_{n1}Y_n'(kr_m) = \\ -H_n^{(2)'}(k_0a)Y_n(ka)J_n'(kr_m) + \frac{\eta}{\eta_0}H_n^{(2)}(k_0a)Y_n'(ka)J_n'(kr_m) + \\ H_n^{(2)'}(k_0a)Y_n'(kr_m)J_n(ka) - \frac{\eta}{\eta_0}H_n^{(2)}(k_0a)Y_n'(kr_m)J_n'(ka). \quad (3.114) \end{aligned}$$

Combining the like terms gives

$$f_{n1}J'_n(kr_m) + \bar{f}_{n1}Y'_n(kr_m) = H_n^{(2)'}(k_0a) [Y'_n(kr_m)J_n(ka) - Y_n(ka)J'_n(kr_m)] - \frac{\eta}{\eta_0} H_n^{(2)}(k_0a) [Y'_n(kr_m)J'_n(ka) - Y'_n(ka)J'_n(kr_m)]. \quad (3.115)$$

The last step is to simplify the equation by defining F_{1mn} and \bar{F}_{1mn} :

$$f_{n1}J'_n(kr_m) + \bar{f}_{n1}Y'_n(kr_m) = F_{1mn}H_n^{(2)'}(k_0a) - \frac{\eta}{\eta_0}\bar{F}_{1mn}H_n^{(2)}(k_0a) \quad (3.116)$$

$$F_{1mn} = Y'_n(kr_m)J_n(ka) - Y_n(ka)J'_n(kr_m) \quad (3.117)$$

$$\bar{F}_{1mn} = Y'_n(kr_m)J'_n(ka) - Y'_n(ka)J'_n(kr_m) \quad (3.118)$$

The last expression to be simplified is the second expression of the second summation:

$$g_{n1}J'_n(kr_m) + \bar{g}_{n1}Y'_n(kr_m) = \varepsilon_n j^n \left[-J'_n(k_0a)Y_n(ka)J'_n(kr_m) + \frac{\eta}{\eta_0}J_n(k_0a)Y'_n(ka)J'_n(kr_m) + J'_n(k_0a)Y'_n(kr_m)J_n(ka) - \frac{\eta}{\eta_0}J_n(k_0a)Y'_n(kr_m)J'_n(ka) \right]. \quad (3.119)$$

Combining like terms gives

$$g_{n1}J'_n(kr_m) + \bar{g}_{n1}Y'_n(kr_m) = \varepsilon_n j^n \left[J'_n(k_0a) [Y'_n(kr_m)J_n(ka) - Y_n(ka)J'_n(kr_m)] - \frac{\eta}{\eta_0}J_n(k_0a) [Y'_n(kr_m)J'_n(ka) - Y'_n(ka)J'_n(kr_m)] \right]. \quad (3.120)$$

Simplifying the equation using F_{1mn} and \bar{F}_{1mn} gives

$$g_{n1}J'_n(kr_m) + \bar{g}_{n1}Y'_n(kr_m) = \varepsilon_n j^n \left[J'_n(k_0a)F_{1mn} - \frac{\eta}{\eta_0}J_n(k_0a)\bar{F}_{1mn} \right]. \quad (3.121)$$

Using each of these expressions, equation (3.105) becomes

$$\begin{aligned}
C_n & \left[G(\phi_m) \frac{1}{r} \sum_{n=0}^{\infty} \left[F_{mn} H_n^{(2)'}(k_0 a) - \frac{\eta}{\eta_0} \bar{F}_{mn} H_n^{(2)}(k_0 a) \right] n \sin(n\phi_m) \right. \\
& \left. + \bar{G}(\phi_m) k \sum_{n=0}^{\infty} \left[F_{1mn} H_n^{(2)'}(k_0 a) - \frac{\eta}{\eta_0} \bar{F}_{1mn} H_n^{(2)}(k_0 a) \right] \cos(n\phi_m) \right] = \\
& - E_0 \varepsilon_n j^n \left[G(\phi_m) \frac{1}{r} \sum_{n=0}^{\infty} \left[F_{mn} J_n'(k_0 a) - \frac{\eta}{\eta_0} \bar{F}_{mn} J_n(k_0 a) \right] n \sin(n\phi_m) \right. \\
& \left. + \bar{G}(\phi_m) k \sum_{n=0}^{\infty} \left[F_{1mn} J_n'(k_0 a) - \frac{\eta}{\eta_0} \bar{F}_{1mn} J_n(k_0 a) \right] \cos(n\phi_m) \right]. \quad (3.122)
\end{aligned}$$

Truncating the sum at $n=N$ and using $N+1$ matching points, (3.122) can be written as a matrix equation of the form $\sum A_{mn} C_n = B_m$, which can be solved for C_n .

After finding C_n , the last step is to insert the value of C_n into electric scattered field (3.68):

$$E_\phi^s = j E_0 \sum_{n=0}^{\infty} C_n H_n^{(2)'}(k_0 r) \cos(n\phi) \quad (3.123)$$

For $k_0 r \gg 1$ The Hankel function can be approximated using the following equation:

$$H_n^{(2)'}(k_0 r) = -\sqrt{\frac{2j}{\pi k_0 r}} j^{n+1} e^{-jk_0 r} \quad (3.124)$$

Substituting this into (3.123) gives:

$$E_\phi^s = E_0 \sqrt{\frac{2j}{\pi k_0 r}} \sum_{n=0}^{\infty} C_n j^n e^{-jk_0 r} \cos(n\phi) \quad (3.125)$$

3.4 TEz Case Comparison

The TEz case comparison is to check the derivation for the elliptical case with the circular case that was derived in Heike Vollmer's thesis [10]. The ellipse is now a circle with constant radius $r_m = b$. As done in the TMz case, only the n th term will be used in the comparison for simplicity. Since the metallic core is now a circle, and the coating has radius $a_1 = a_2$, the $G(\phi)$ expression now gives:

$$G(\phi) = \frac{(a_1 - a_1) \sin(\phi) \cos(\phi)}{\sqrt{a_1^2 (\sin(\phi))^2 + a_1^2 (\cos(\phi))^2}} = 0. \quad (3.126)$$

For $\bar{G}(\phi)$, letting a_1 equal to a_2 , gives:

$$\bar{G}(\phi) = \frac{a_1 (\sin(\phi))^2 + a_1 (\cos(\phi))^2}{\sqrt{a_1^2 (\sin(n\phi))^2 + a_1^2 (\cos(\phi))^2}} = \frac{a_1}{\sqrt{a_1^2}} = 1. \quad (3.127)$$

Starting with the tangent electric field equal to zero at the dielectric material interface with the metallic core and solving for C_n , gives:

$$\begin{aligned} C_n \left[G(\phi) \frac{1}{r} \sum_{n=0}^{\infty} \left[\frac{\eta_0}{\eta} F_{mn} H_n^{(2)'}(k_0 a) - \bar{F}_{mn} H_n^{(2)}(k_0 a) \right] n \sin(n\phi_m) \right. \\ \left. + \bar{G}(\phi) k \sum_{n=0}^{\infty} \left[\frac{\eta_0}{\eta} F_{1mn} H_n^{(2)'}(k_0 a) - \bar{F}_{1mn} H_n^{(2)}(k_0 a) \right] \cos(n\phi_m) \right] = \\ - E_0 \varepsilon_n j^n \left[G(\phi) \frac{1}{r} \sum_{n=0}^{\infty} \left[\frac{\eta_0}{\eta} F_{mn} J_n'(k_0 a) - \bar{F}_{mn} J_n(k_0 a) \right] n \sin(n\phi_m) \right. \\ \left. + \bar{G}(\phi) k \sum_{n=0}^{\infty} \left[\frac{\eta_0}{\eta} F_{1mn} J_n'(k_0 a) - \bar{F}_{1mn} J_n(k_0 a) \right] \cos(n\phi_m) \right]. \quad (3.128) \end{aligned}$$

Simplifying the equation using (3.126) and (3.127) gives:

$$C_n \left[k \sum_{n=0}^{\infty} \left[\frac{\eta_0}{\eta} F_{1mn} H_n^{(2)'}(k_0 a) - \bar{F}_{1mn} H_n^{(2)}(k_0 a) \right] \cos(n\phi_m) \right] =$$

$$- E_0 \varepsilon_n j^n \left[k \sum_{n=0}^{\infty} \left[\frac{\eta_0}{\eta} F_{1mn} J_n'(k_0 a) - \bar{F}_{1mn} J_n(k_0 a) \right] \cos(n\phi_m) \right]. \quad (3.129)$$

Orthogonality of the cosine function can be applied since $r_m = b$ is a constant.

Also, substituting for F_{1mn} and \bar{F}_{1mn} from equations (3.41) and (3.42) with the original Bessel functions for the comparison gives:

$$C_n \left[\frac{\eta_0}{\eta} [Y_n'(kr_m) J_n(ka) - Y_n(ka) J_n'(kr_m)] H_n^{(2)'}(k_0 a) \right.$$

$$\left. - [Y_n'(kr_m) J_n'(ka) - Y_n'(ka) J_n'(kr_m)] H_n^{(2)}(k_0 a) \right] =$$

$$- E_0 \varepsilon_n j^n \left[\frac{\eta_0}{\eta} [Y_n'(kr_m) J_n(ka) - Y_n(ka) J_n'(kr_m)] J_n'(k_0 a) \right.$$

$$\left. - [Y_n'(kr_m) J_n'(ka) - Y_n'(ka) J_n'(kr_m)] J_n(k_0 a) \right] \quad (3.130)$$

Define D and L to simplify the fraction:

$$D = \frac{J_n(ka)}{J_n(k_0 a)} - \frac{Y_n(ka) J_n'(kr_m)}{Y_n'(kr_m) J_n(k_0 a)} \quad (3.131)$$

$$L = \frac{J_n'(ka)}{J_n'(k_0 a)} - \frac{Y_n'(ka) J_n'(kr_m)}{Y_n'(kr_m) J_n'(k_0 a)}. \quad (3.132)$$

Solving for C_n gives:

$$C_n = \frac{-E_0 \varepsilon_n j^n \left[D - \frac{1}{\sqrt{\varepsilon_r}} L \right] \frac{J_n(k_0 a)}{H_n^{(2)}(k_0 a)}}{D \frac{H_n^{(2)'}(k_0 a) J_n(k_0 a)}{H_n^{(2)}(k_0 a) J_n'(k_0 a)} - \frac{1}{\sqrt{\varepsilon_r}} L}. \quad (3.133)$$

This expression matches with the expression for C_n in Heike Vollmer's thesis on [10, p. 18] with minor corrections, since the radii are named by different methods.

CHAPTER 4

Computational Considerations

4.1 Computation Method

The computer code written to calculate the frequency domain data for the TE_z and TM_z scattered electric field has the following structure: placement of the ellipse matching points, calculation of the values of the Bessel functions, normalization of the matrix entries, and evaluation of the matrix. Appropriate placement of the points on the ellipse is necessary so that the matrix is not singular. Placement of the points on the ellipse is done using the following formula:

$$\theta_i = \frac{i}{N+1}\pi + \frac{\pi}{2(N+1)}, \quad i = 0, 1, \dots, N \quad (4.1)$$

After the ellipse is set up and the step size and number of the frequency points is chosen, the wave numbers are calculated. The Bessel functions for the matrix are calculated using a routine provided by Dr. Edward Rothwell based on the formulas in Abramowitz [1]. The results from the Bessel functions are scaled down by applying a natural logarithm to the calculated values to prevent a numerical overflow when the actual value of the Bessel functions are used. For the TM_z case, equation (3.48) has $H_n^{(2)'}(k_0a)$ factored from the expansion coefficient as shown:

$$\sum_{n=0}^{\infty} C'_n \left[\frac{\eta}{\eta_0} F_{mn} - \bar{F}_{mn} \frac{H_n^{(2)}(k_0 a)}{H_n^{(2)'}(k_0 a)} \right] \cos(n\phi_m) =$$

$$- \sum_{n=0}^{\infty} \varepsilon_n j^n \left[\frac{\eta}{\eta_0} J'_n(k_0 a) F_{mn} - \bar{F}_{mn} J_n(k_0 a) \right] \cos(n\phi_m) \quad (4.2)$$

where as

$$C'_n = C_n H_n^{(2)'}(k_0 a). \quad (4.3)$$

And equation (3.51) becomes:

$$E_z^s = E_0 \sqrt{\frac{2}{\pi k_0 r}} e^{-j(k_0 r - \pi/4)} \sum_{n=0}^{\infty} \frac{C'_n}{H_n^{(2)'}(k_0 a)} \cos(n\phi) e^{-jn\pi/2} \quad (4.4)$$

This normalization allows the usage of larger arguments and orders of the Hankel function without overflowing the variable in FORTRAN. Two other methods for normalization that were explored are dividing through by $H_n^{(2)'}(k_0 a)$ and dividing through by $H'_{max}(k_0 a)$. Dividing equation (3.48) by $H_n^{(2)'}(k_0 a)$ gives:

$$\sum_{n=0}^{\infty} C_n \left[\frac{\eta}{\eta_0} F_{mn} - \bar{F}_{mn} \frac{H_n^{(2)}(k_0 a)}{H_n^{(2)'}(k_0 a)} \right] \cos(n\phi_m) =$$

$$- \sum_{n=0}^{\infty} \varepsilon_n j^n \left[\frac{\eta}{\eta_0} \frac{J'_n(k_0 a)}{H_n^{(2)'}(k_0 a)} F_{mn} - \bar{F}_{mn} \frac{J_n(k_0 a)}{H_n^{(2)'}(k_0 a)} \right] \cos(n\phi_m). \quad (4.5)$$

The division by $H_n^{(2)'}(k_0 a)$ was rejected because the results did not always match the case without normalization. Dividing equation (3.48) by $H'_{max}(k_0 a)$ gives:

$$\sum_{n=0}^{\infty} C_n \left[\frac{\eta}{\eta_0} F_{mn} - \bar{F}_{mn} \frac{H_n^{(2)}(k_0 a)}{H'_{max}(k_0 a)} \right] \cos(n\phi_m) =$$

$$- \sum_{n=0}^{\infty} \varepsilon_n j^n \left[\frac{\eta}{\eta_0} \frac{J'_n(k_0 a)}{H'_{max}(k_0 a)} F_{mn} - \bar{F}_{mn} \frac{J_n(k_0 a)}{H'_{max}(k_0 a)} \right] \cos(n\phi_m). \quad (4.6)$$

The division by $H_{max}^{(2)'}(k_0a)$ created zeros for all points in the data range.

After the matrix is set up, the next step is to solve matrix using an LU decomposition routine. Lastly the C_n term is inserted into equation (3.51) or equation (3.125) to get the scattered electric field value. For the TMz case, the FORTRAN code is in Appendix A, and for the TEz case, the FORTRAN code is in Appendix B.

4.2 Flat Case

The coated planar surface or the flat case is the standard reference for the comparison in the time domain using the E-pulse technique. The equation that is used to create the scattered electric field for the flat case is [9]:

$$R = \frac{\frac{\eta - \eta_0}{\eta + \eta_0} - e^{-2jkd}}{1 - \frac{\eta - \eta_0}{\eta + \eta_0} e^{-2jkd}} \quad (4.7)$$

Here d is the coating thickness and $\eta = \sqrt{\mu_0/(\epsilon_r \epsilon_0)}$. To compare to the coated ellipse, values of $d = .1$ m and $\epsilon_r = 9$ are used. The equation is coded in FORTRAN and is shown in Appendix C. Magnitude and phase plots of R from (4.6) are shown in figures 4.1 and 4.2, respectively. The magnitude of the flat case is always 1 because the incident electromagnetic wave is entirely reflected back from the flat surface. The phase plot shows the typical pattern of variation between 180 to -180 degrees. Applying a 32768 point FFT to the frequency domain data gives the time domain data shown in 4.3. The series of pulses represents the multiple reflection within the planar coating. Note that the waveform is zero in between the pulses.

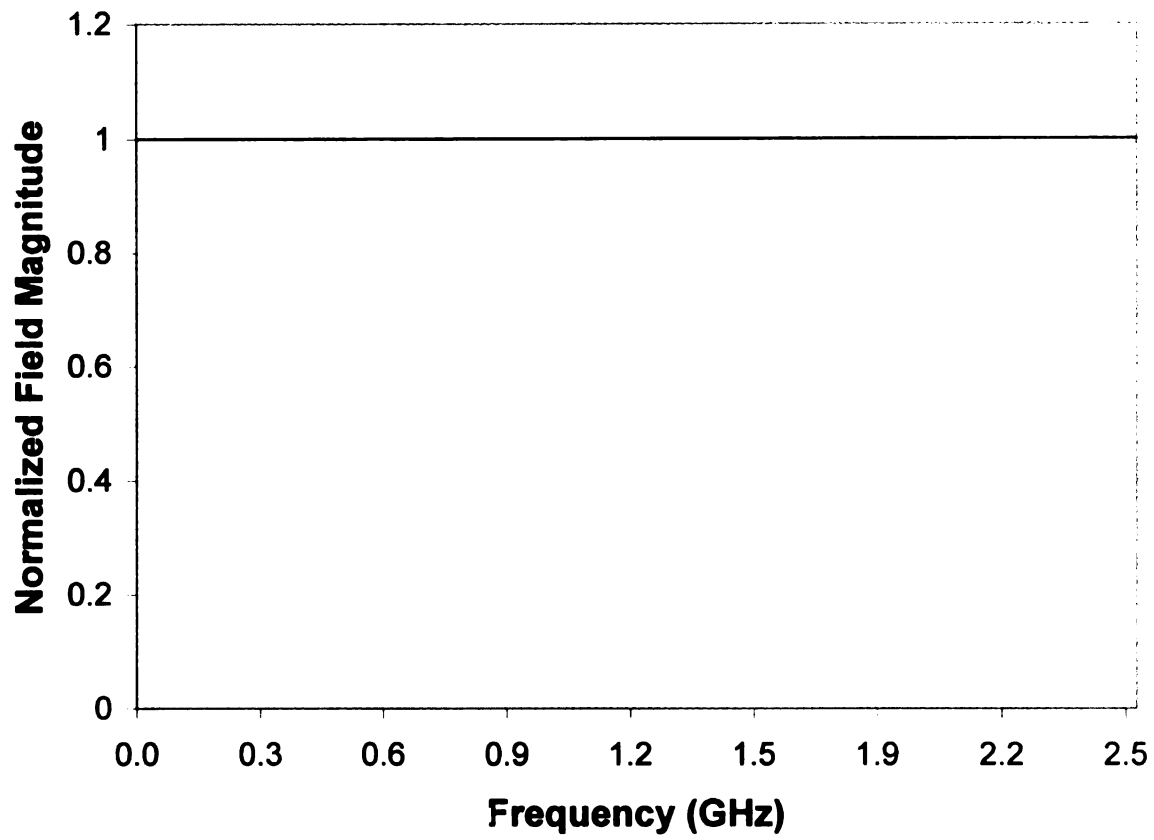


Figure 4.1. Flat case normalized field magnitude vs. frequency with $d = .1$ m, $\epsilon_r = 9$, $\mu_r = 1$

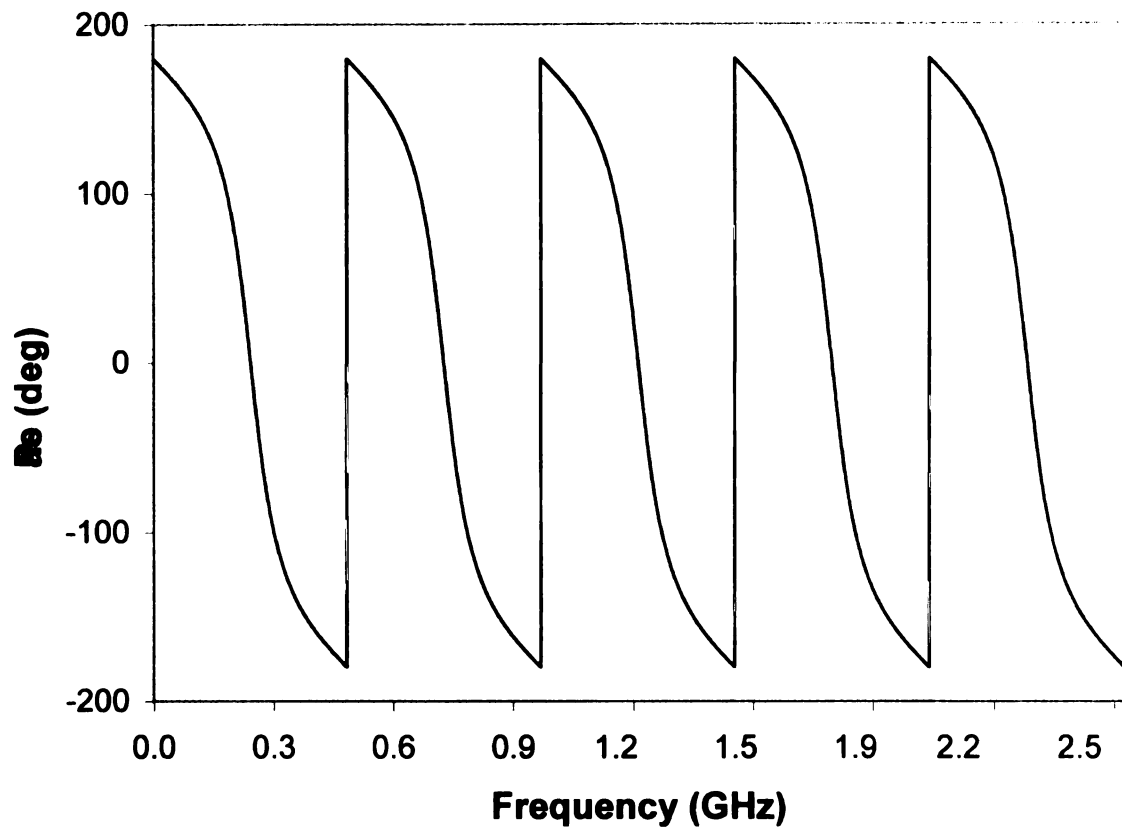


Figure 4.2. Flat case phase vs. frequency with $d = .1$ m, $\epsilon_r = 9$, $\mu_r = 1$

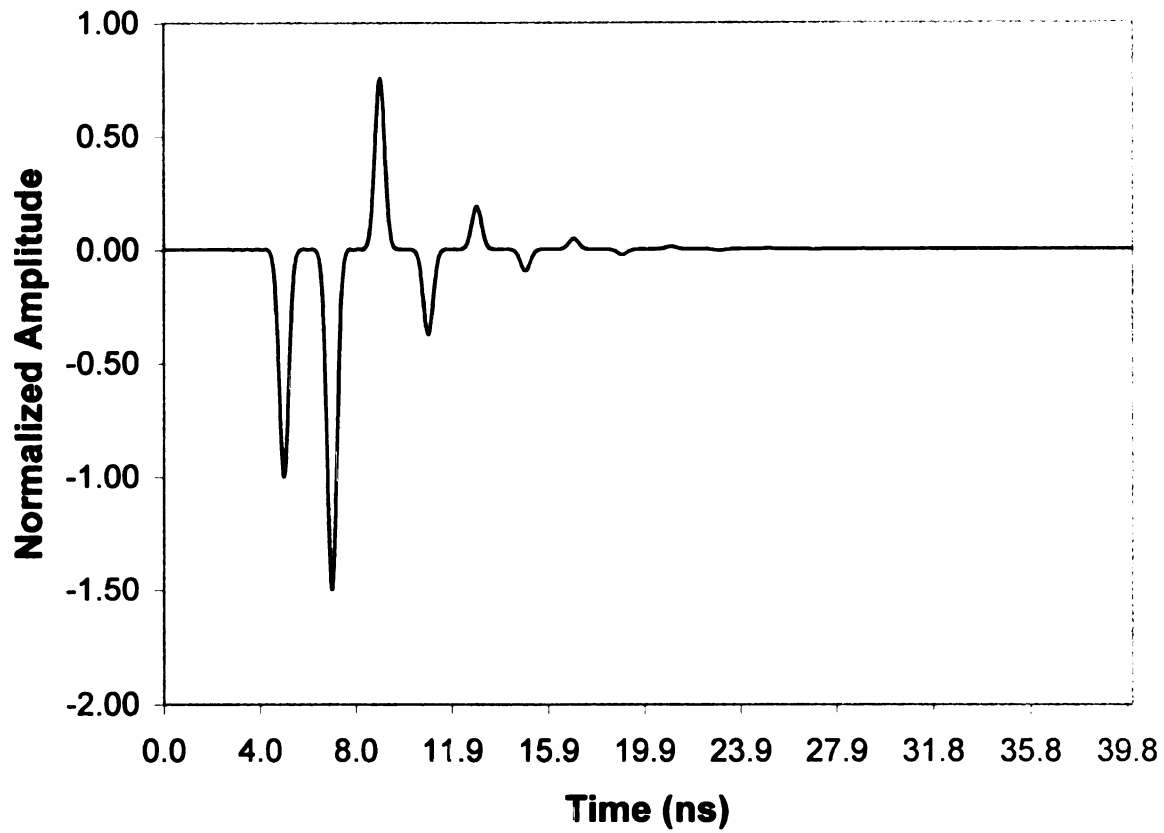


Figure 4.3. Flat case normalized amplitude vs. time with $d = .1$ m, $\epsilon_r = 9$, $\mu_r = 1$

4.3 Circular Case

One way to check to see if the equations for the scattered electric field are derived correctly is to compare the C_n terms of the elliptical case to the circular case. The circular special case occurs when the major axis and minor axis are equal in length. Since in Heike Vollmer's thesis [10], the circular case data was already calculated, the elliptical case formulas can be setup to match those of the circular case. The equations (3.56) and (3.133) for the TMz case and the TEz case, respectively are used for comparison with the C_n term from Heike Vollmer's thesis. As shown in sections 3.2 and 3.4, the C_n are the same. Data is calculated using the elliptical case with the major and minor axes set to the chosen radius of the circular case are found to be identical to the data shown in Heike Vollmer's thesis.

4.4 Echo Width of Elliptical Metallic Core

Another way to check that the scattered electric field equations are derived correctly is to calculate the two dimensional radar cross section or echo width of the uncoated elliptical cylinder [5]. At high frequencies, the echo width of a curved surface approaches π times the radius of curvature at the plane-wave contact point. Let $x(\phi)$ and $y(\phi)$ describe points on the surface parameterized by the variable ϕ . Then the radius of curvature is given by the following [12]:

$$R = \frac{((x')^2 + (y')^2)^{3/2}}{x'y'' - y'x''}. \quad (4.8)$$

The x,y coordinates, the first derivative, and the second derivative of x,y coordinates are:

$$x = a_1 \cos \theta \quad y = a_2 \sin \theta \quad (4.9)$$

$$x' = -a_1 \sin \theta \quad y' = a_2 \cos \theta \quad (4.10)$$

$$x'' = -a_1 \cos \theta \quad y'' = -a_2 \sin \theta. \quad (4.11)$$

Substituting into equation (4.7) the formulas for x, y and their derivatives gives:

$$R = \frac{((-a_1 \sin \theta)^2 + (a_2 \cos \theta)^2)^{3/2}}{(-a_1 \sin \theta)(-a_2 \sin \theta) - (-a_1 \cos \theta)(a_2 \cos \theta)}. \quad (4.12)$$

Simplifying the equation for the radius of curvature at any angle yields:

$$R = \frac{((a_1 \sin \theta)^2 + (a_2 \cos \theta)^2)^{3/2}}{a_1 a_2}. \quad (4.13)$$

Along the x-axis where $\theta = 0^\circ$, the radius of curvature is:

$$R = \frac{a_2^3}{a_1 a_2} = \frac{a_2^2}{a_1}. \quad (4.14)$$

Along the y-axis where $\theta = 90^\circ$, the radius of curvature is:

$$R = \frac{a_1^3}{a_1 a_2} = \frac{a_1^2}{a_2} \quad (4.15)$$

The echo width σ of the metallic cylinder can be calculated using the FORTRAN program in Appendices A and B to find the value of E_z^s using $\epsilon_r = 1$ and substituting the value into the definition [2, 11-102]:

$$\sigma = 2\pi \left[\frac{r |E_z^s|^2}{E_0^2} \right]. \quad (4.16)$$

Figure 4.4 shows the echo width found using $a_1 = 1.4$ m and $a_2 = 1.3$ m, with x as the major axis. The radius of curvature with x as the major axis using equation (4.13) is 1.21 m, giving a high-frequency limit to the echo width of 3.79 m. The value of the echo width for $k = 4.0$ 1/m from Figure 4.4 is 3.89 m. Figure 4.5 shows the echo width found using $a_1 = 1.4$ m and $a_2 = 1.45$ m, with y as the major axis. The radius of curvature with y as the major axis found using equation (4.14) is 1.51 m, giving a high-frequency limit to the echo width of 4.72 m. The value of the echo width for $k = 4.0$ 1/m from Figure 4.5 is 4.79 m.

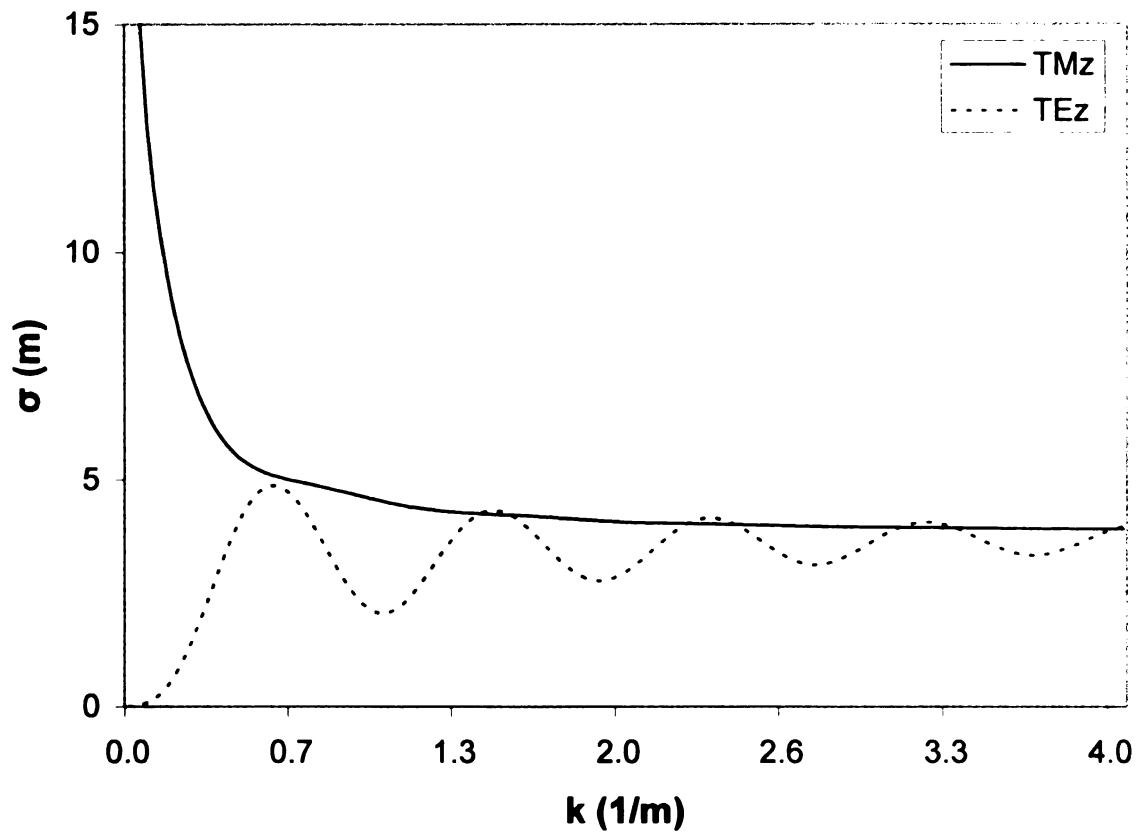


Figure 4.4. Echo width vs wave number, x as major axis, $a_1 = 1.4$ m, $a_2 = 1.3$ m.

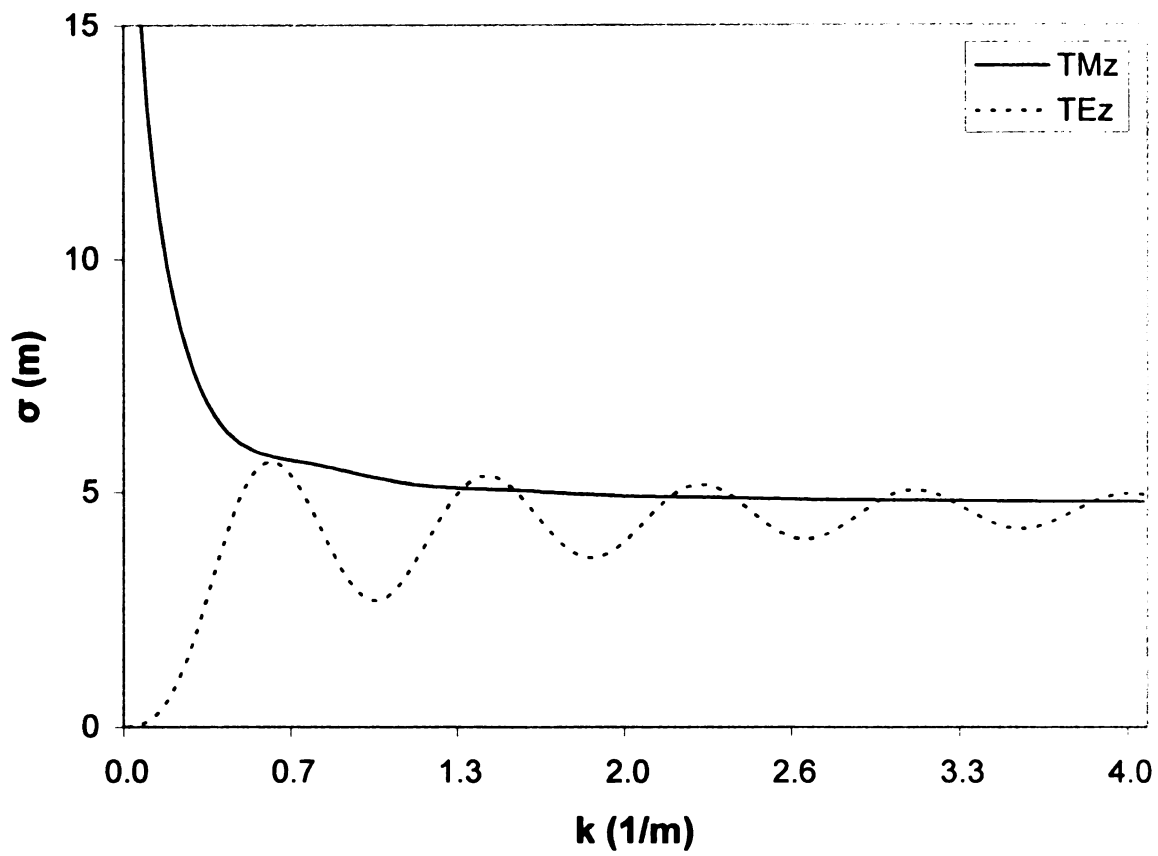


Figure 4.5. Echo width vs wave number, y as major axis, $a_1 = 1.4$ m, $a_2 = 1.45$ m.

CHAPTER 5

Results for the Elliptical Case

5.1 Frequency Response

The frequency domain plots of the TMz and the TEz cases are created using either the x axis or the y axis as the major axis. The major axis that is chosen greatly affects the results of the numerical calculations as shown in the plots. The TMz and the TEz cases with the same major axis produce a similar result with the largest difference occurring at the lower frequencies. After the results are calculated, magnitudes are normalized by multiplying the data by $\sqrt{r/a}/E_0$, for a normalized field magnitude. The various sizes that are chosen shows the variance of the different cases with a small, medium, and a large radius of the cylinders.

The frequency domain for the TMz cases uses equation (3.51) for the scattered electric field. The C_n term is found by solving the matrix equation(3.48). The FORTRAN software used to calculate the frequency domain data in appendix A. For the TEz case, the scattered electric field is given by equation (3.125). The C_n term for the TEz case is the matrix equation (3.122). The FORTRAN software used calculating the frequency domain data is in appendix B. The dielectric thickness on the x axis is 0.1 m and the dielectric constant, $\epsilon_r = 9$. The number of points on the ellipse is chosen to be 275, since the TMz cases at $a = 2$ m needs that many points

to converge the data. The number of steps for the frequency domain data affects the time needed in the time domain data. The x major axis uses 500 steps for the frequency domain since the wrap around in time domain does not occur. However, with y as the major axis cases, the window in the time domain is not big enough with 500 steps, 2000 steps are needed to have the creeping wave decay out.

The magnitude of the TMz scattered electric field with x as the major axis, in the frequency domain becomes less oscillatory as the radius increases as shown in Figures 5.1, 5.2, and 5.3. Another characteristic shown in all the TMz scattering electric field plots is when the frequency approaches DC, the magnitude goes toward infinity. For the TMz scattered electric field plots with y as the major axis, Figures 5.4, 5.5, and 5.6 shows an increased rate of oscillations as the radius of the cylinder increases. In Figures 5.7, 5.8, and 5.9, the TEz scattered electric field having x as the major axis has a similar shape to the TMz with the same major axis, but the lowest frequencies now approach zero instead of infinity. For the TEz scattered electric field with y as the major axis, the oscillations are occurring at a higher rate than the TMz case as shown in Figures 5.10, 5.11, and 5.12. The phase plot shown in Figure 5.17 is typical of all the phase plots with the major difference being that the slope of the phase is steeper for a larger cylinder radius.

The field scattered by a conducting elliptical cylinder without a dielectric coating is needed to construct difference data. The difference data is created by subtracting the field scattered by the uncoated cylinder from the field scattered by the coated cylinder, and is used for comparison of the results of the E-pulse technique. The two elliptical metallic core plots are shown as typical results for the TMz and the TEz cases in Figures 5.13 and 5.15. In each of these plots, ϵ_r was set to 1.01 to achieve zero coating. The TEz scattered electric field magnitude from the elliptical metallic core have the lowest frequencies approaching zero and at higher frequencies approaching a constant. For the TMz scattered electric field from the

metallic core, the field at the lowest frequencies approaches infinity and the higher frequencies approaching a constant. The magnitude difference shown in Figures 5.14 and 5.16 is typical of the difference data. The TMz difference data no longer goes to infinity as the frequency approaches zero. This result produces a time-domain waveform that is closer to zero between reflections than is the original data. The result of the difference data is converted to the time domain and the time domain data has the E-pulse technique applied. The results of using difference data with the E-pulse technique are explored in the next chapter.

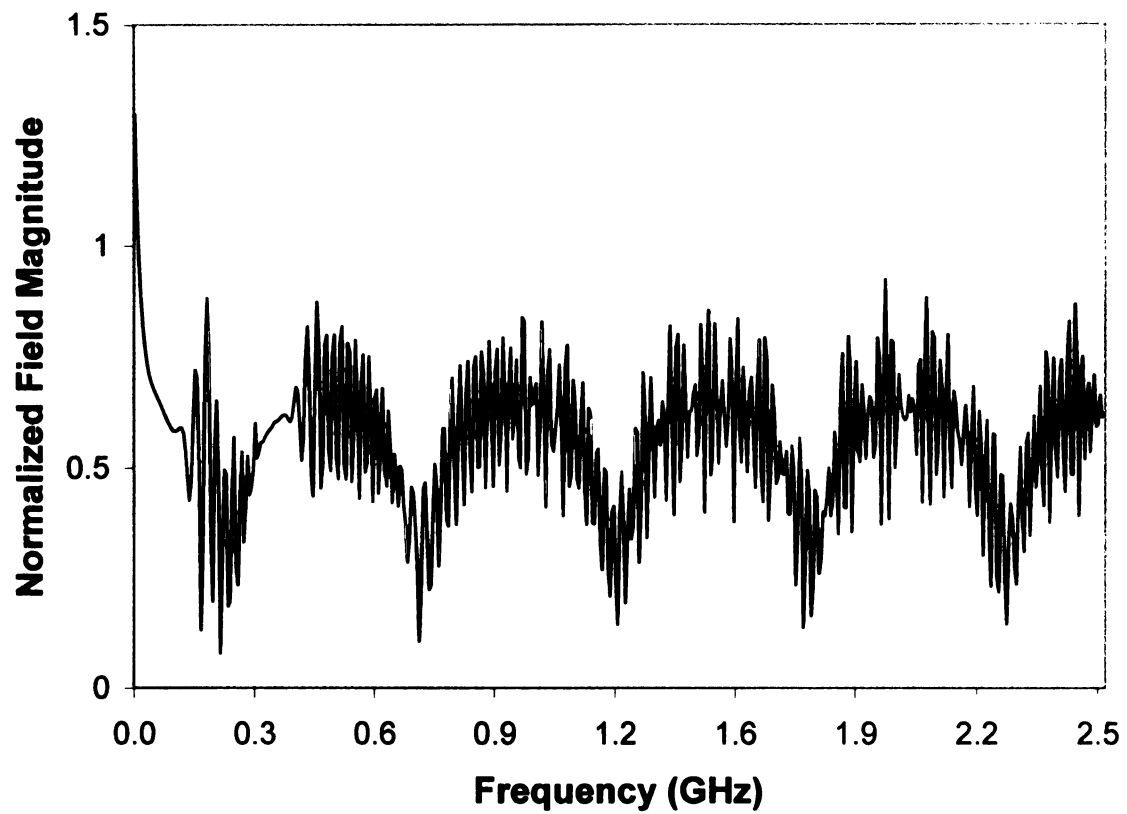


Figure 5.1. TMz normalized field magnitude vs. frequency, $a = .9$ m, $a_1 = .8$ m, $a_2 = .7$ m, with x as the major axis.

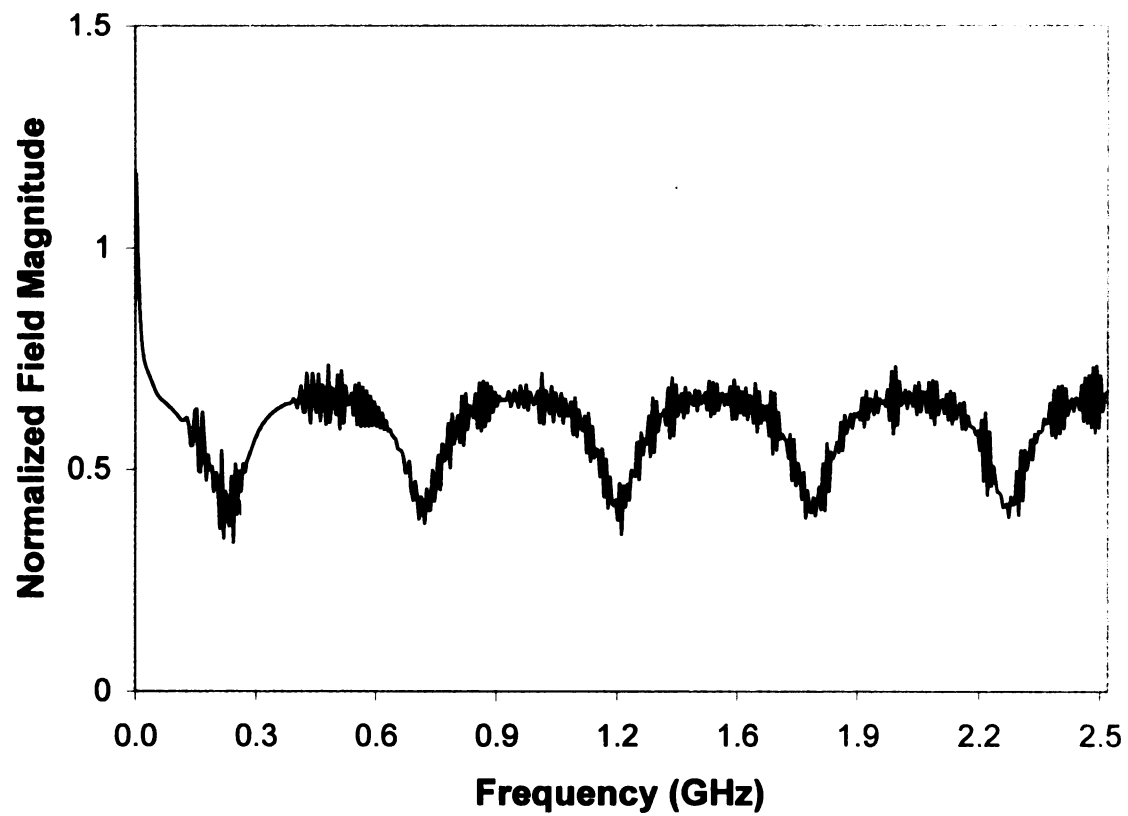


Figure 5.2. TMz normalized field magnitude vs. frequency, $a = 1.5$ m, $a_1 = 1.4$ m, $a_2 = 1.3$ m, with x as the major axis.

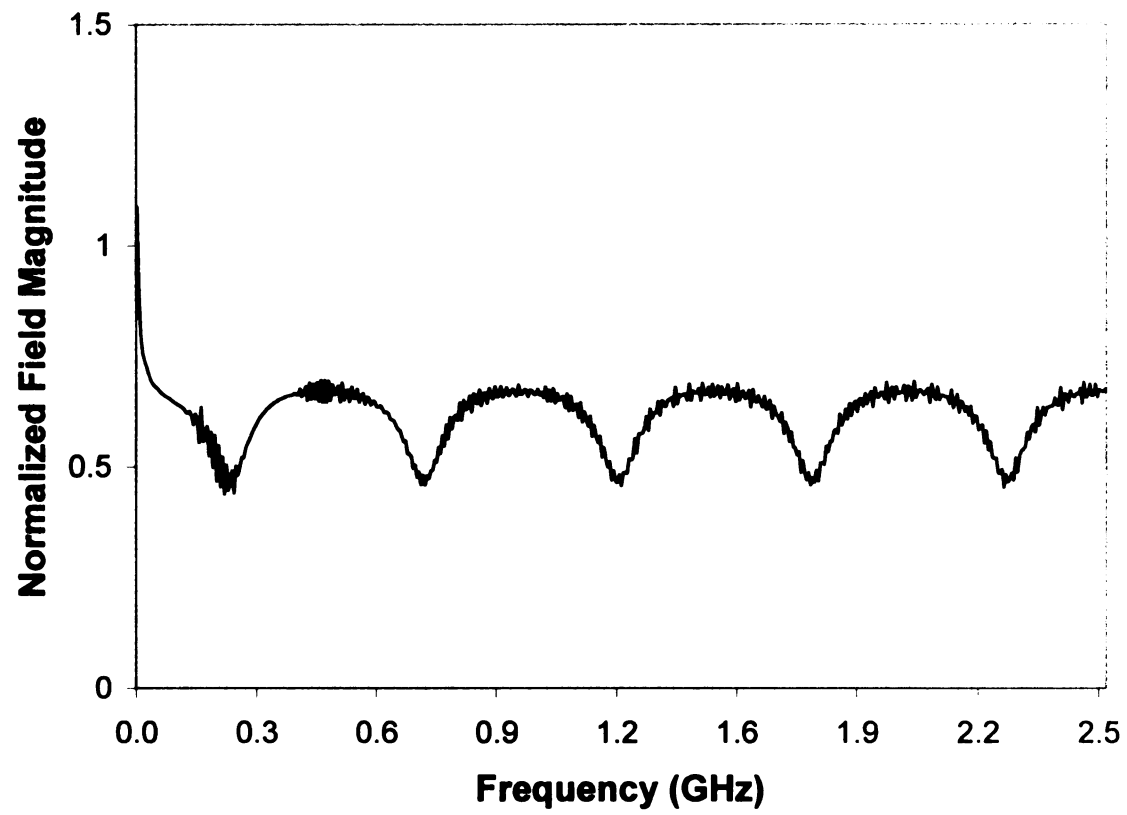


Figure 5.3. TMz normalized field magnitude vs. frequency, $a = 2$ m, $a_1 = 1.9$ m, $a_2 = 1.8$ m, with x as the major axis.

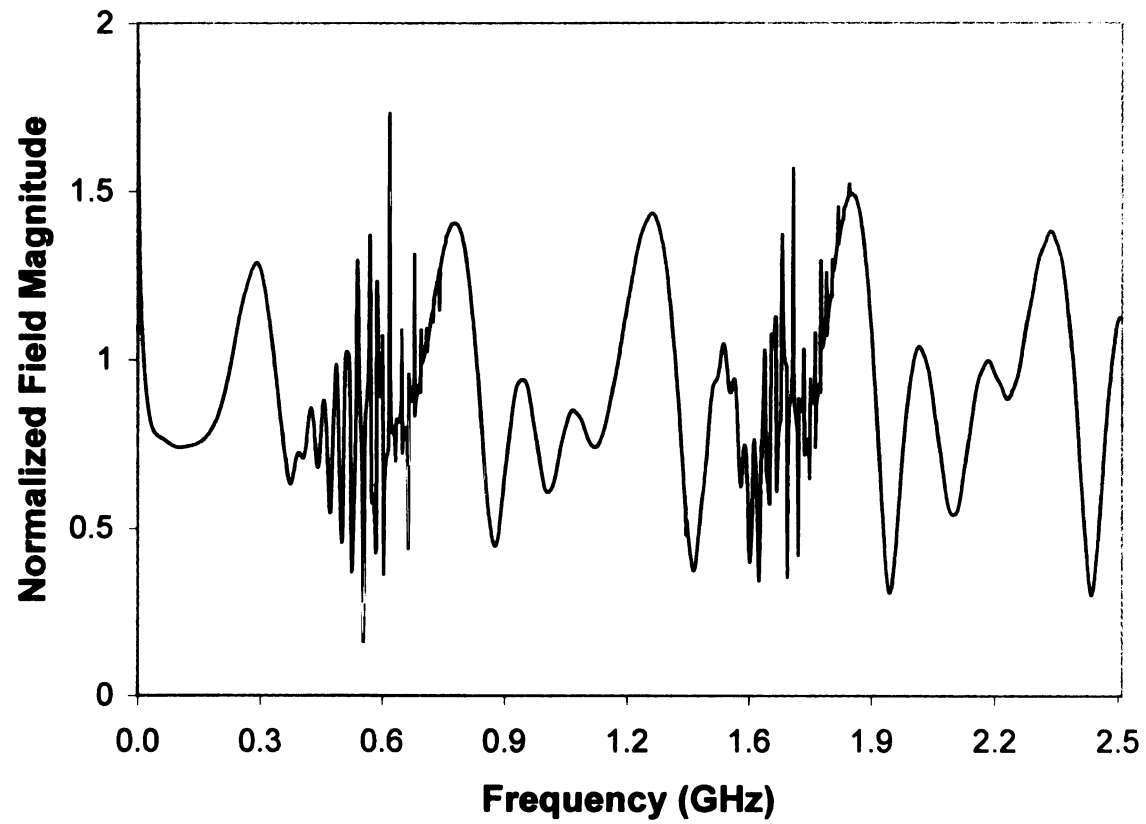


Figure 5.4. TMz normalized field magnitude vs. frequency, $a = .9$ m, $a_1 = .8$ m, $a_2 = .85$ m, with y as the major axis.

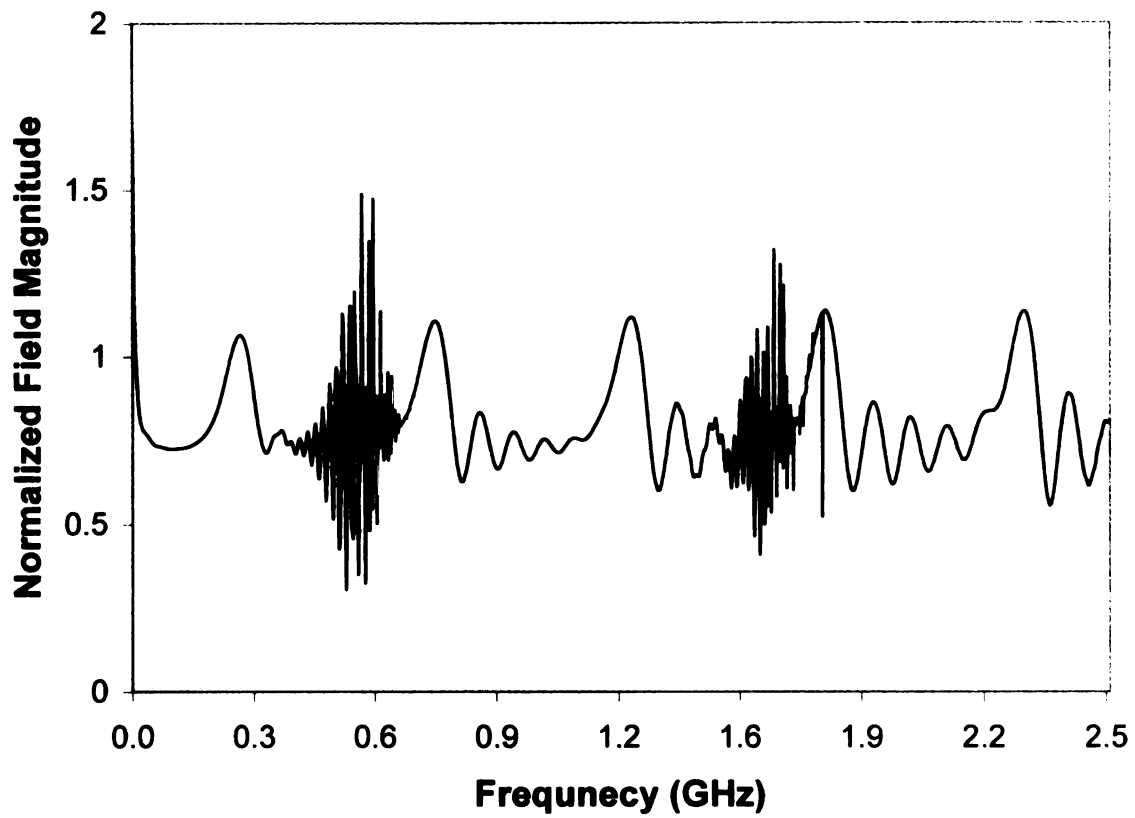


Figure 5.5. TMz normalized field magnitude vs. frequency, $a = 1.5$ m, $a_1 = 1.4$ m, $a_2 = 1.45$ m, with y as the major axis.

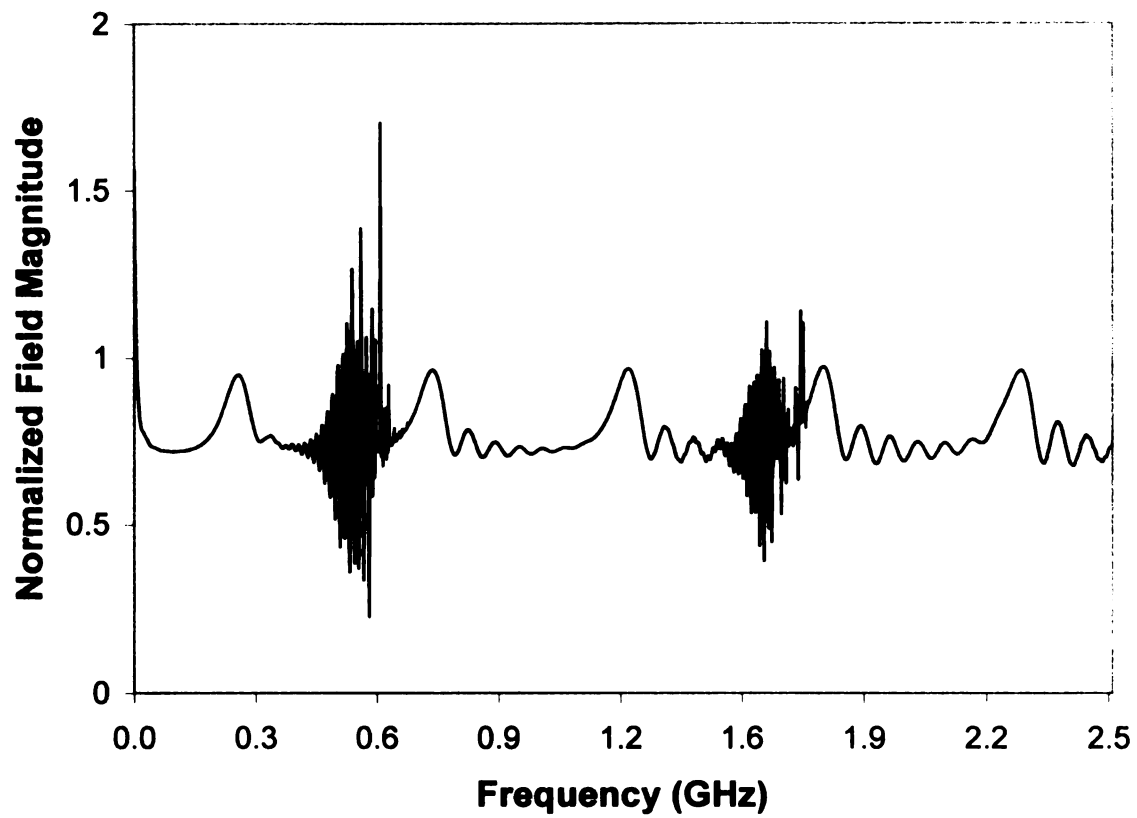


Figure 5.6. TMz normalized field magnitude vs. frequency. $a = 2$ m, $a_1 = 1.9$ m, $a_2 = 1.95$ m, with y as the major axis.

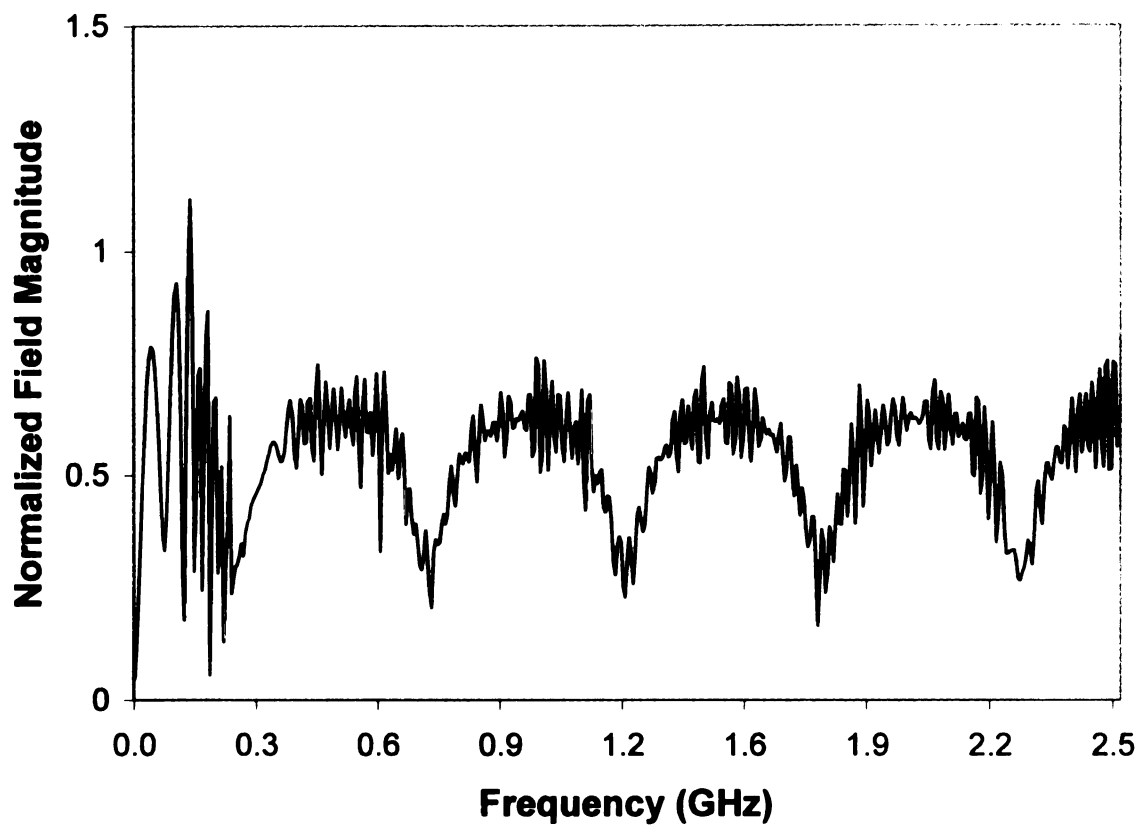


Figure 5.7. TE_z normalized field magnitude vs. frequency, $a = .9$ m, $a_1 = .8$ m, $a_2 = .7$ m, with x as the major axis.

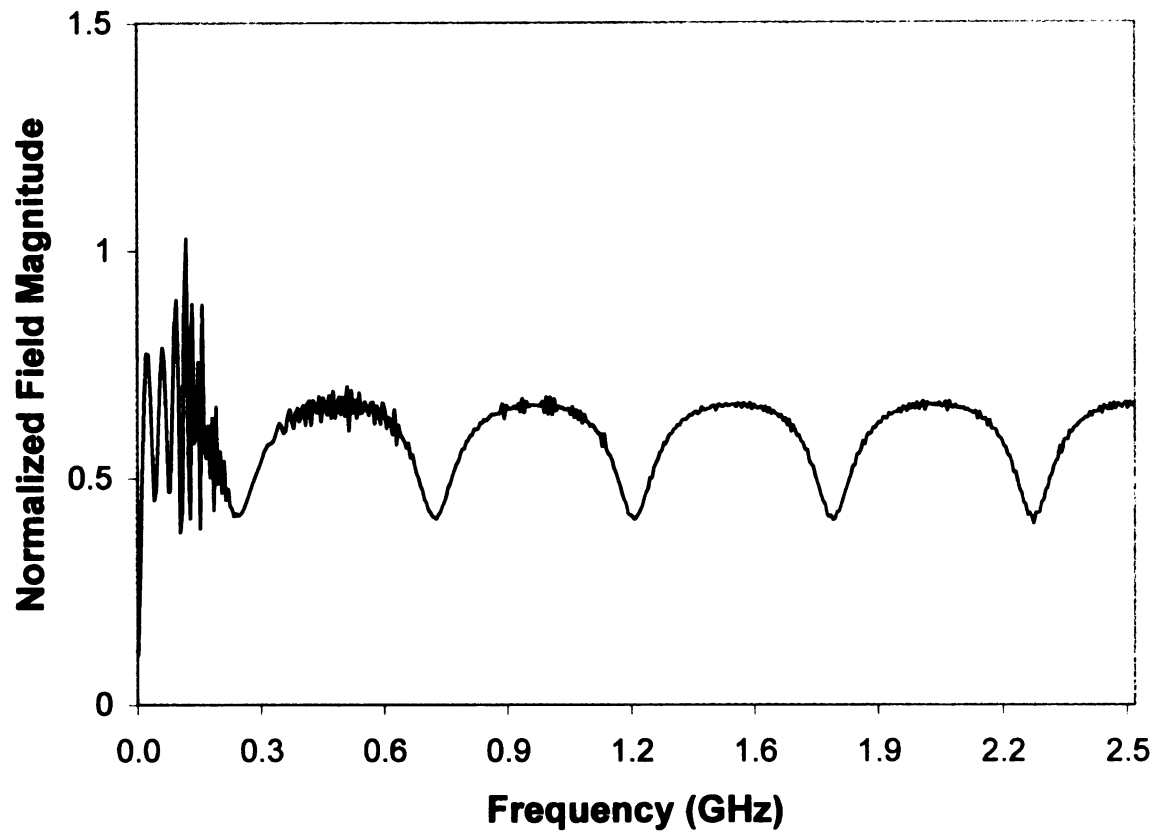


Figure 5.8. TE_z normalized field magnitude vs. frequency, $a = 1.5$ m, $a_1 = 1.4$ m, $a_2 = 1.3$ m, with x as the major axis.

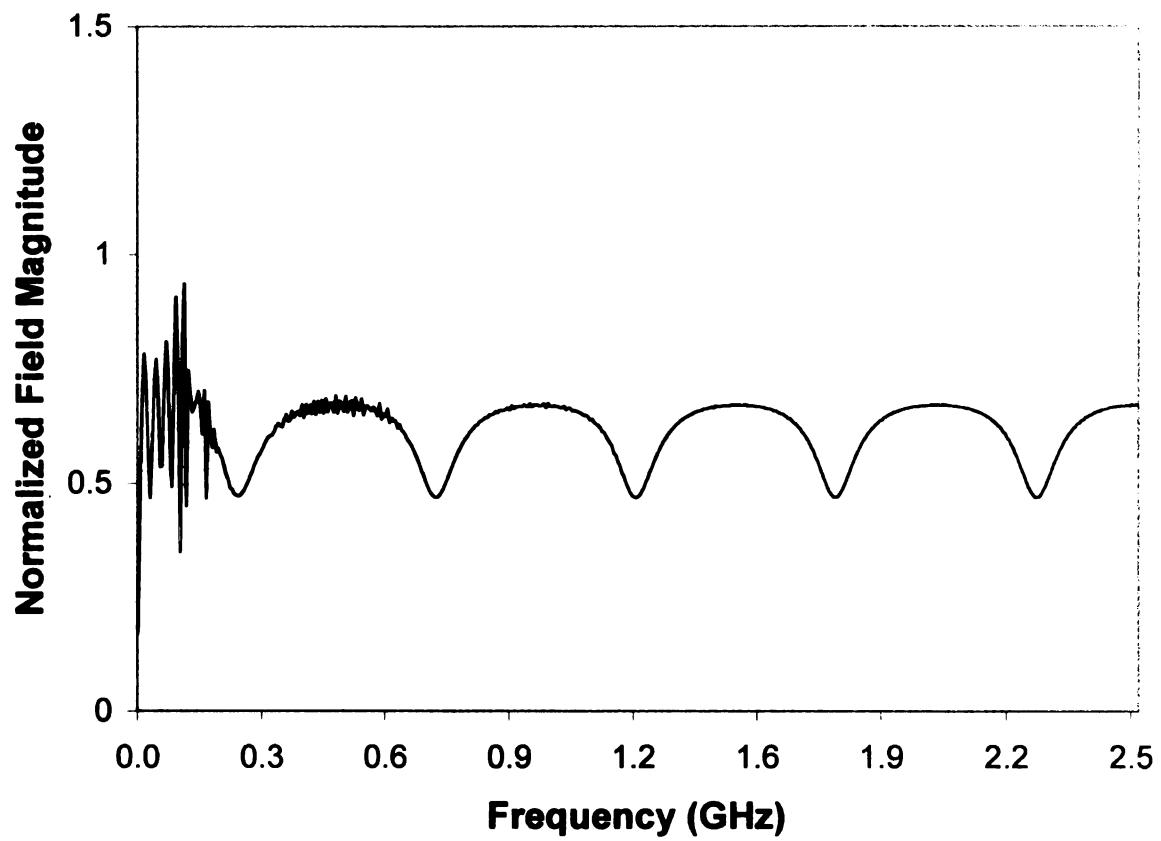


Figure 5.9. TE_z normalized field magnitude vs. frequency, $a = 2$ m, $a_1 = 1.9$ m, $a_2 = 1.8$ m, with x as the major axis.

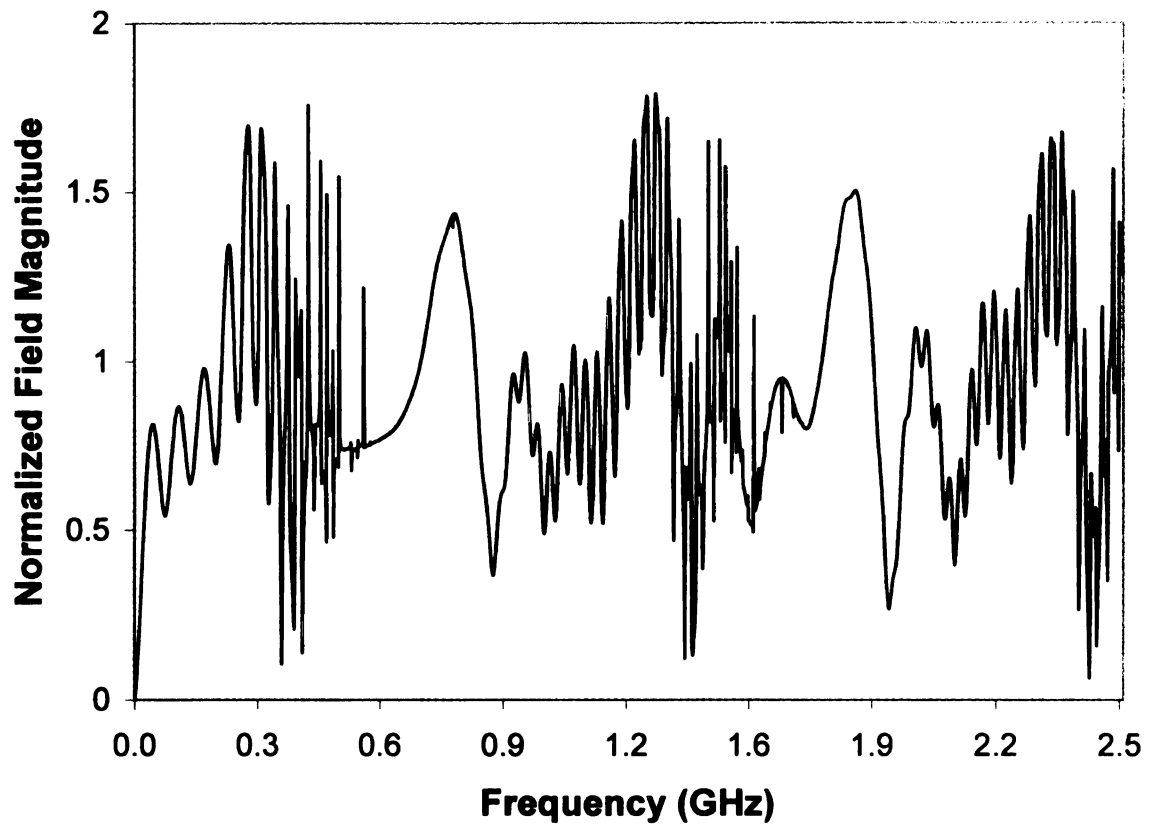


Figure 5.10. TE_z normalized field magnitude vs. frequency, $a = .9$ m, $a_1 = .8$ m, $a_2 = .85$ m, with y as the major axis.

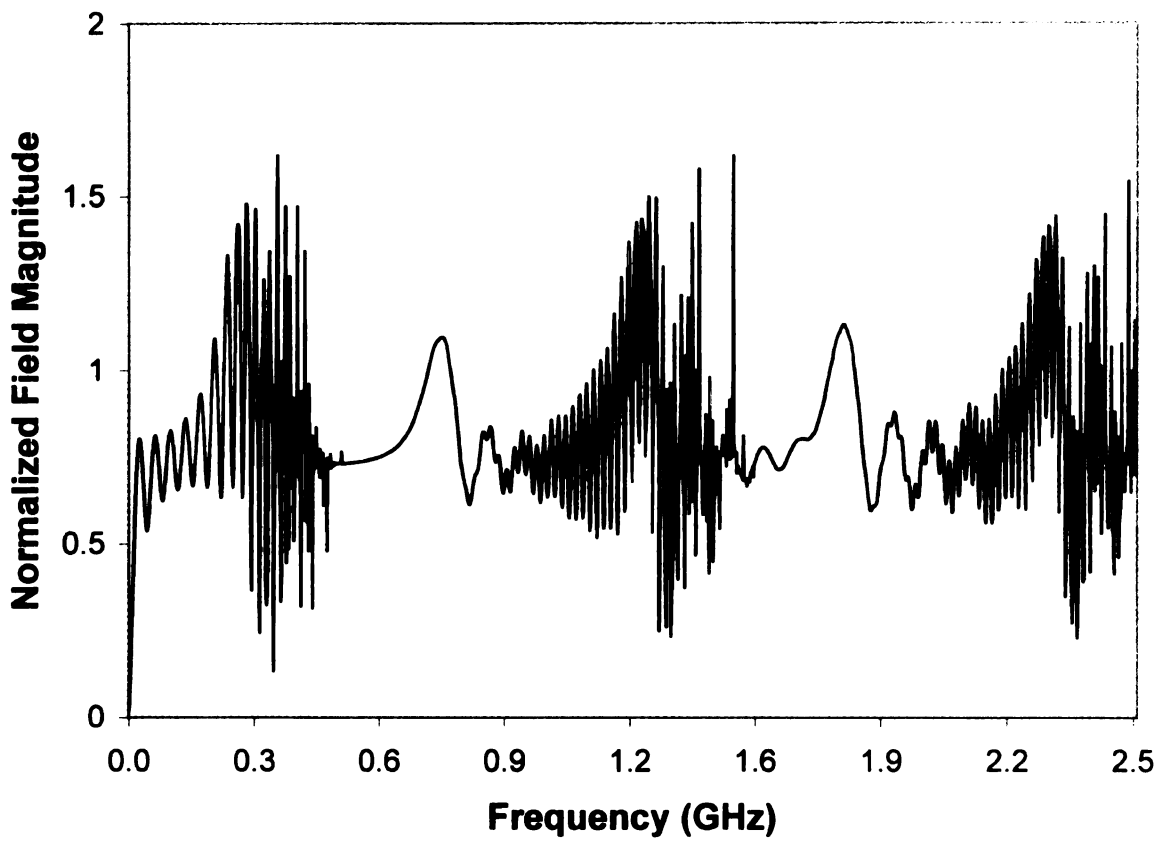


Figure 5.11. TE_z normalized field magnitude vs. frequency, $a = 1.5$ m, $a_1 = 1.4$ m, $a_2 = 1.45$ m, with y as the major axis.

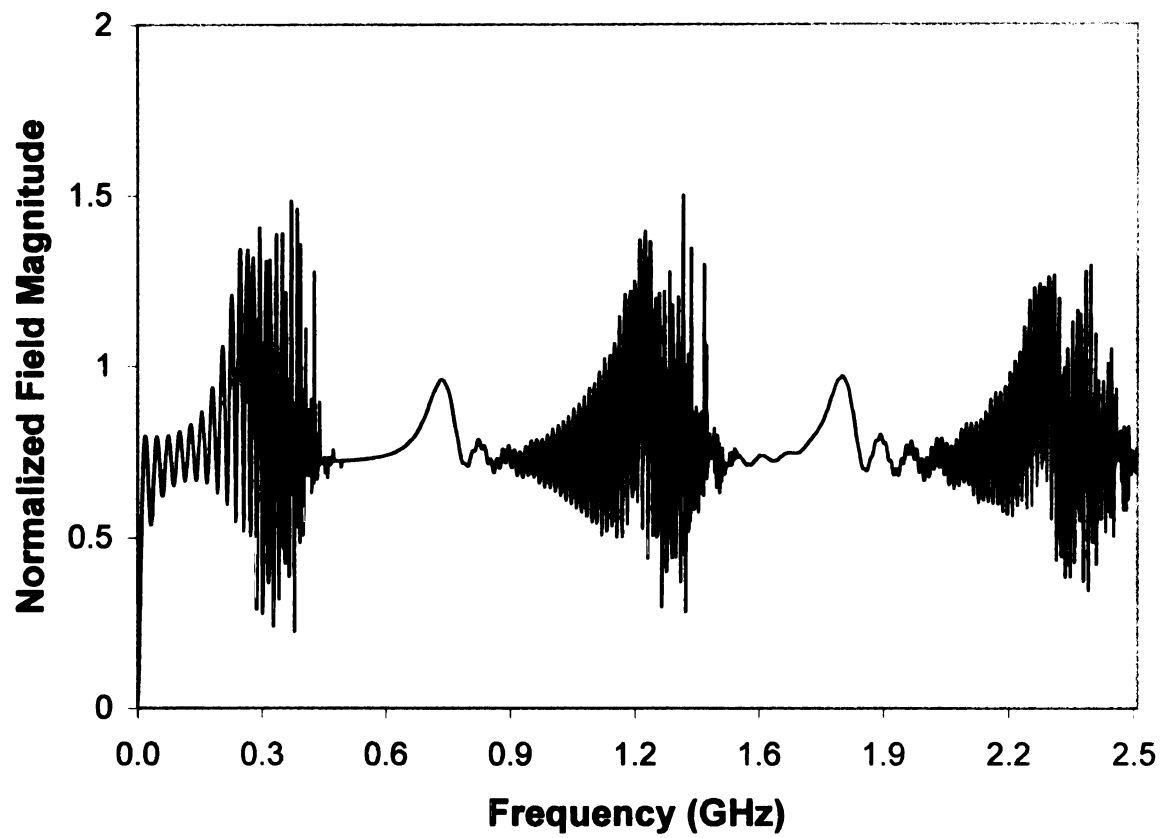


Figure 5.12. TE_z normalized field magnitude vs. frequency, $a = 2$ m, $a_1 = 1.9$ m, $a_2 = 1.95$ m, with y as the major axis.

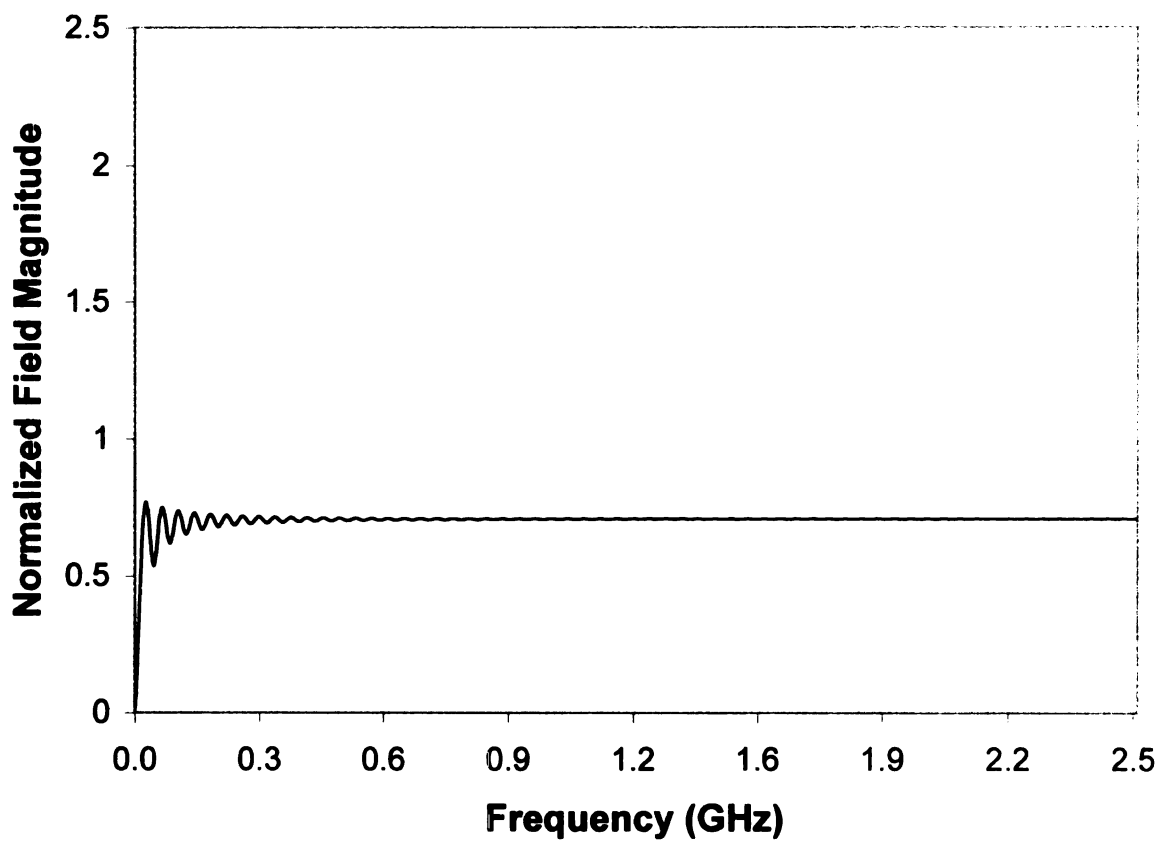


Figure 5.13. TEz normalized field magnitude metallic elliptical cylinder vs. frequency, $a = 1.5$ m, $a_1 = 1.4$ m, $a_2 = 1.45$ m, with y as the major axis.

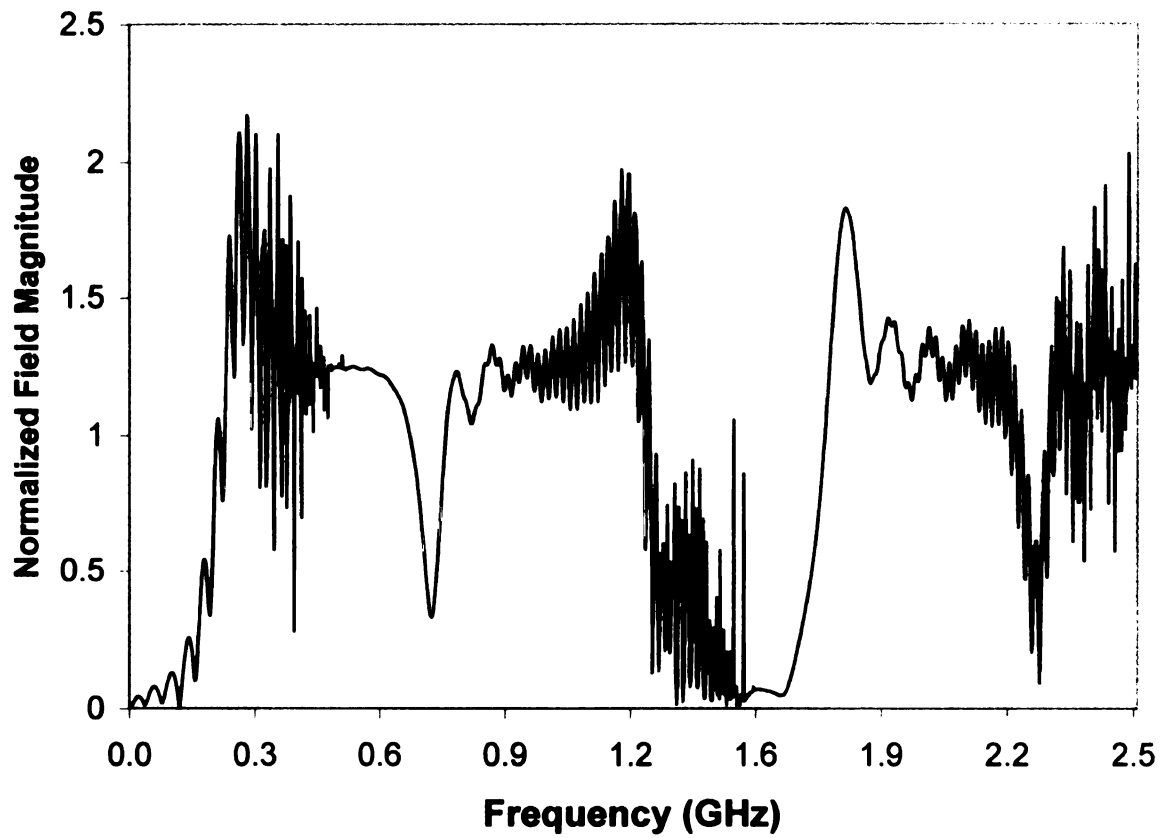


Figure 5.14. TE_z normalized field magnitude with metallic elliptical cylinder subtracted off vs. frequency. $a = 1.5$ m, $a_1 = 1.4$ m, $a_2 = 1.45$ m, with y as the major axis.

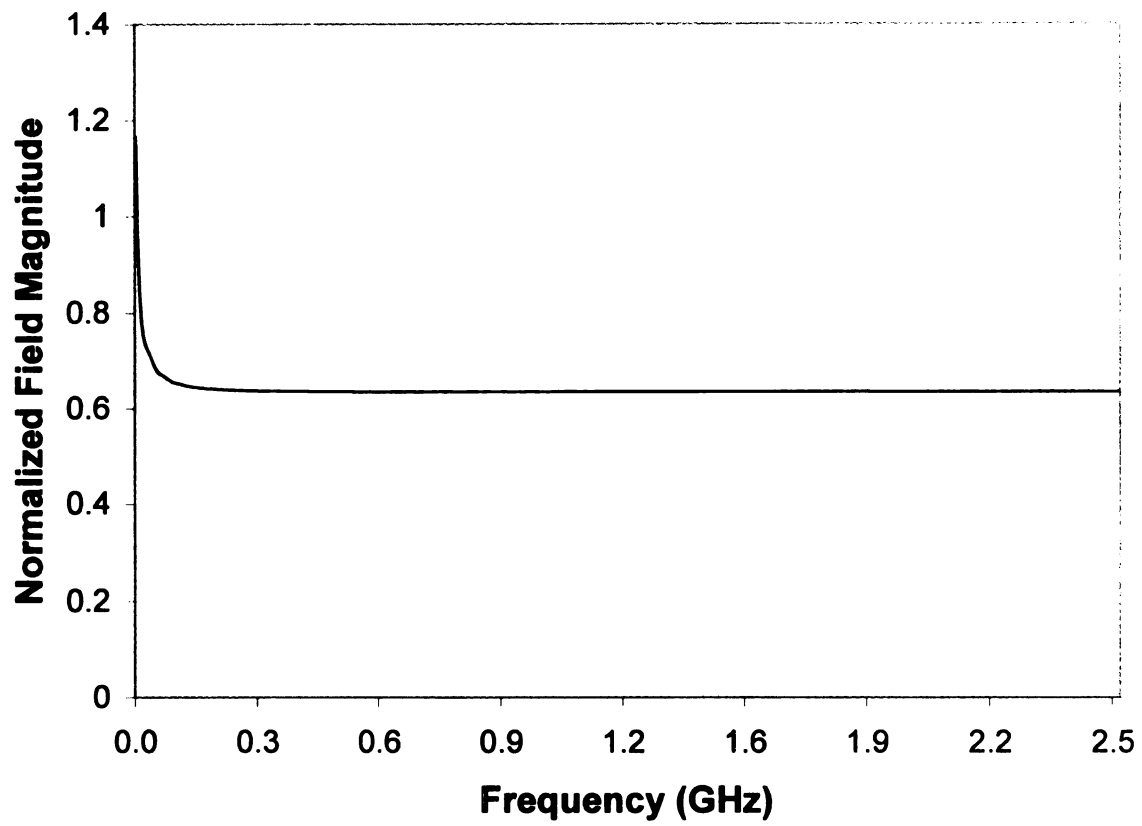


Figure 5.15. TMz normalized field magnitude metallic elliptical cylinder vs. frequency, $a = 1.5$ m, $a_1 = 1.4$ m, $a_2 = 1.3$ m, with x as the major axis.

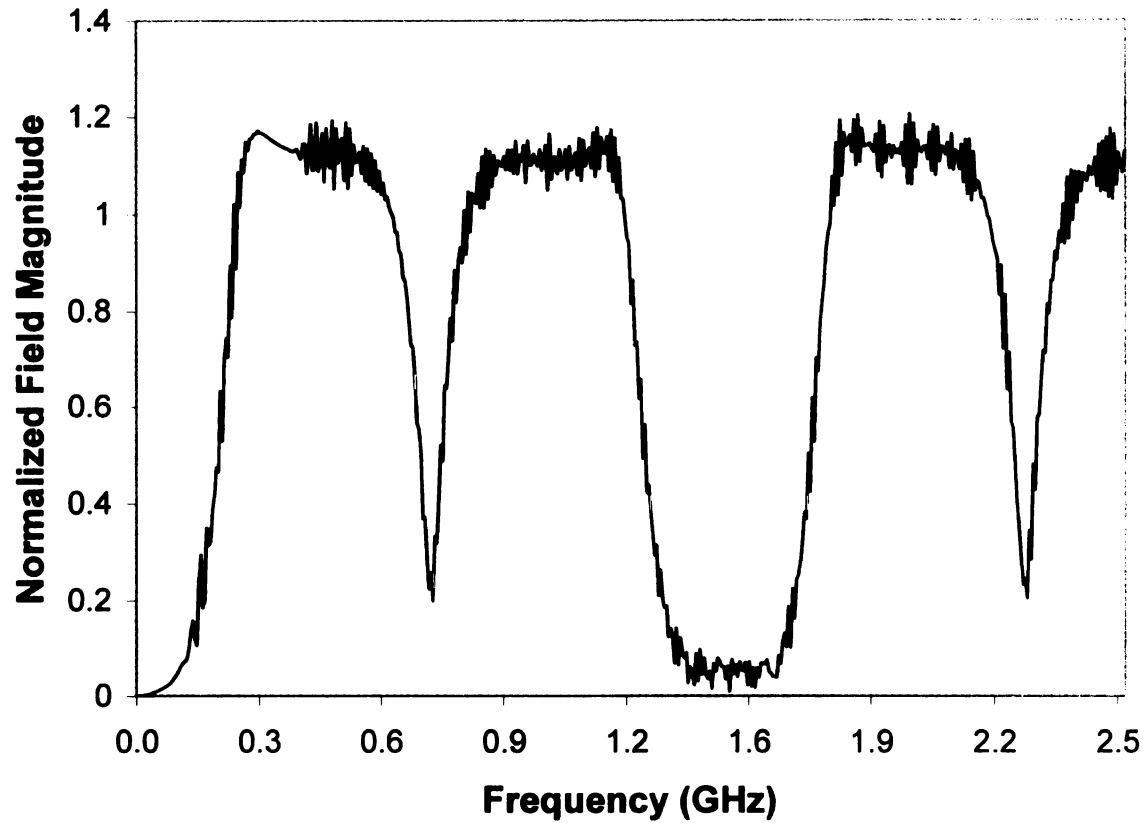


Figure 5.16. TMz normalized field magnitude with metallic elliptical cylinder subtracted off vs. frequency, $a = 1.5$ m, $a_1 = 1.4$ m, $a_2 = 1.3$ m, with x as the major axis.

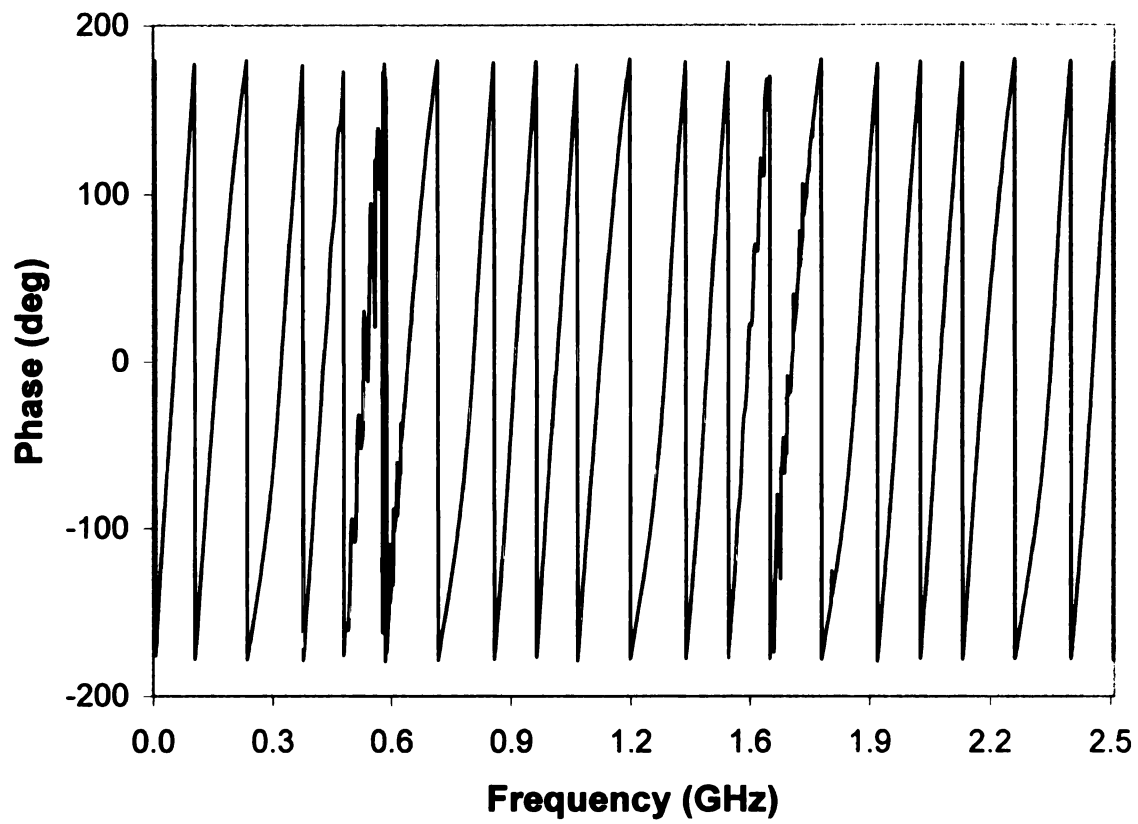


Figure 5.17. TMz phase vs. frequency, $a = 1.5$ m, $a_1 = 1.4$ m, $a_2 = 1.45$ m, with y as the major axis.

5.2 Time Domain Results

Once the frequency domain data has been created, the FFT is applied to get time domain data. The program WaveCalc developed by John Ross (www.johnross.com) has the FFT needed to calculate time domain data. The first step is to apply a gaussian-modulated cosine of $\tau = 0.5$ and centered at zero frequency to weight the frequency domain data properly. The FFT is applied using zero padding to 32768 points and the time domain data is calculated. The next step is to normalize the data with the amplitude of the initial reflection set equal to one, and to time-shift the waveform so that the initial reflections occur at the same time. With this setup, the relative values of the various amplitudes can be compared, and the time origin is set to be at the point where the incident wave is contacting the dielectric material. The succession of pulses seen in the time domain data is explained as a series of multiple reflection as shown in Figures 5.18 and 5.19.

In Figures 5.20, 5.21, 5.22, and 5.23, the data shows the full ranges of time obtain from the FFT for four combinations of orientation and polarization. The TMz case of Figure 5.20 with x as the major axis has the smallest amplitude of the creeping wave for the configurations considered. The TMz case with y as the major axis has a creeping wave that is larger than with x as the major axis. The creeping wave arrives earlier and has a strong repetition lasting longer than the case where x is the major axis. This requires that the data be computed to 800 nanoseconds in order to avoid wrap-around in the FFT. Changing the polarization results in a larger creeping wave for TEz with the x axis as the major axis compared with TMz case with the same major axis. The largest creeping wave occurs with TEz polarization with y as the major axis, as shown in Figure 5.23.

The next set of plots shows the effects of cylinder size on the reflection of the pulse. The TMz case with x as the major axis has the most similar time waveforms

with the two larger outer radii cases almost matching, as shown in Figure 5.24.

Note that the creeping wave for the smallest arise returns earliest, and can be seen in the plot. With y as the major axis for the TMz case, the curves are not a similar as when x is major axis. For the TEz case with x as the major axis, the curves are closer than in the TMz case with the same major axis; however, the creeping wave starts to show up sooner in the smaller outer radii cases as shown in Figure 5.26.

The TEz case with y as the major axis shown in Figure 5.27, has a much greater variance among various outer radii cases, comparably to the TMz case with the same major axis. The creeping wave for the TEz cases arrives earlier in time than for the TMz cases.

The planar surface case is the standard that is used in the E-pulse technique for comparison with the various configurations of the cylinder. The field scattered normally from a planar coated conductor with a dielectric thickness of 0.1 m and a dielectric constant of $\epsilon_r = 9$ is computed using equation (4.1) and compared to the field scattered from the coated cylinder as shown in Figures 5.28 to 5.39. The amplitude of the flat case is normalized so that the amplitude of the initial reflection is the same as in the cylinder case. With $a = .9$ m, all the plots have the creeping wave appearing, since the time needed to travel around the cylinder is less than 40 nanoseconds. The TMz case with $a = .9$ m and x as the major axis has a smaller relative amplitude compared with the flat case as shown in Figure 5.28. The TEz case with x as the major axis and $a = .9$ m, as shown in Figure 5.34, is similar to the TMz case, but the creeping wave is larger in amplitude. For the TMz and TEz cases with y as the major axis and $a = .9$ m relative amplitude of successive pulse is larger than that of flat case as seen in Figures 5.31 and 5.37. For the TEz case, the creeping wave is larger than that of TMz case. With $a = 1.5$ m, the creeping wave is only appearing in the TEz case, since the traversal time needed for the TMz case is longer than 40 nanoseconds. In Figures 5.29 and 5.35, the TEz and TMz cases with

x as the major axis and $a = 1.5$ m, the relative amplitude is still smaller than that of the flat case. For the TE_z and TM_z with y as the major axis and $a = 1.5$ m, relative amplitude is larger than that of the flat case but smaller than when $a = .9$ m as seen in Figures 5.32 and 5.38. When $a = 2$ m, the creeping wave takes longer than 40 nanoseconds, so no creeping wave appears in the plot. For Figures 5.30 and 5.36, the TE_z and TM_z cases have a relative amplitude that is smaller than the flat case, but getting closer to the flat case than with the smaller radii. The TM_z and TE_z case with $a = 2$ m and y as the major axis is larger in amplitude than the flat case as shown in Figures 5.33 and 5.39. In all of these plots it is seen that as the radius of curvature gets bigger, the field scattered from the cylinder gets closer to the field reflected from the planar coated conductor. This suggests that it might be possible to use the E-pulse for the flat case with cylinders of large radius.

A comparison of the difference between the placement of the major axis, as shown in Figures 5.40 and 5.41, shows that the relative amplitude of the field with y as the major axis is greater than that with x as the major axis. This occurs because the y major axis has a greater radius of curvature than that of the x major axis. For the TE_z case, the creeping wave occurs simultaneously, with the y major axis having a larger amplitude than the x major axis as shown in Figure 5.41. The subtraction of the metallic core data from the frequency data results in the time domain having a flatter response at the cost of adding a false peak as shown in Figures 5.42, 5.43, 5.44, and 5.45. With both TM_z cases, the subtracted case is closer to the flat case than that non-subtracted case. For the TE_z cases, subtracting off the metallic core does result in the time domain waveform being flatter than the non-subtracted case. However, the subtracted case results in a larger EDN number than the non-subtracted case, with the results being explored in the next chapter.

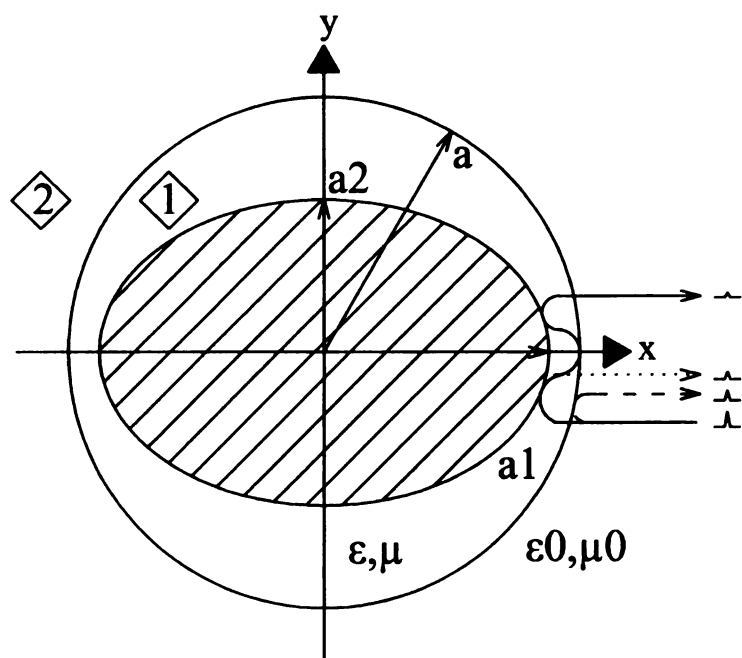


Figure 5.18. The electromagnetic pulse multiple reflections, x is the major axis of the ellipse.

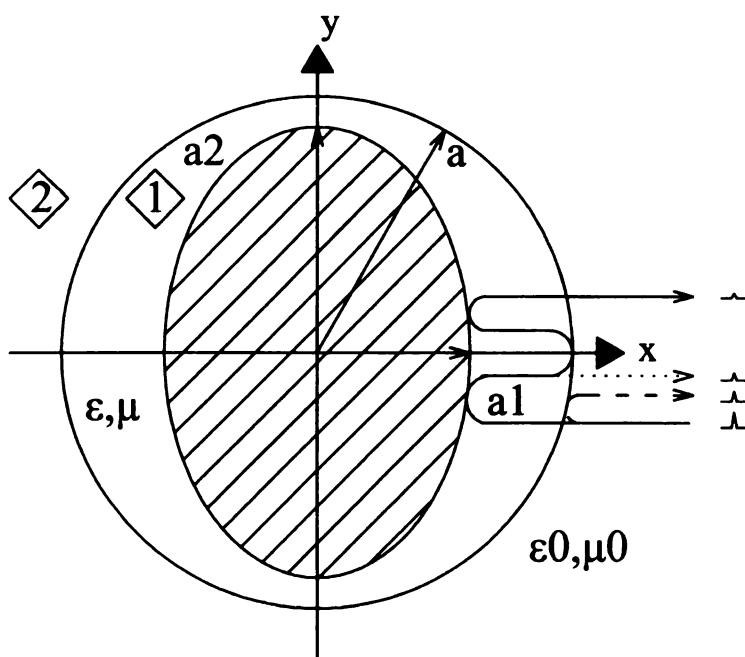


Figure 5.19. The electromagnetic pulse multiple reflection, y is the major axis of the ellipse.

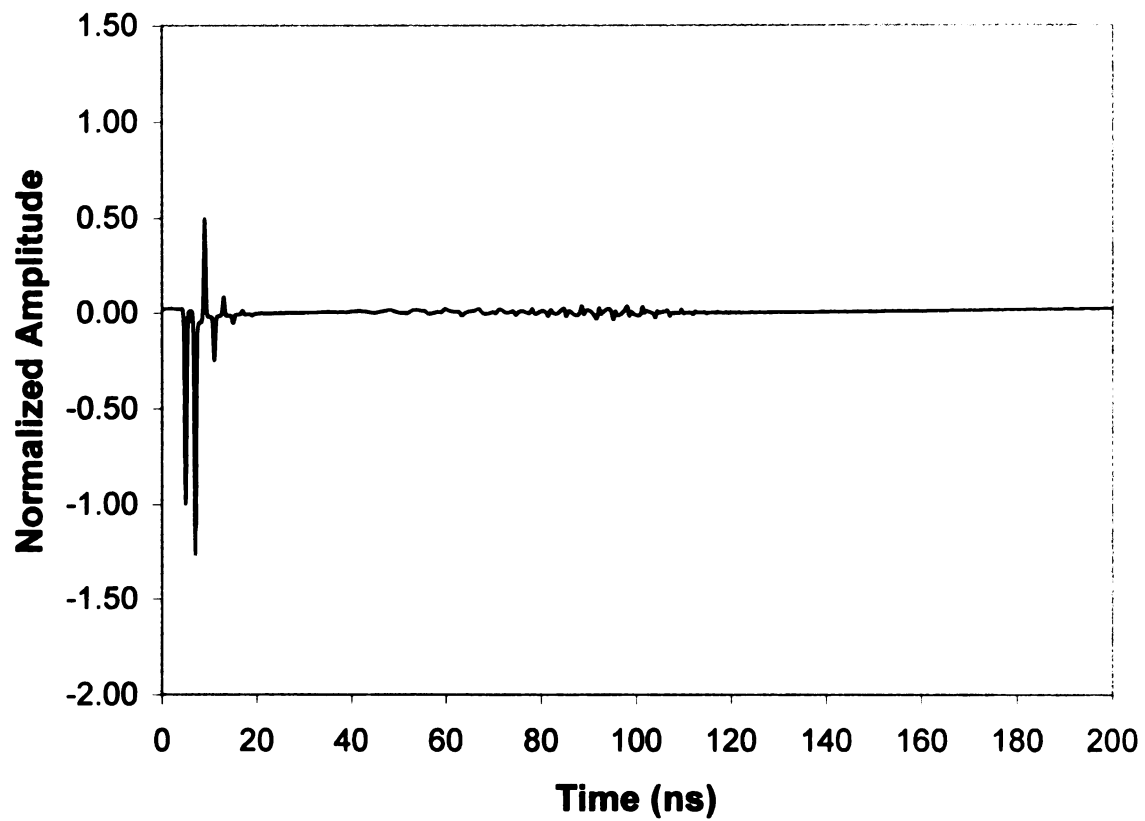


Figure 5.20. TMz normalized amplitude vs. time, $a = 1.5$ m, $a_1 = 1.4$ m, $a_2 = 1.3$ m, with x as the major axis.

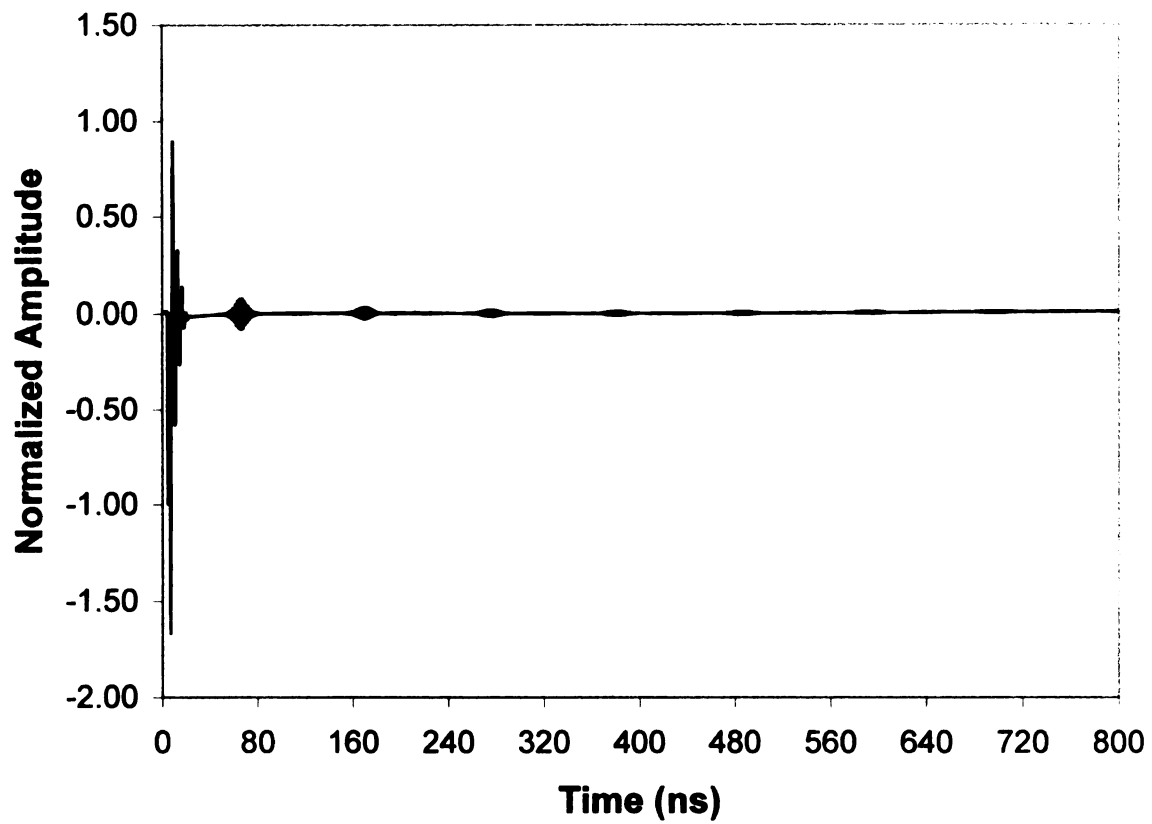


Figure 5.21. TMz normalized amplitude vs. time, $a = 1.5$ m, $a_1 = 1.4$ m, $a_2 = 1.45$ m, with y as the major axis.

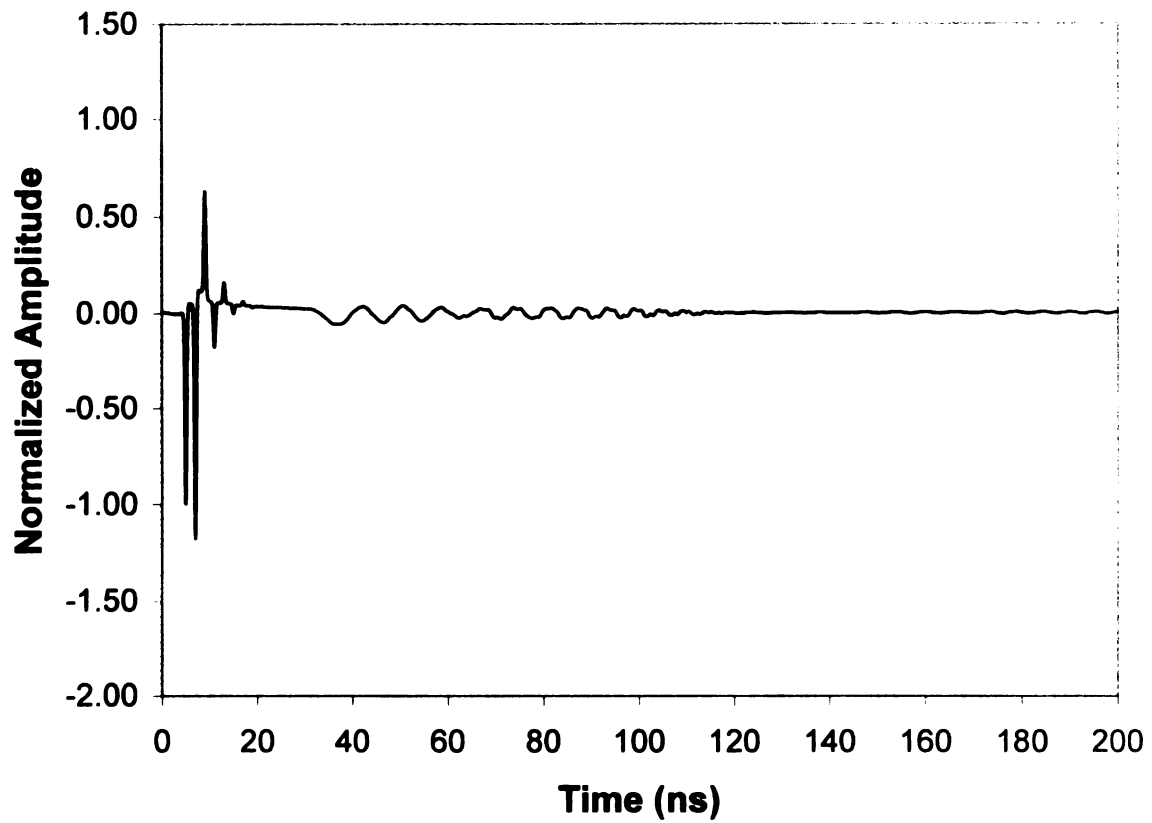


Figure 5.22. TE_z normalized amplitude vs. time, $a = 1.5$ m, $a_1 = 1.4$ m, $a_2 = 1.3$ m, with x as the major axis.

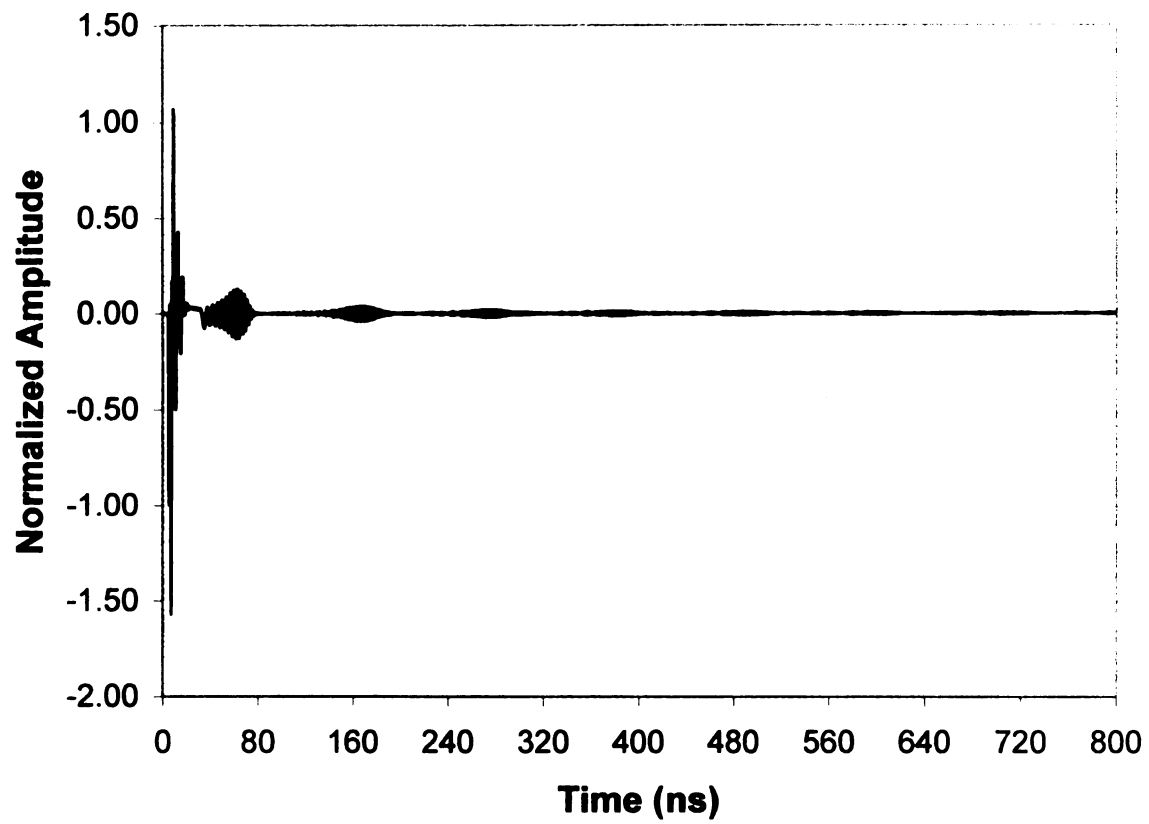


Figure 5.23. TEz normalized amplitude vs. time, $a = 1.5$ m, $a_1 = 1.4$ m, $a_2 = 1.45$ m, and with y as the major axis.

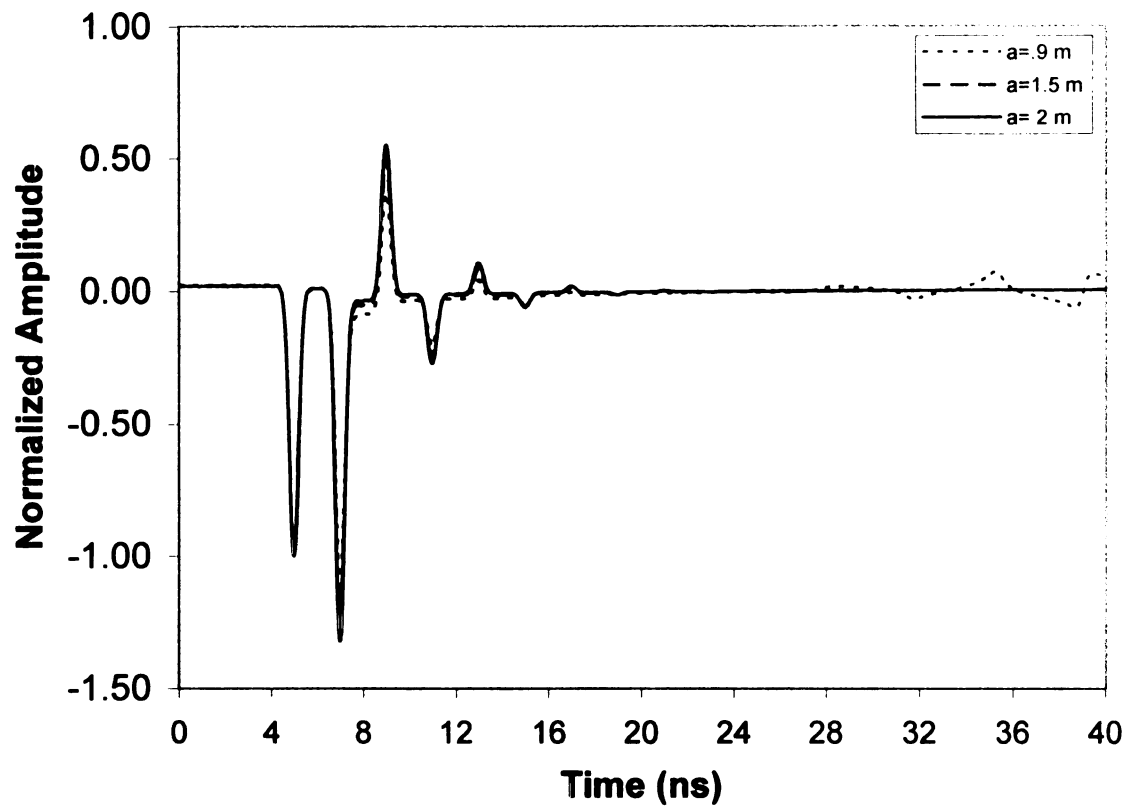


Figure 5.24. TMz normalized amplitude vs. time with $a = .9$ m, 1.5 m, 2 m and with x as the major axis.

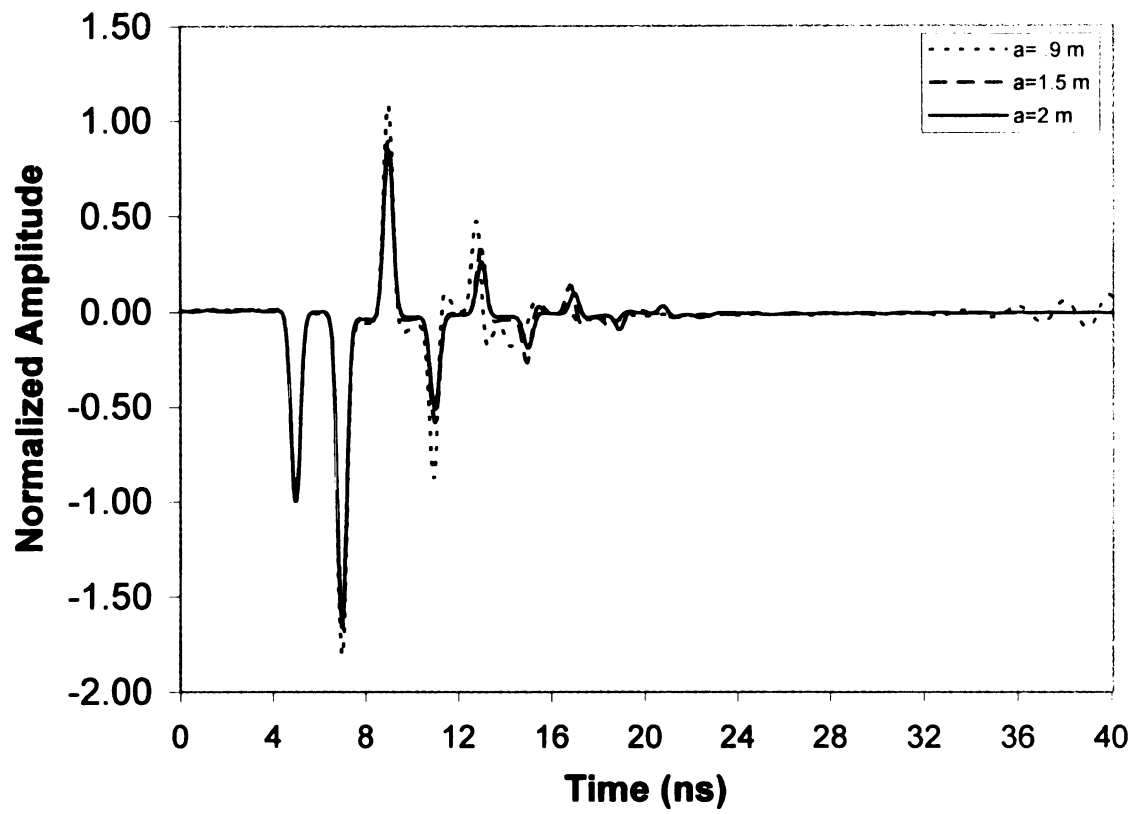


Figure 5.25. TMz normalized amplitude vs. time with $a = .9 \text{ m}$, 1.5 m , 2 m and with y as the major axis.

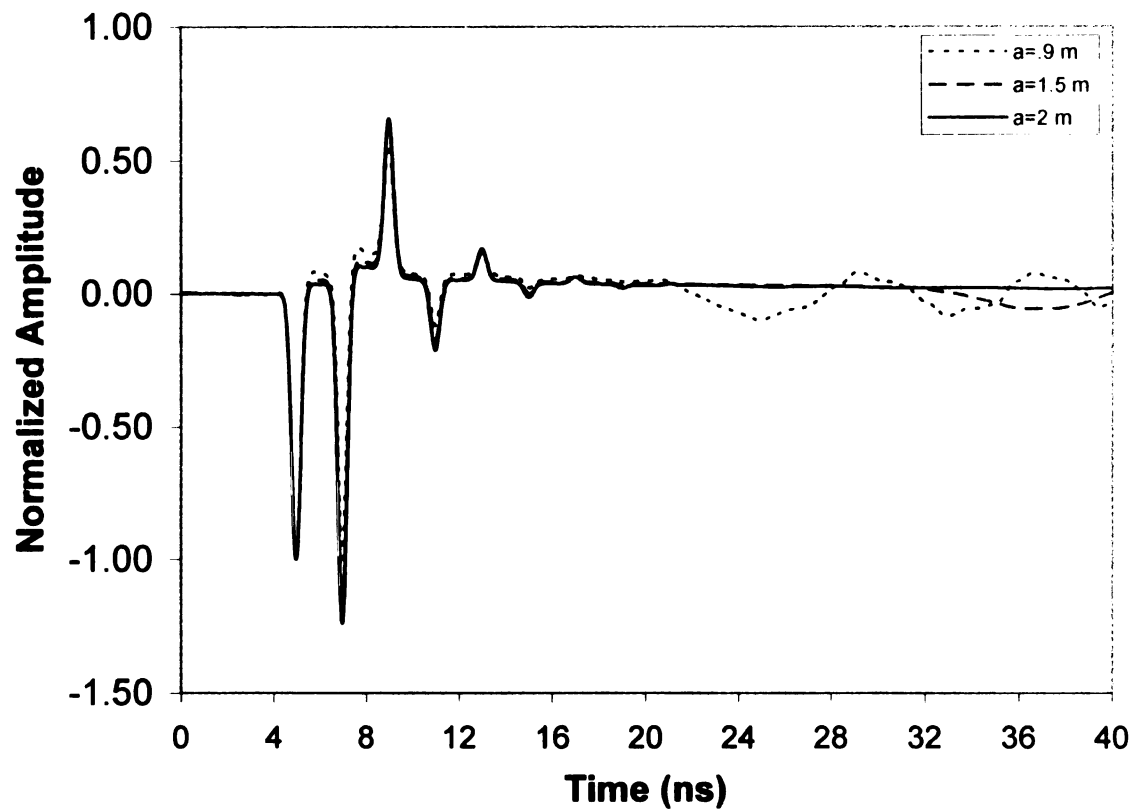


Figure 5.26. TE_z normalized amplitude vs. time with $a = .9$ m, 1.5 m, 2 m and with x as the major axis.

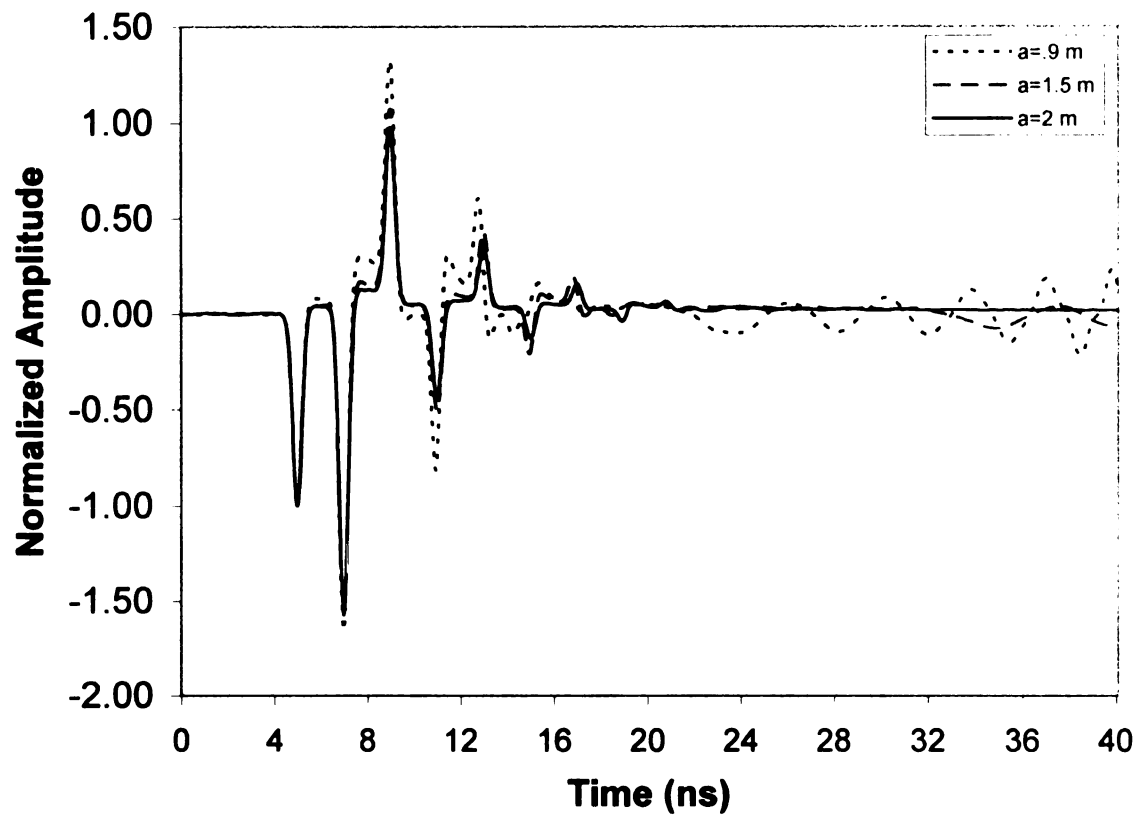


Figure 5.27. TEz normalized amplitude vs. time with $a = .9$ m, 1.5 m, 2 m and with y as the major axis.

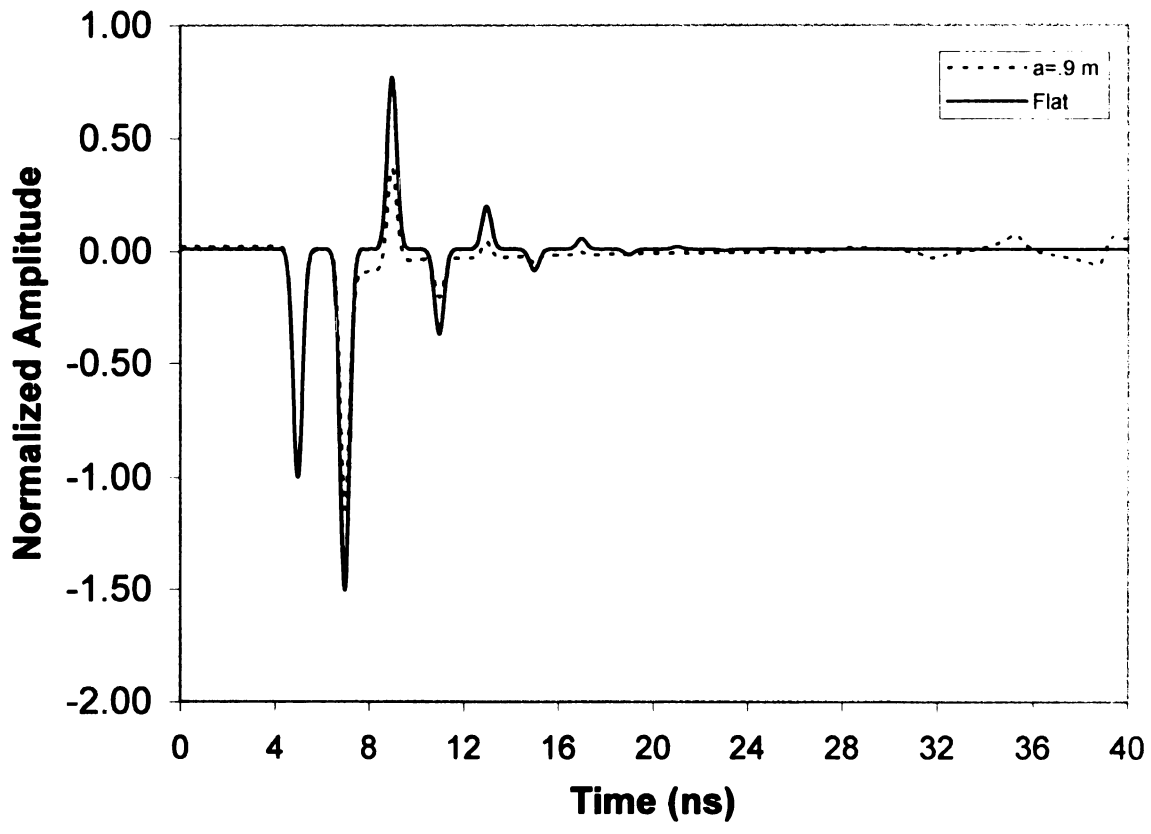


Figure 5.28. TMz normalized amplitude vs. time comparison of flat with $a = .9$ m and with x as the major axis.

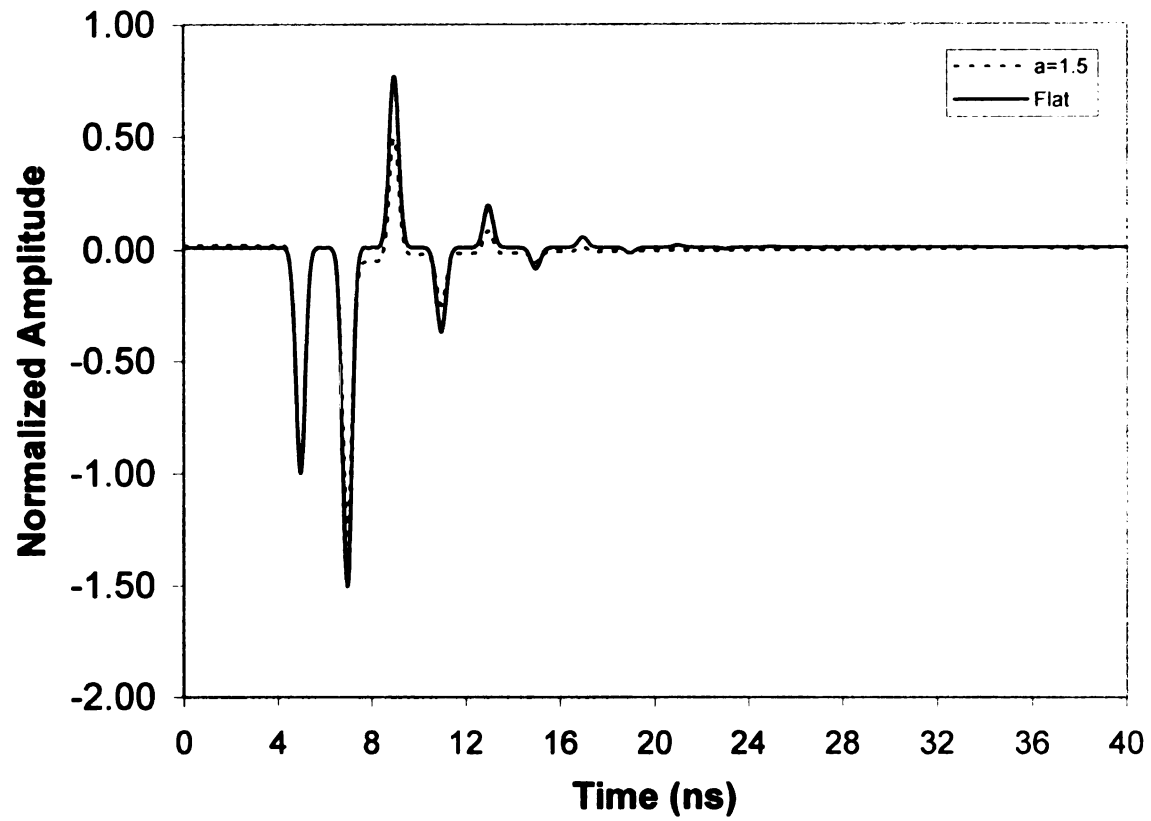


Figure 5.29. TMz normalized amplitude vs. time comparison of flat with $a = 1.5$ m and with x as the major axis.

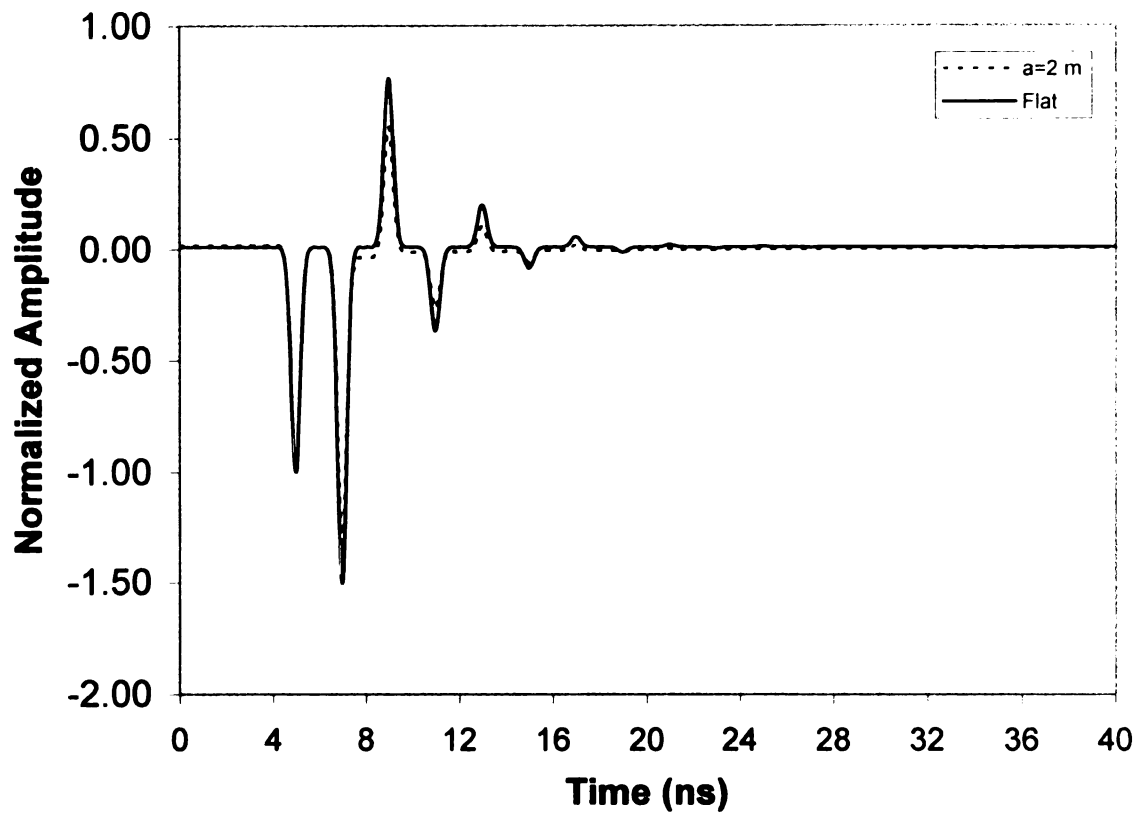


Figure 5.30. TMz normalized amplitude vs. time comparison of flat with $a = 2.0$ m and with x as the major axis.

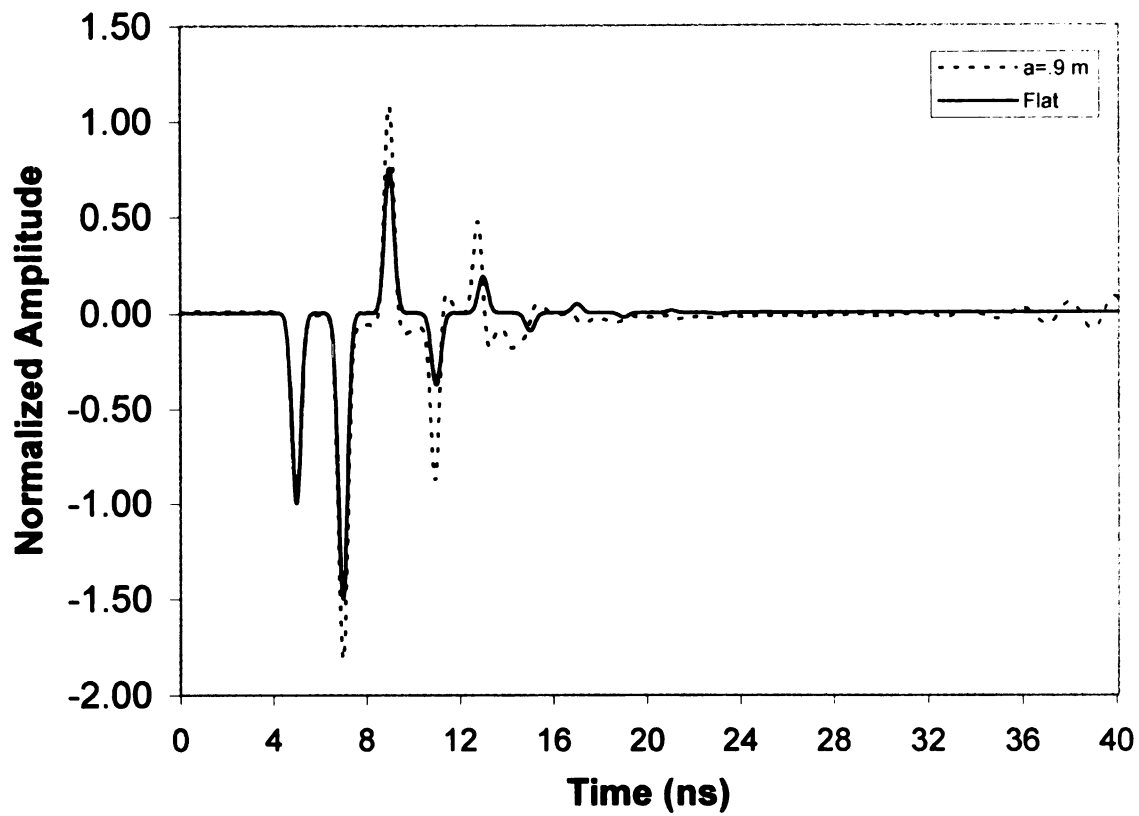


Figure 5.31. TMz normalized amplitude vs. time comparison of flat with $a = .9$ m and with y as the major axis.

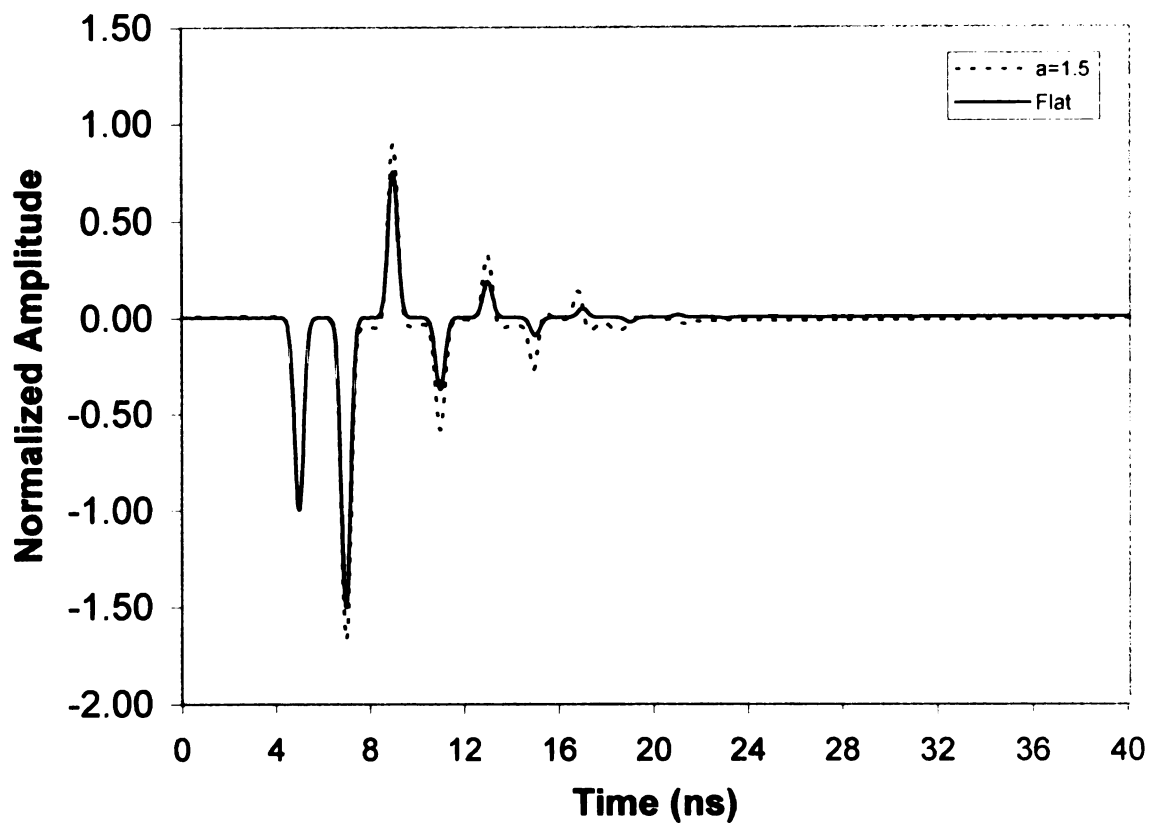


Figure 5.32. TMz normalized amplitude vs. time comparison of flat with $a = 1.5$ m and with y as the major axis.

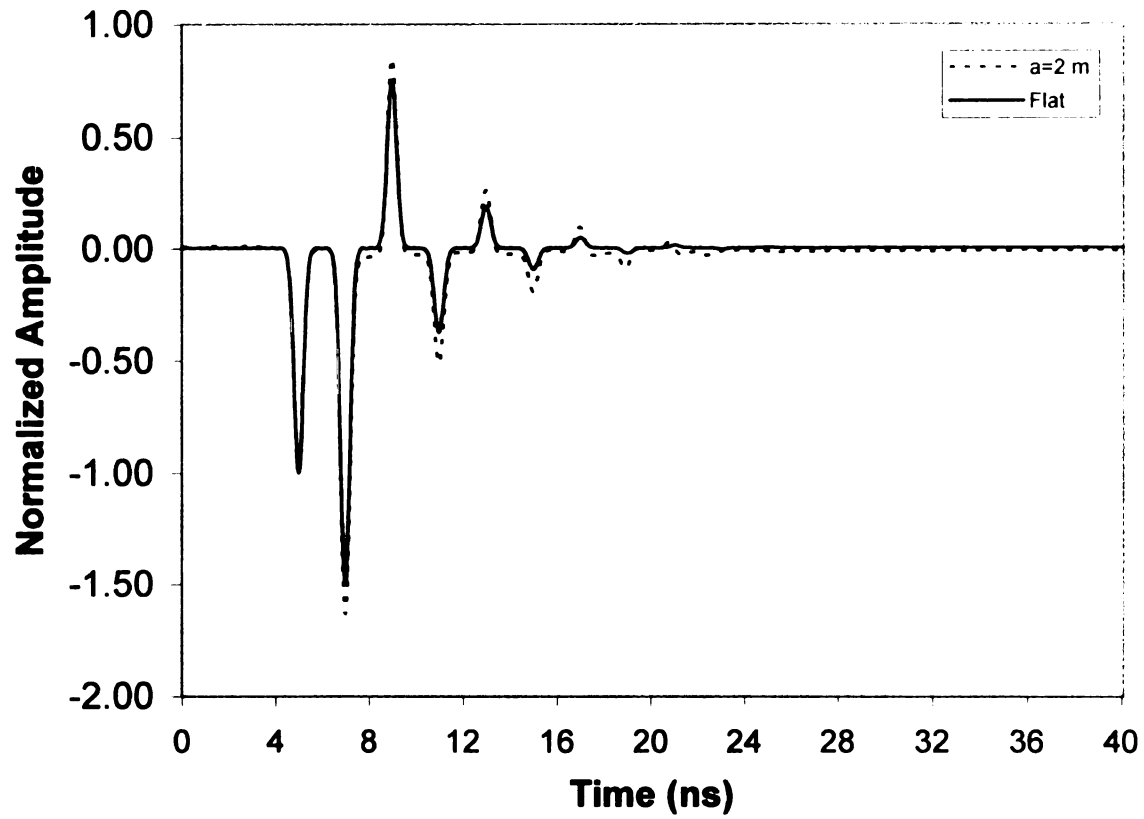


Figure 5.33. TMz normalized amplitude vs. time comparison of flat with $a = 2.0$ m and with y as the major axis.

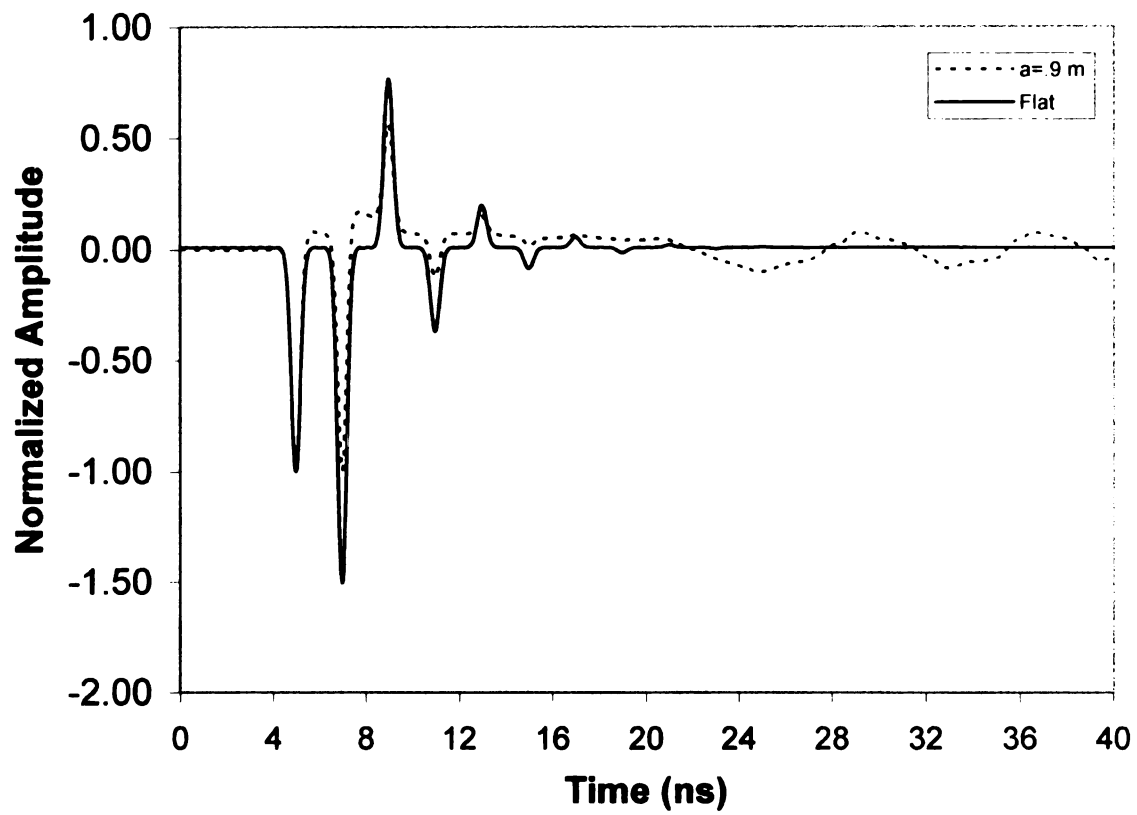


Figure 5.34. TEz normalized amplitude vs. time comparison of flat with $a = .9$ m and with x as the major axis.

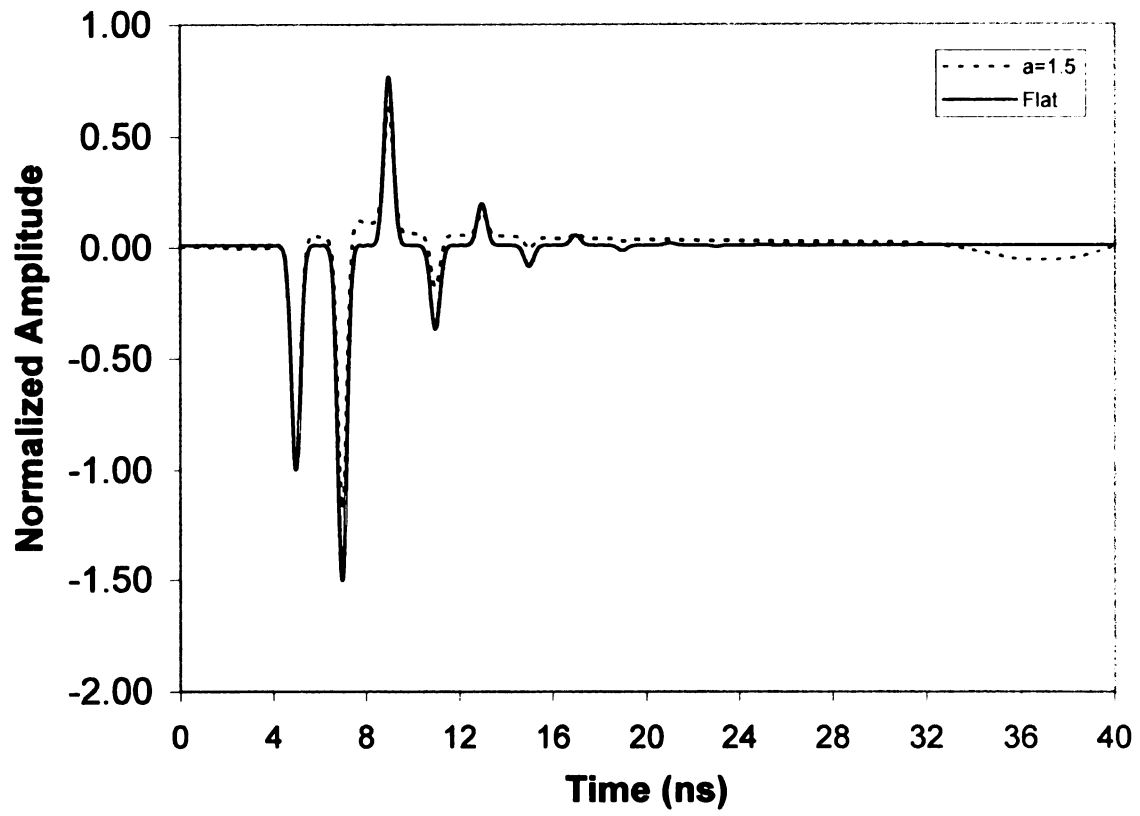


Figure 5.35. TEz normalized amplitude vs. time comparison of flat with $a = 1.5$ m and with x as the major axis.

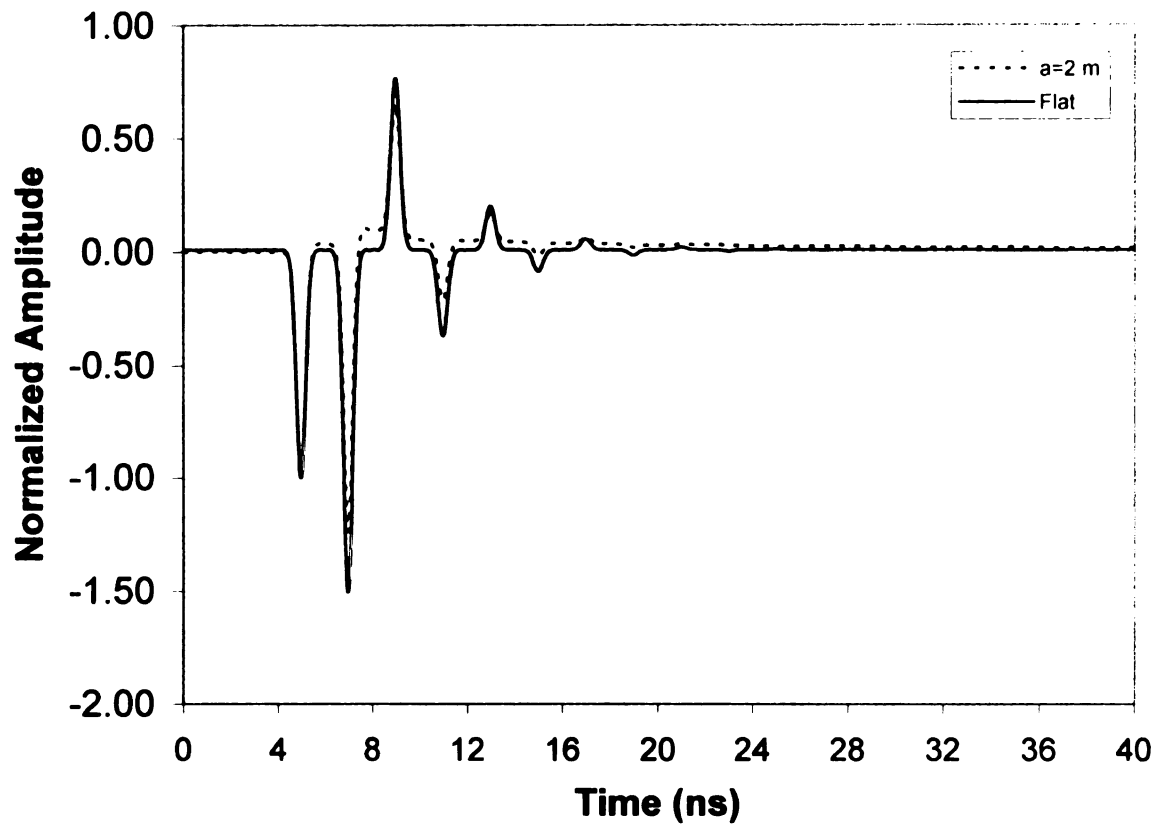


Figure 5.36. TEz normalized amplitude vs. time comparison of flat with $a = 2.0$ m and with x as the major axis.

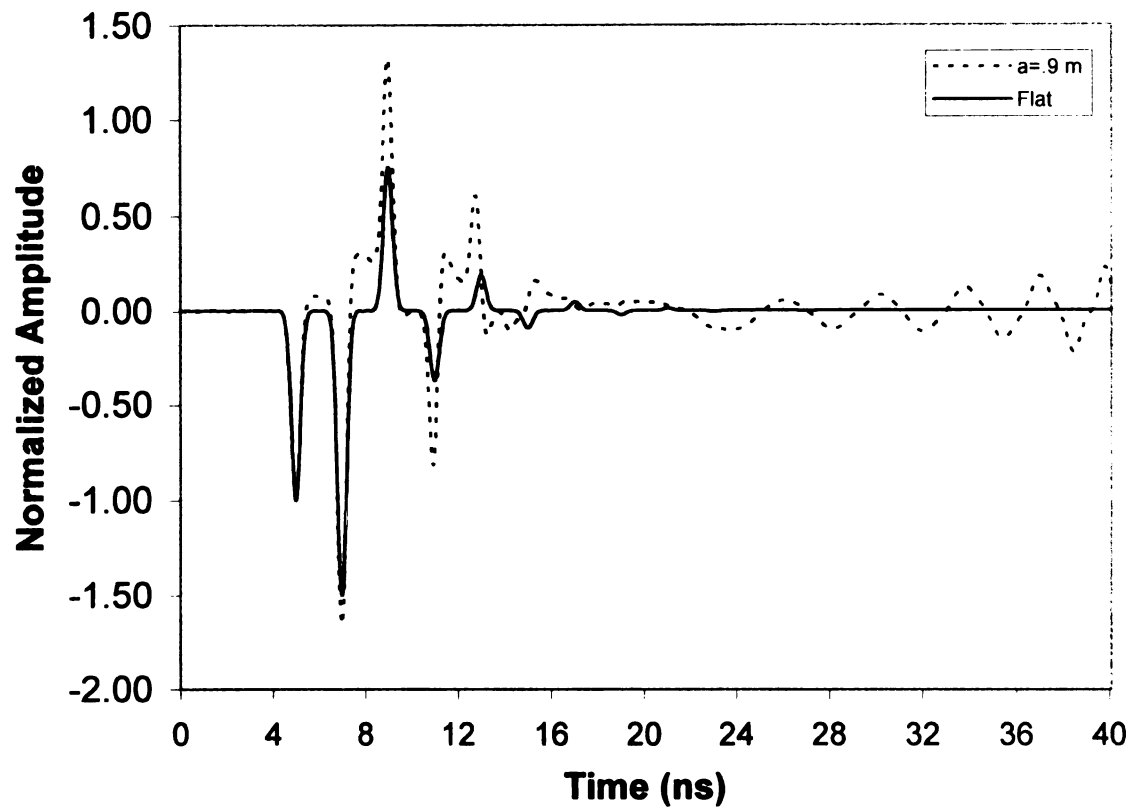


Figure 5.37. TEz normalized amplitude vs. time comparison of flat with $a = .9$ m and with y as the major axis.

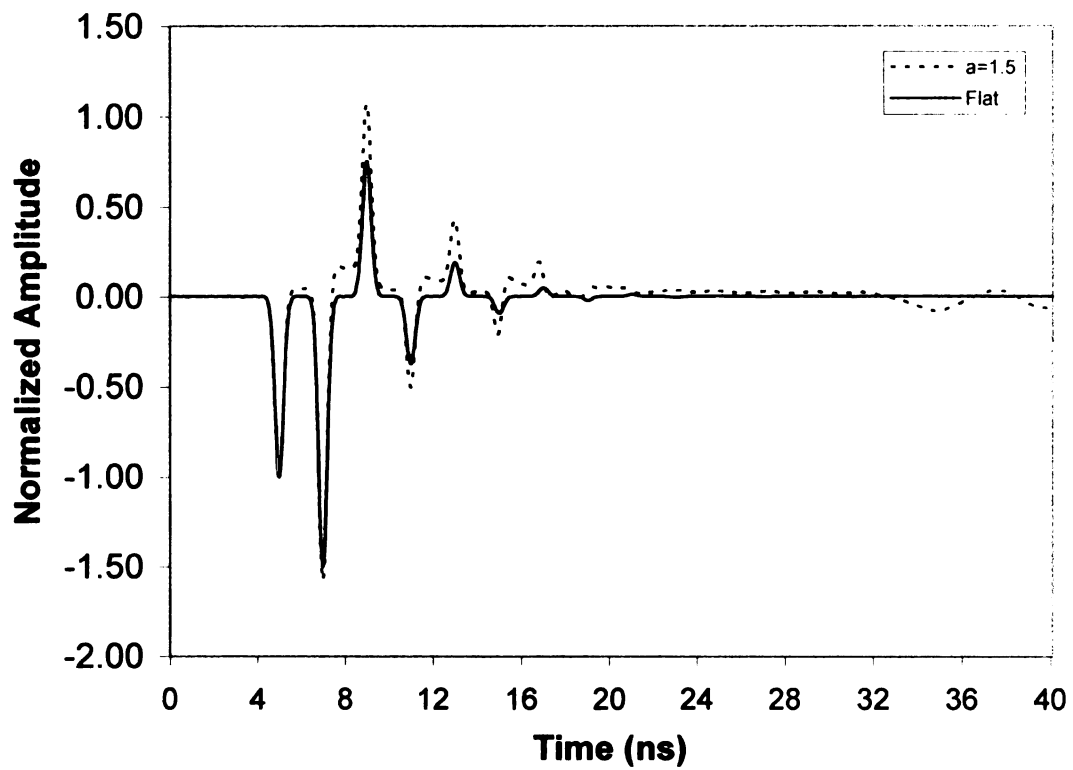


Figure 5.38. TEz normalized amplitude vs. time comparison of flat with $a = 1.5$ m and with y as the major axis.

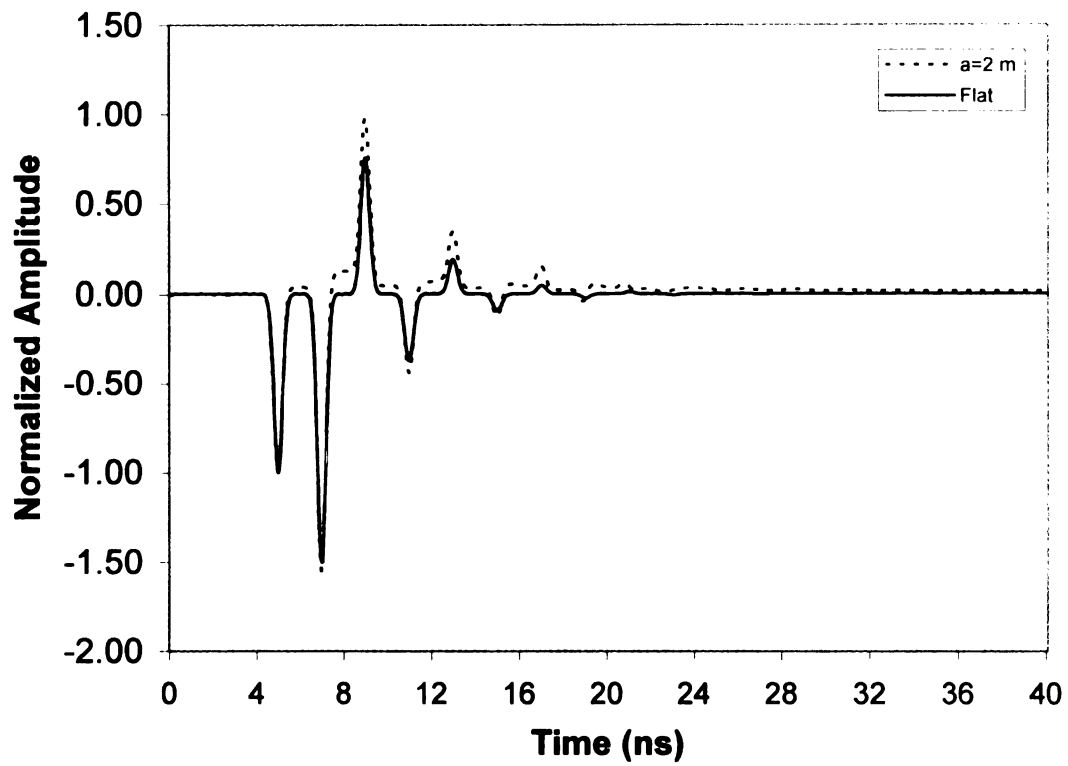


Figure 5.39. TEz normalized amplitude vs. time comparison of flat with $a = 2.0$ m and with y as the major axis.

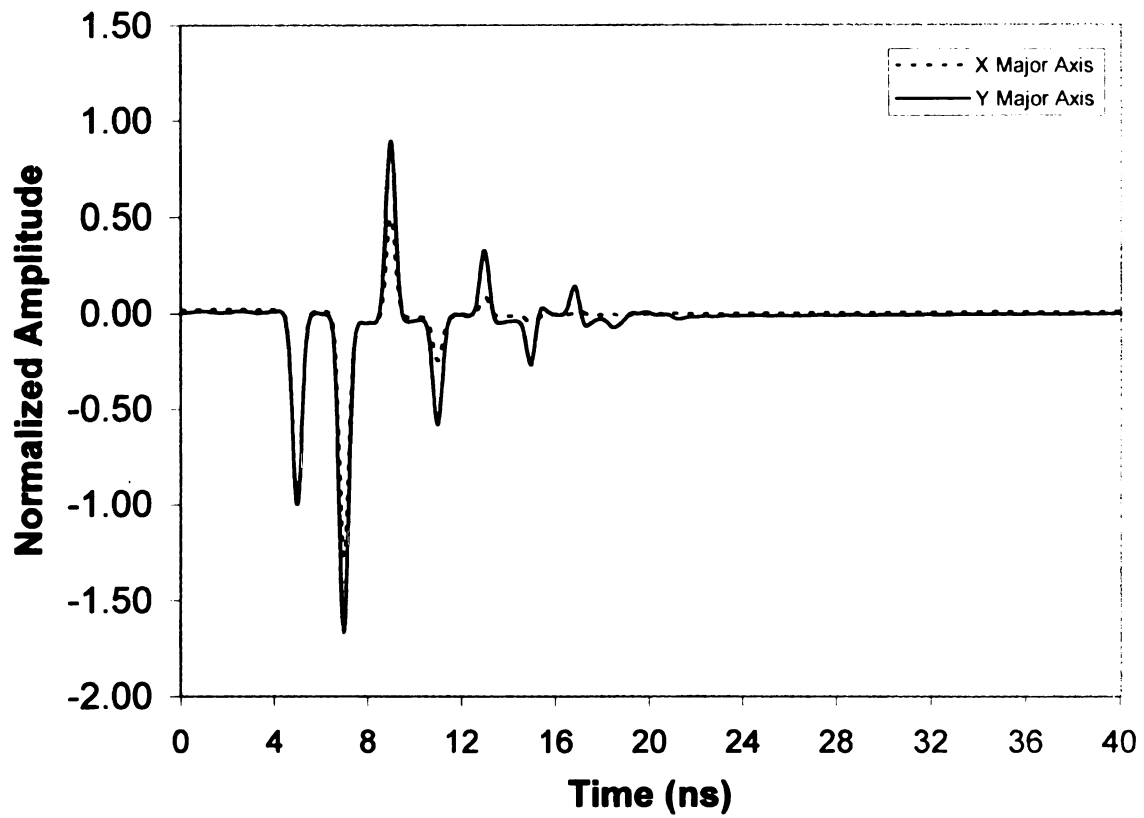


Figure 5.40. TMz normalized amplitude vs. time comparison of x vs y as the major axis, $a = 1.5$ m.

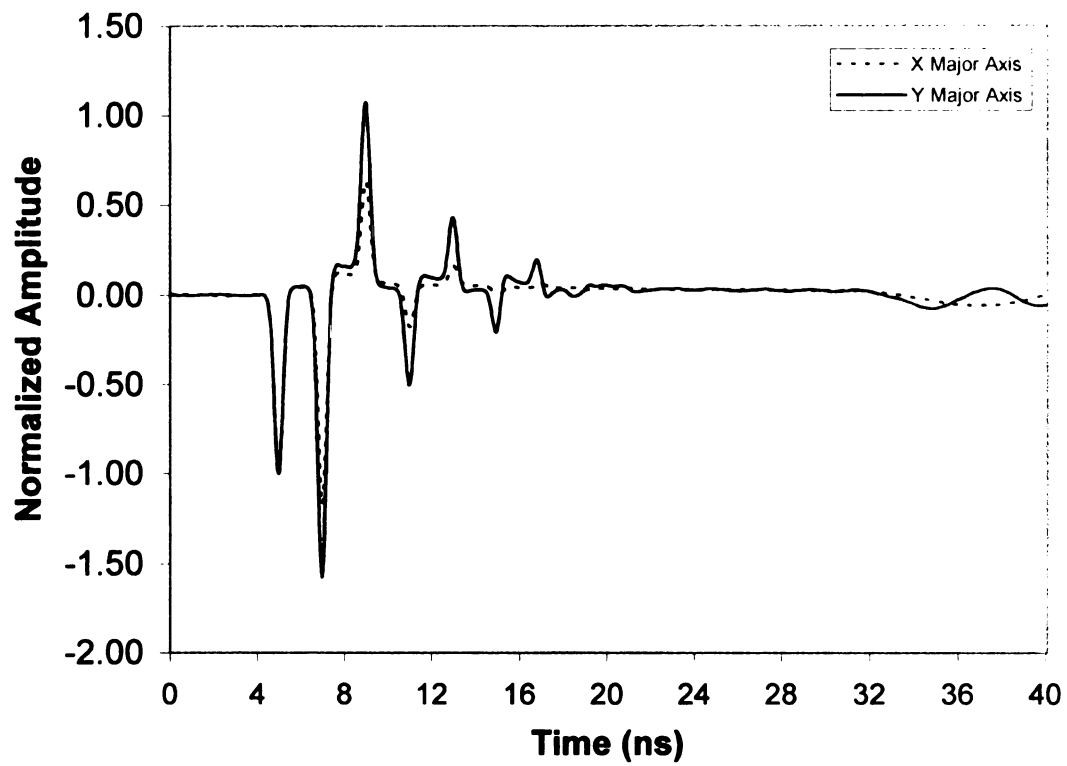


Figure 5.41. TEz normalized amplitude vs. time comparison of x vs y as the major axis, $a = 1.5$ m.

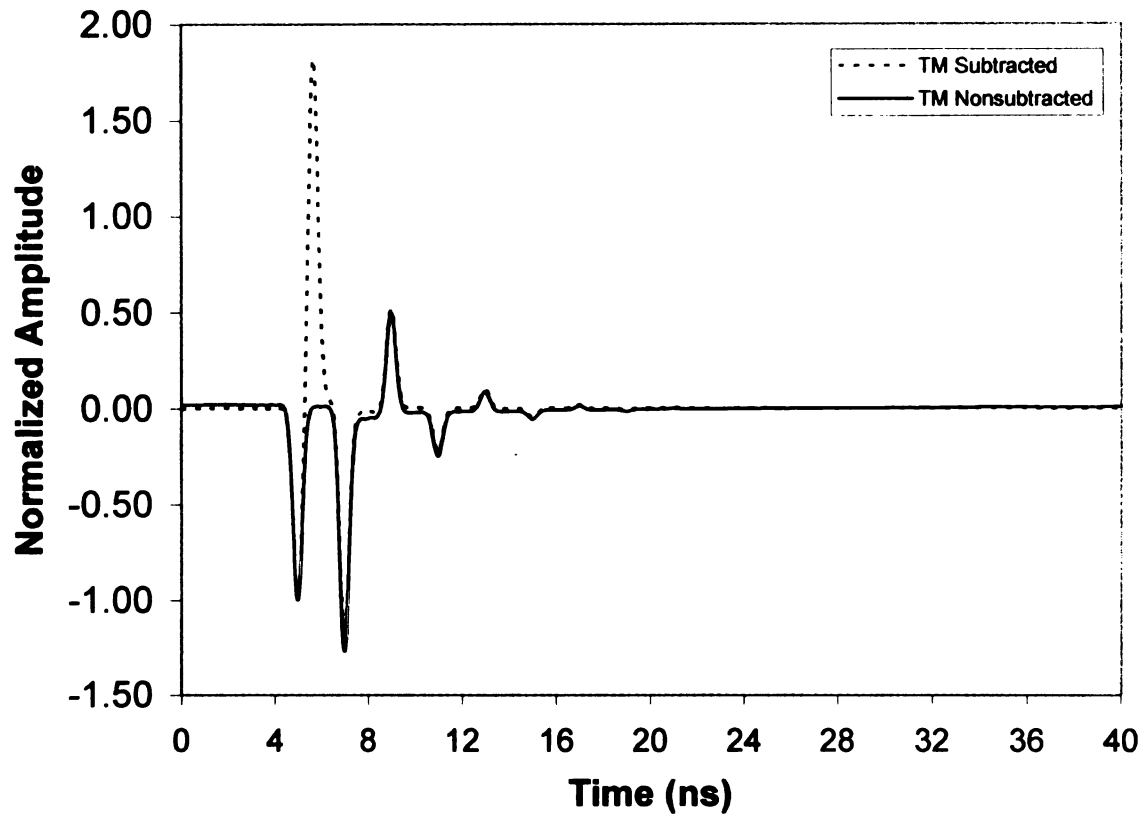


Figure 5.42. TMz normalized amplitude vs. time comparison of standard cylinder response with subtracted metallic core response with $a = 1.5$ m and x as the major axis.

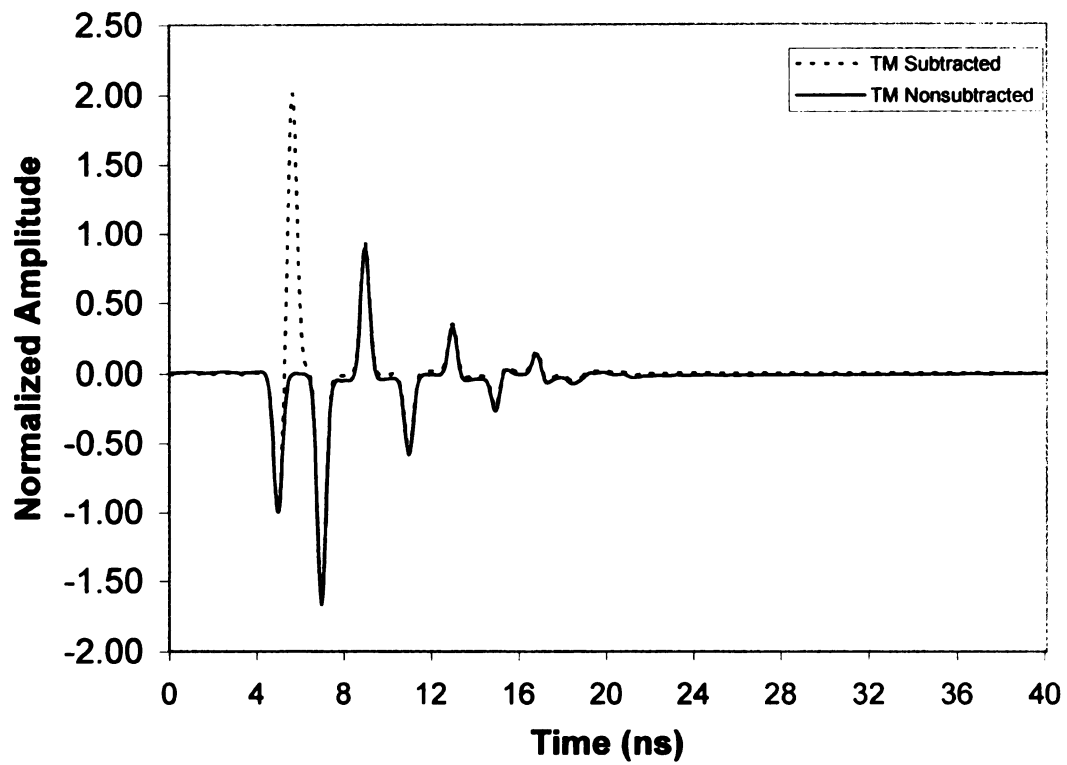


Figure 5.43. TMz normalized amplitude vs. time comparison of standard cylinder response with subtracted metallic core response with $a = 1.5$ m and y as the major axis.

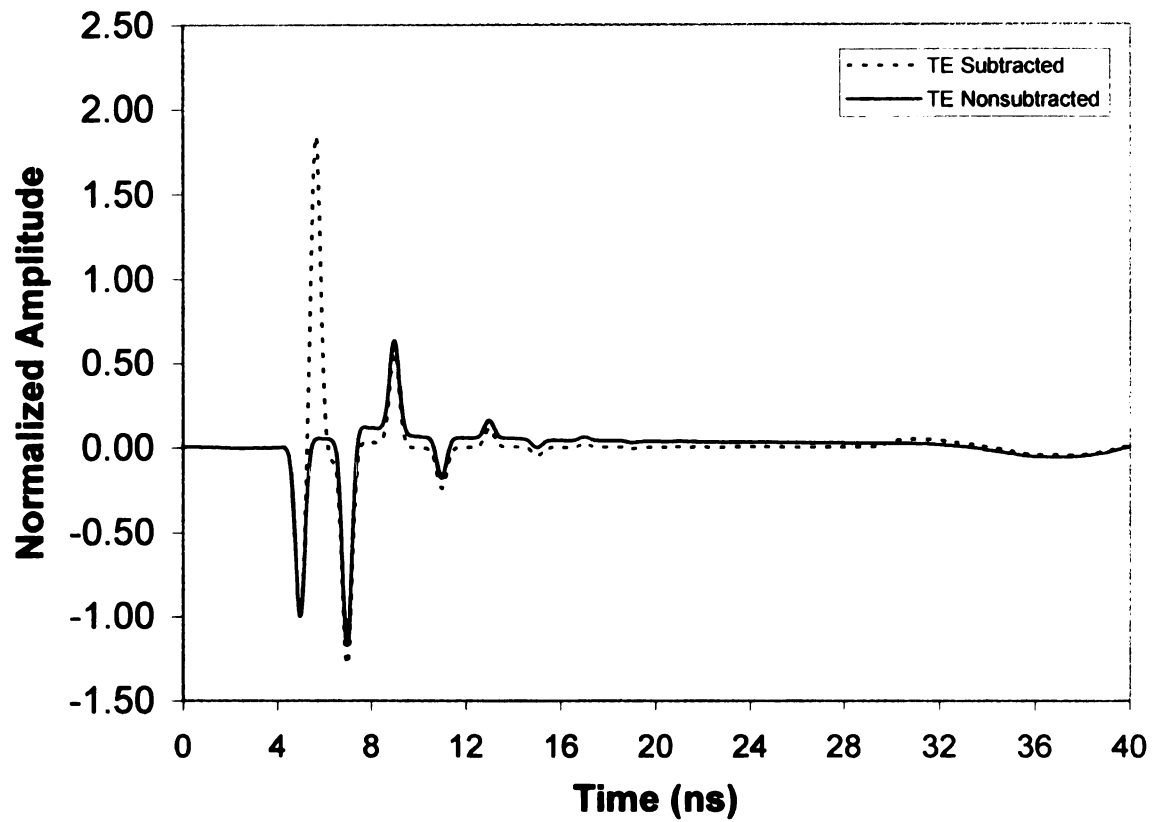


Figure 5.44. TE_z normalized amplitude vs. time comparison of standard cylinder response with subtracted metallic core response with $a = 1.5$ m and x as the major axis.

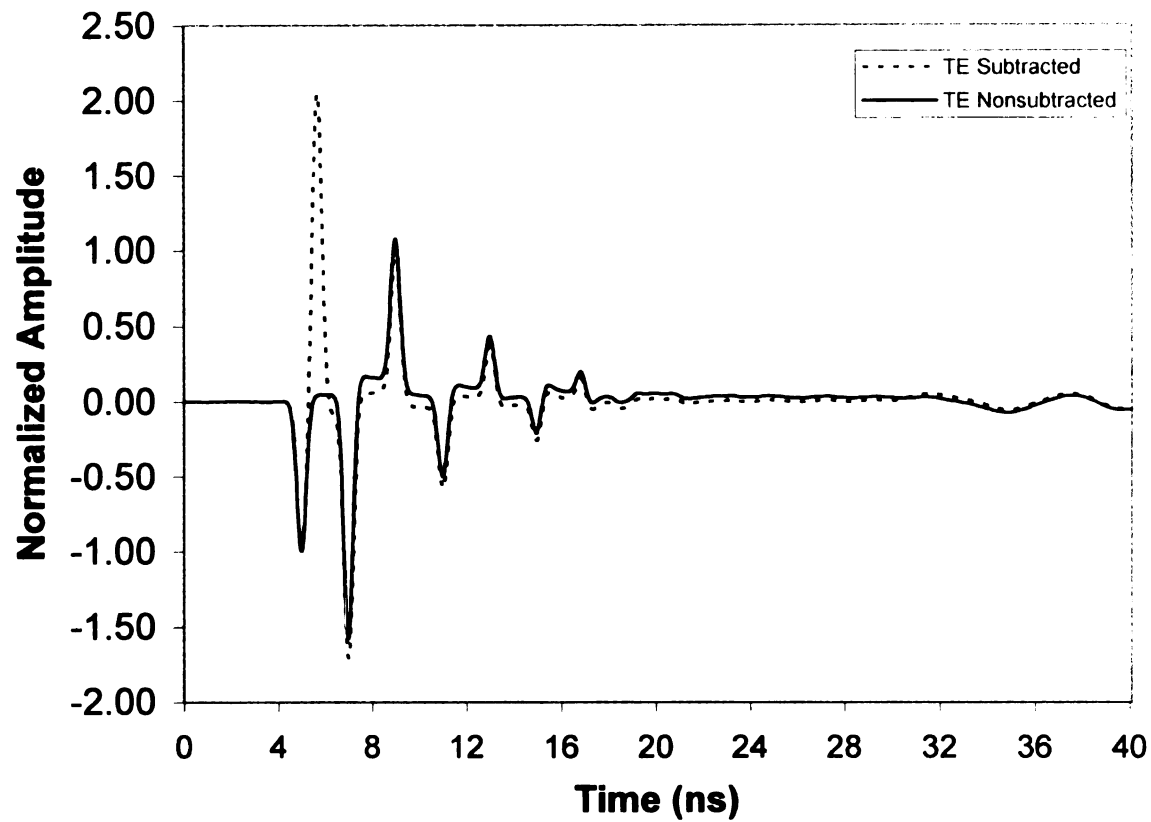


Figure 5.45. TEz normalized amplitude vs. time comparison of standard cylinder response with subtracted metallic core response with $a = 1.5$ m and y as the major axis.

CHAPTER 6

E-pulse Results

In this chapter the E-pulse technique is used to measure the difference between the field scattered by a coated elliptical conductor and a coated planar surface. The E-pulse for the flat case calculated using the technique of Garrett Stenholm's thesis [8] is shown in Figure 6.1. The E-pulse of Figure 6.1 is convolved with data in Figure 4.3 to calculate the waveform shown in Figure 6.2. As expected, after a time T_L , which is the sum of the E-pulse duration and the two-way transit time through the coating, the convolution is almost zero. After the flat case waveform is convolved with the E-pulse, the coated cylinder's time domain data is convolved with the E-pulse and the results are compared.

Figures 6.3 - 6.5 and 6.9 - 6.11 show the convolutions of the planar surface E-pulse with the scattered field waveforms for coated ellipses with x as the major axis. It is seen that the convolutions are in the late time, but not as flat as the convolution with the planar waveform. For the TM $_z$ and TE $_z$ cases with x as the major axis and $a = .9$ m, the response is small for the last 16 nanoseconds as seen in Figures 6.3 and 6.9. As the outer radius increases to $a = 1.5$ m, the TE $_z$ and the TM $_z$ response become closer the flat case as seen in Figures 6.4 and 6.10. When $a = 2$ m, the difference between the flat case and the TE $_z$ and TM $_z$ cases with x as the major axis is even smaller as shown in Figures 6.5 and 6.11. Figures 6.6 - 6.8 and

6.12 - 6.14 shows similar results for the case where y is the major axis. When the y axis is the major axis, the difference is sizable between the large and small cylinder radii. For the TE $_z$ and TM $_z$ cases with y as the major axis and $a = .9$ m, the last 16 nanoseconds show large oscillations as seen in Figures 6.6 and 6.12. As the outer radius increases to $a = 1.5$, the TE $_z$ and TM $_z$ cases become flatter, as seen in Figures 6.7 and 6.13. When $a = 2$ m, the TE $_z$ and the TM $_z$ cases in Figures 6.8 and 6.14 have only small oscillations occurring in the last 16 nanoseconds. As expected, the convolution data becomes more flat as the cylinder radius increases, since larger cylinder radii producing data that is closer to the flat case.

It was shown in Heike Vollmer's thesis that subtracting the response of the uncoated cylinder produces a smaller convolved waveform in the late time. The convolution using subtracted cases shown in Figures 6.15 and 6.16 differ mostly in the initial oscillation of the convolved plot. The standard convolution plot has two maximum and two minimums, while the difference convolution plot has four maximums and three minimums. The last 15 nanoseconds have only a small difference between the standard convolution plot and the difference convolution plot. The reason that the difference is small compared to the difference in Heike Vollmer's thesis is that the E-pulse in Figure 6.1 is a DC E-pulse, while the E-pulse used in Heike Vollmer's thesis is a standard E-pulse. The DC E-pulse eliminates the "tail" that is present in the fields scattered by the cylinders.

It is useful to quantify the value of the non-zero late-time convolved signal using the signal energy. This done using the E-pulse discrimination number (EDN) which is calculated from [11] using:

$$EDN = \frac{\int_{T_L}^{T_L + W} c_e^2(t) dt}{\int_0^{T_e} e^2(t) dt \int_{T_L}^{T_L + W} r^2(t) dt} \quad (6.1)$$

Here $e(t)$ is the E-pulse waveform, $r(t)$ is the time domain scattered field signal, and

c_e is the convolution of $e(t)$ and $r(t)$. Also, T_e is the E-pulse duration, T_L is the start of the convolution late-time, and W is the window width of the energy calculation. The EDN that is calculated using data with different major axes is plotted in Figures 6.17 and 6.18. To find the EDN value, T_L was set to 8.7 nanoseconds. The ending time, $T_L + W$, is chosen at the point where the oscillations fade out, but before the convolution with the creeping wave arrives. For the x as the major axis, the EDN value of the non-subtracted TEz case is closest to the flat case. However, for TMz case, the subtracted case is closer than the non-subtracted case to the flat case. The y major axis case is also like the x major axis case having the TEz non-subtracted case closest to the flat case. For the TMz y major axis case, the subtracted and non-subtracted cases are very close to the same value for each size of the outer radius. In all cases, the EDN becomes lower as the radius of the cylinder increases, since the response becomes closer to that of the planar case.

Table 6.1 shows the EDN values for the different polarizations and placement of the major axis. Since the E-pulse used for this data is different than what was used in [11], the results are not comparable.

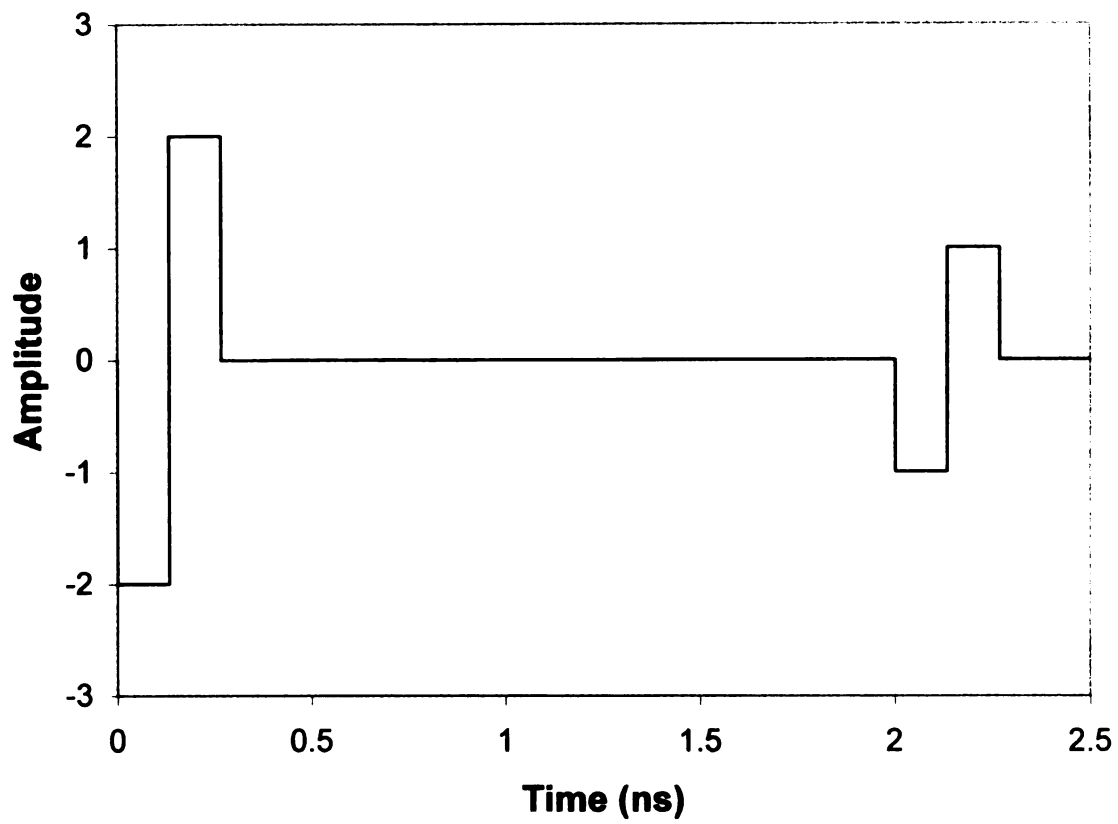


Figure 6.1. E-pulse for the planar coated conductor vs time.

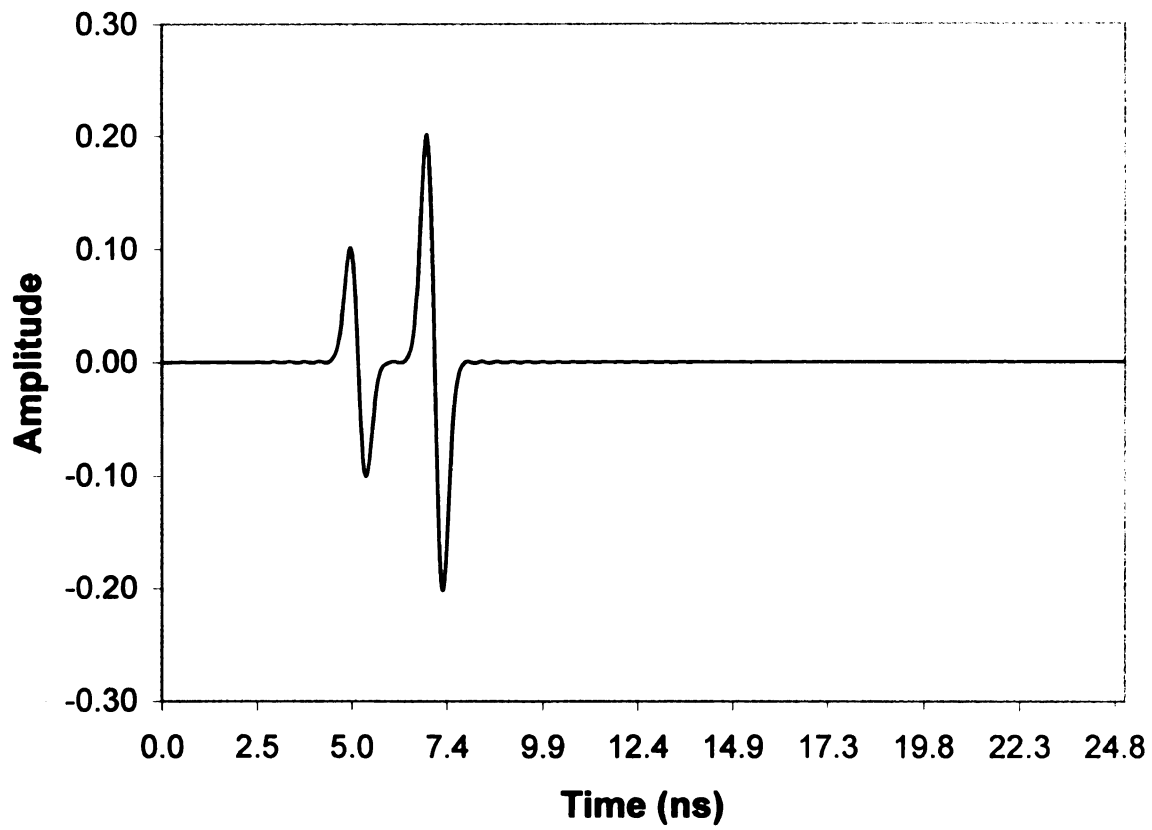


Figure 6.2. Convoluted E-pulse vs. time, flat case.

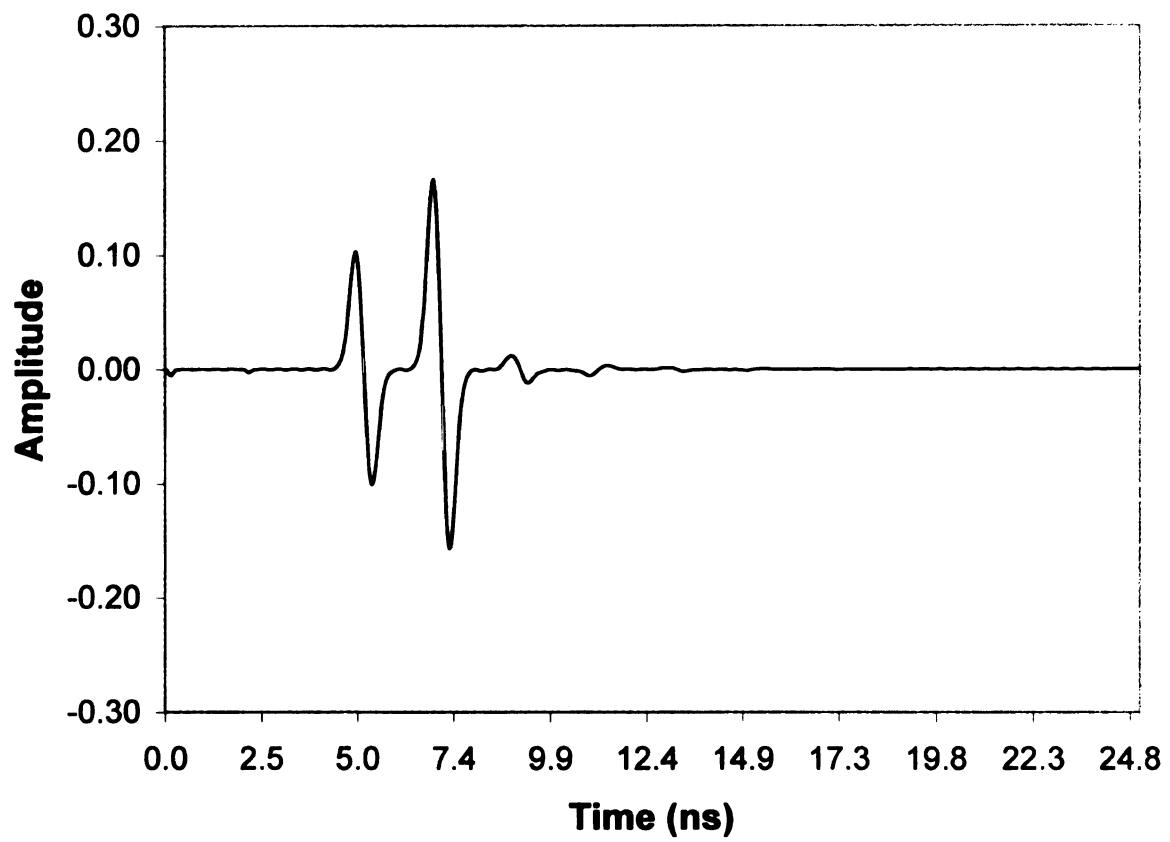


Figure 6.3. TMz convolved E-pulse vs. time, $a = .9$ m, $a_1 = .8$ m, $a_2 = .7$ m, with x as the major axis.

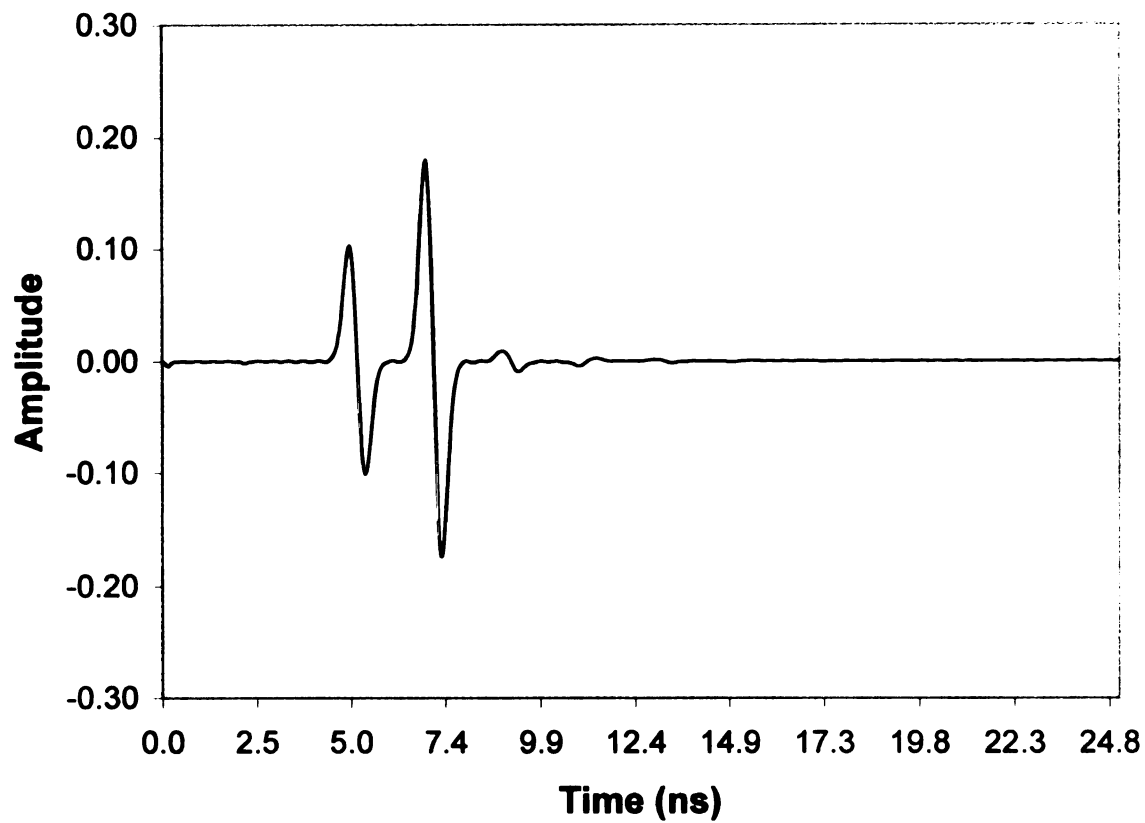


Figure 6.4. TMz convolved E-pulse vs. time, $a = 1.5$ m, $a_1 = 1.4$ m, $a_2 = 1.3$ m, with x as the major axis.

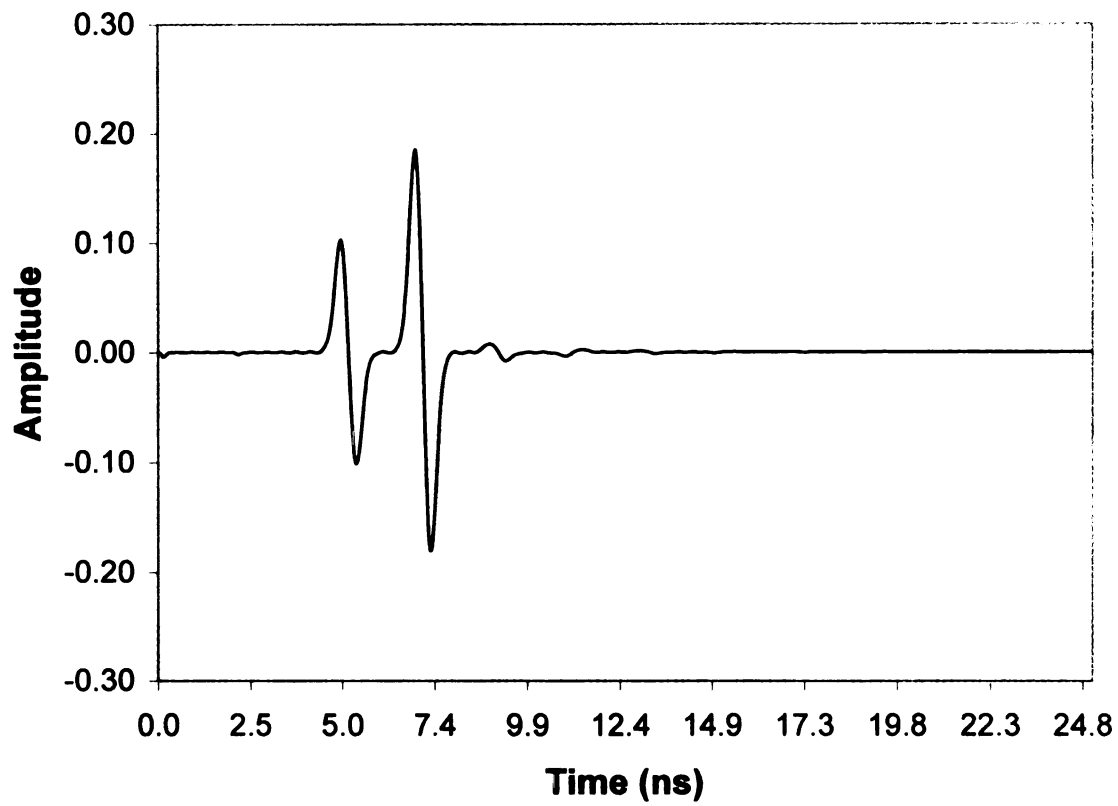


Figure 6.5. TMz convolved E-pulse vs. time, $a = 2$ m, $a_1 = 1.9$ m, $a_2 = 1.8$ m, with x as the major axis.

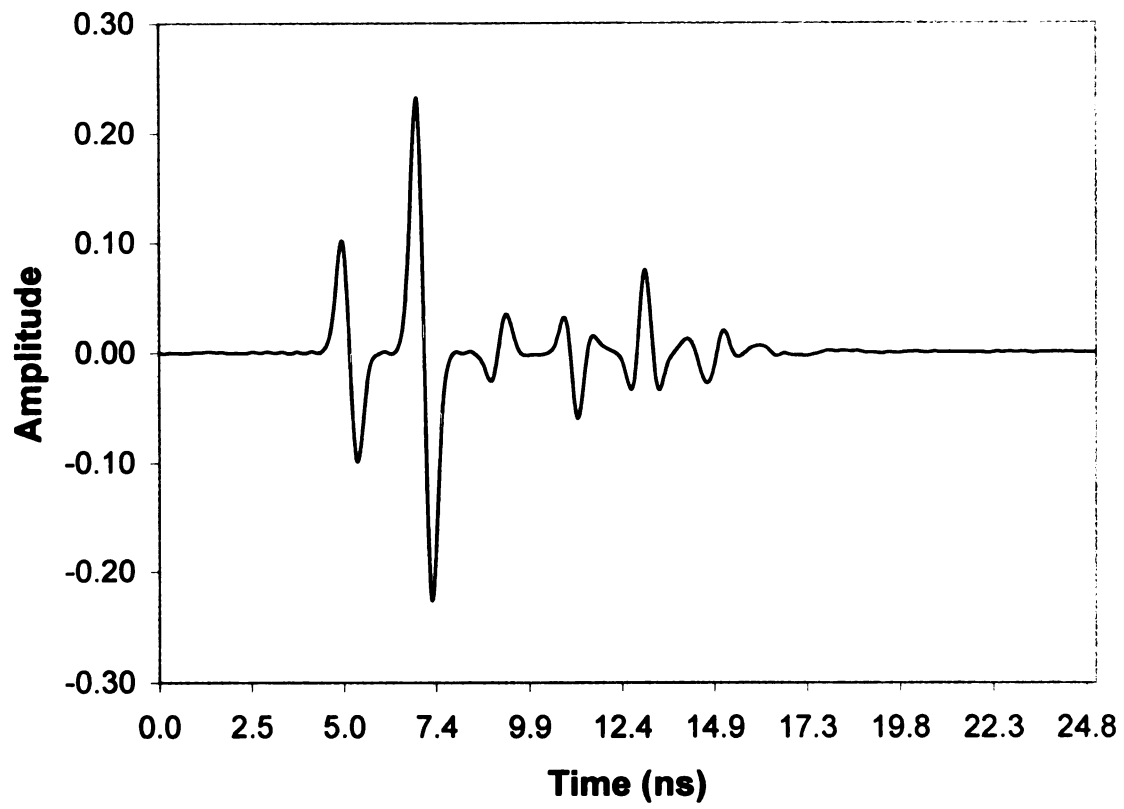


Figure 6.6. TMz convolved E-pulse vs. time, $a = .9$ m, $a_1 = .8$ m, $a_2 = .7$ m, with y as the major axis.

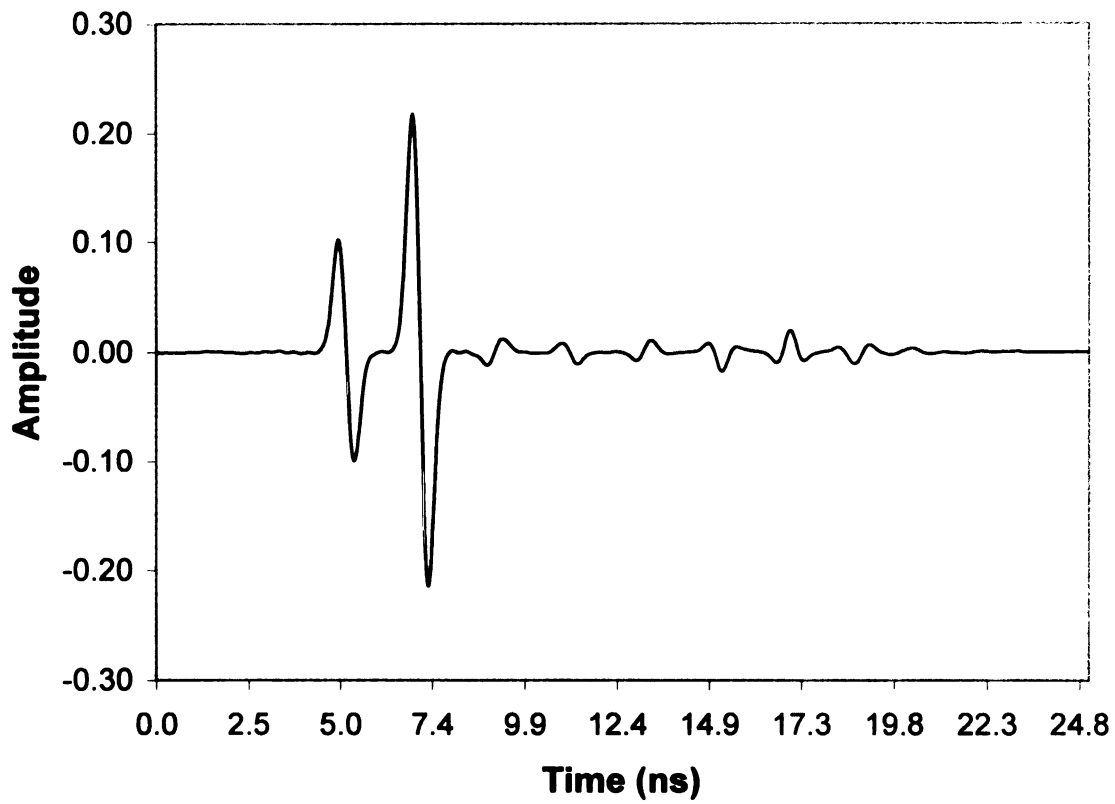


Figure 6.7. TMz convolved E-pulse vs. time, $a = 1.5$ m, $a_1 = 1.4$ m, $a_2 = 1.3$ m. with y as the major axis.

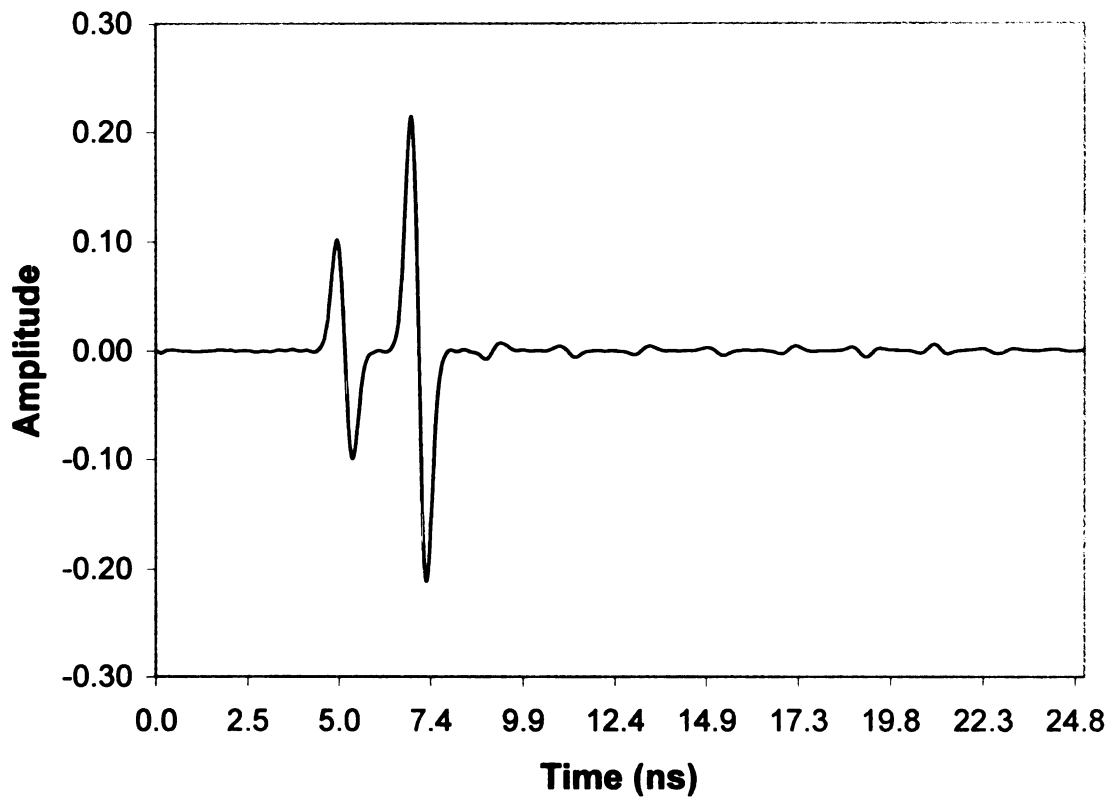


Figure 6.8. TMz convolved E-pulse vs. time, $a = 2$ m, $a_1 = 1.9$ m, $a_2 = 1.8$ m, with y as the major axis.

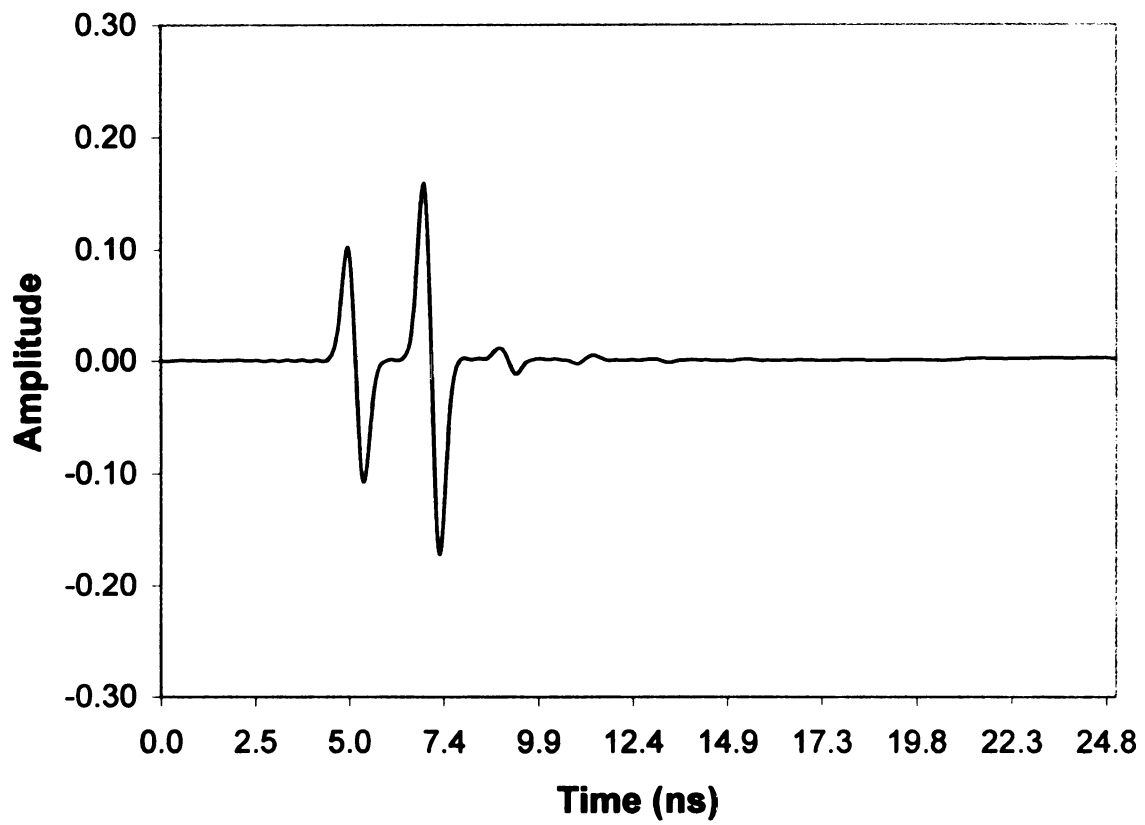


Figure 6.9. TEz convolved E-pulse vs. time, $a = .9$ m, $a_1 = .8$ m, $a_2 = .7$ m, with x as the major axis.

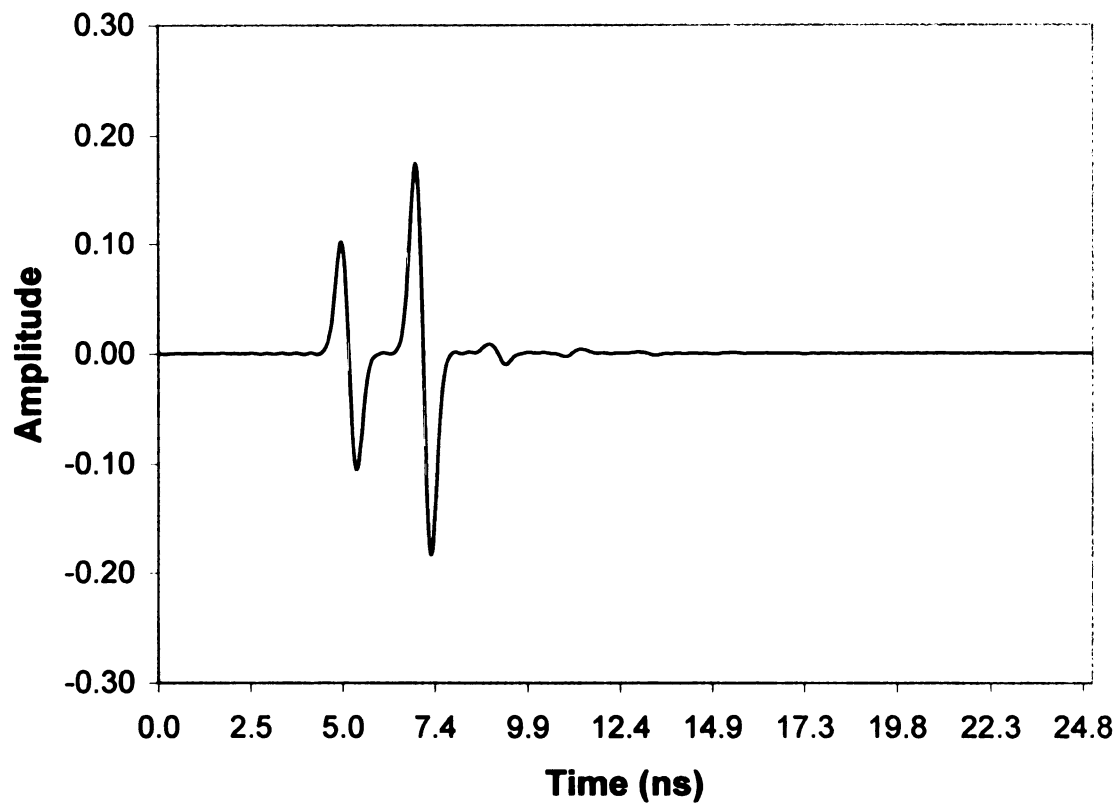


Figure 6.10. TEz convolved E-pulse vs. time, $a = 1.5$ m, $a_1 = 1.4$ m, $a_2 = 1.3$ m, with x as the major axis.

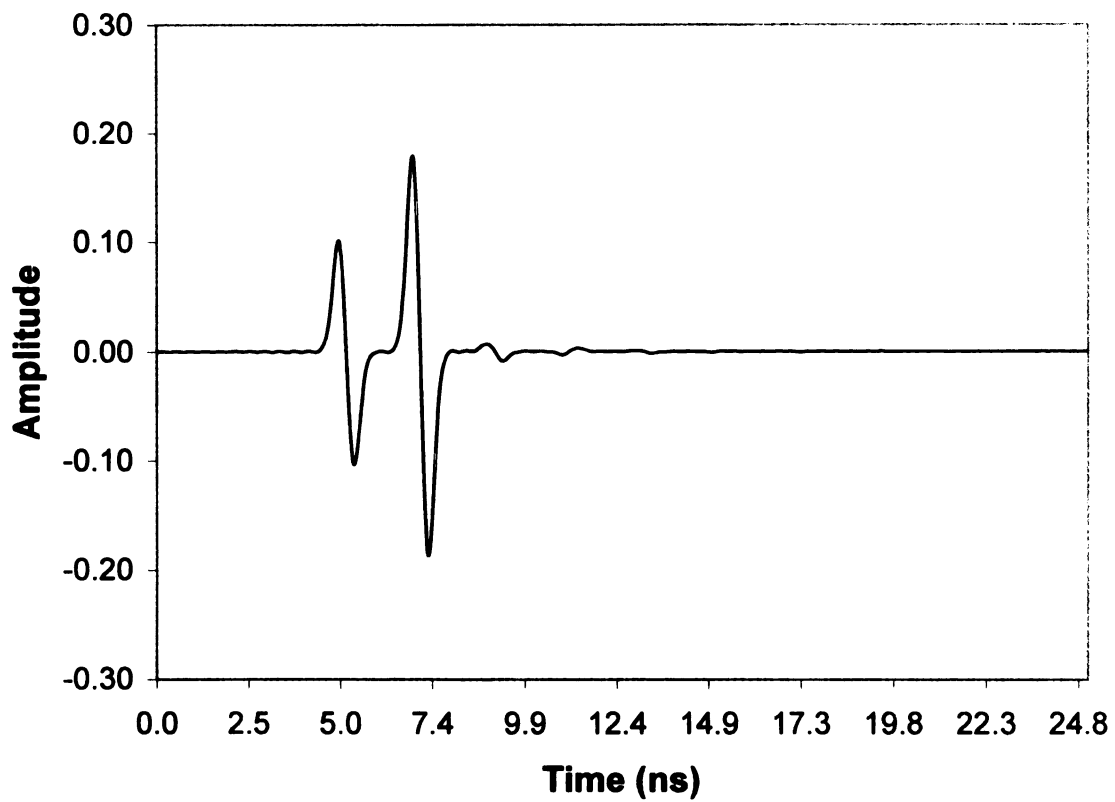


Figure 6.11. TEz convolved E-pulse vs. time, $a = 2$ m, $a_1 = 1.9$ m, $a_2 = 1.8$ m, with x as the major axis.

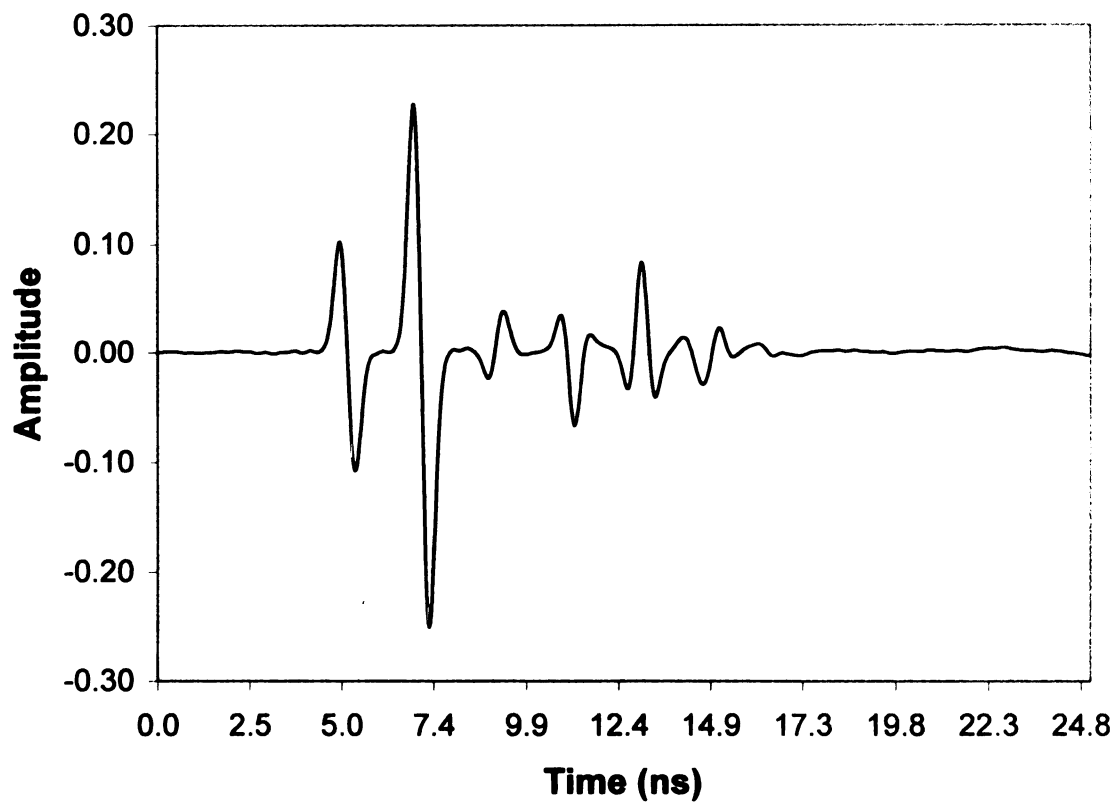


Figure 6.12. TEz convolved E-pulse vs. time, $a = .9$ m, $a_1 = .8$ m, $a_2 = .7$ m, with y as the major axis.

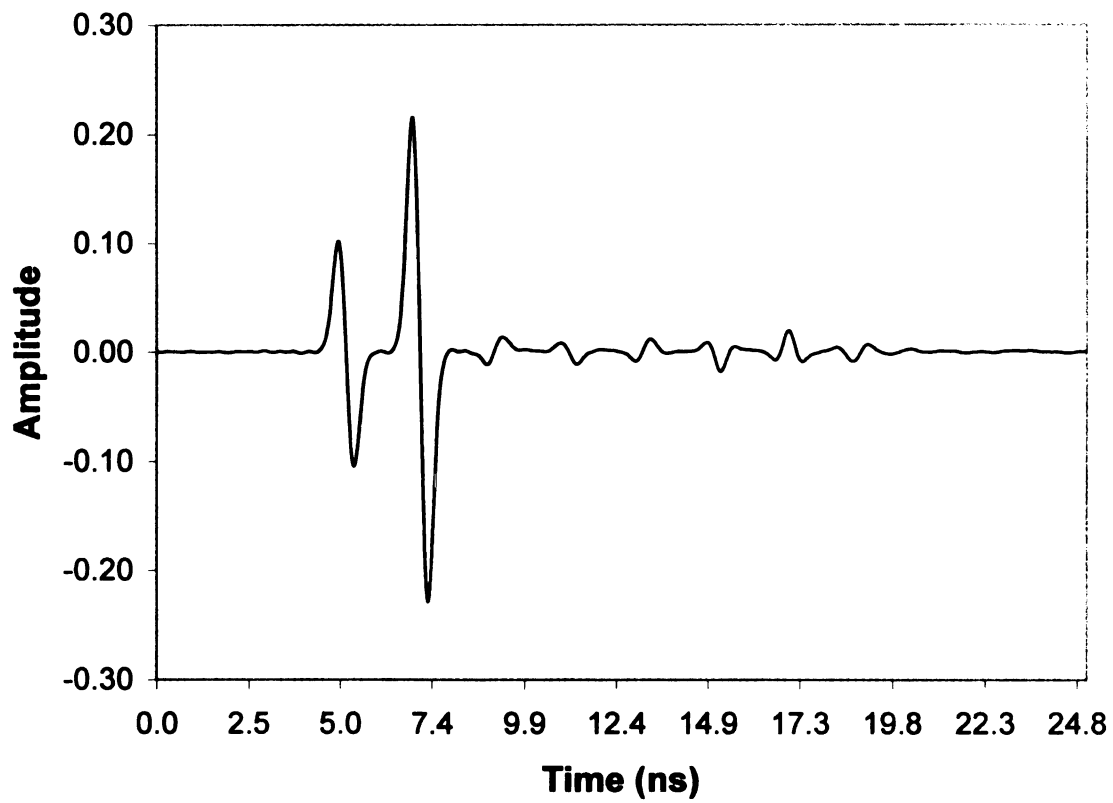


Figure 6.13. TEz convolved E-pulse vs. time, $a = 1.5$ m, $a_1 = 1.4$ m, $a_2 = 1.3$ m, with y as the major axis.

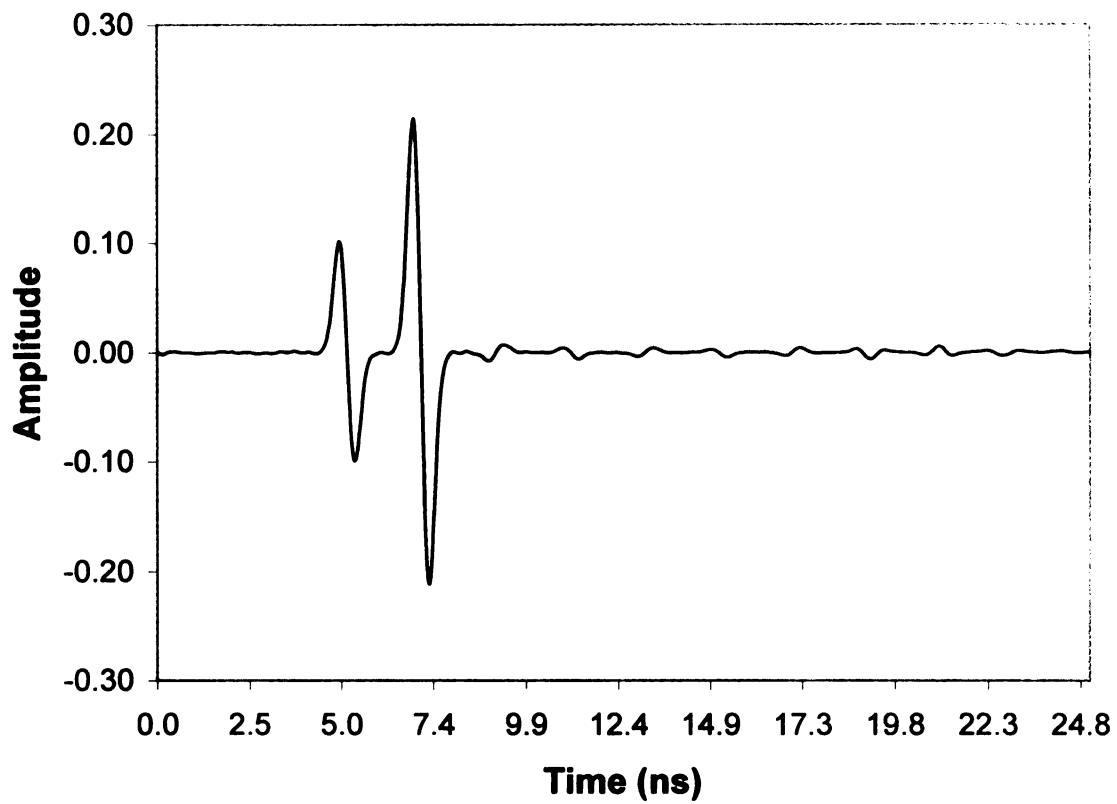


Figure 6.14. TEz convolved E-pulse vs. time, $a = 2$ m, $a_1 = 1.9$ m, $a_2 = 1.8$ m, with y as the major axis.

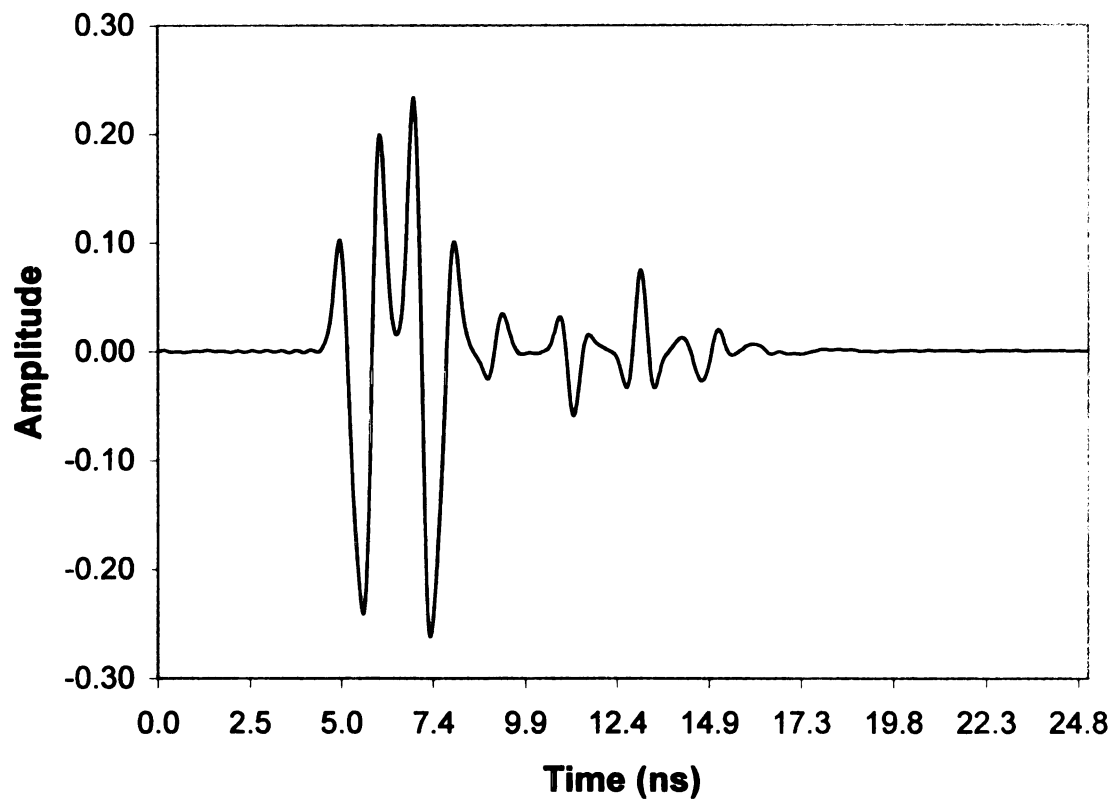


Figure 6.15. TMz subtracted convolved E-pulse vs. time, $a = .9$ m, $a_1 = .8$ m, $a_2 = .7$ m, with y as the major axis.

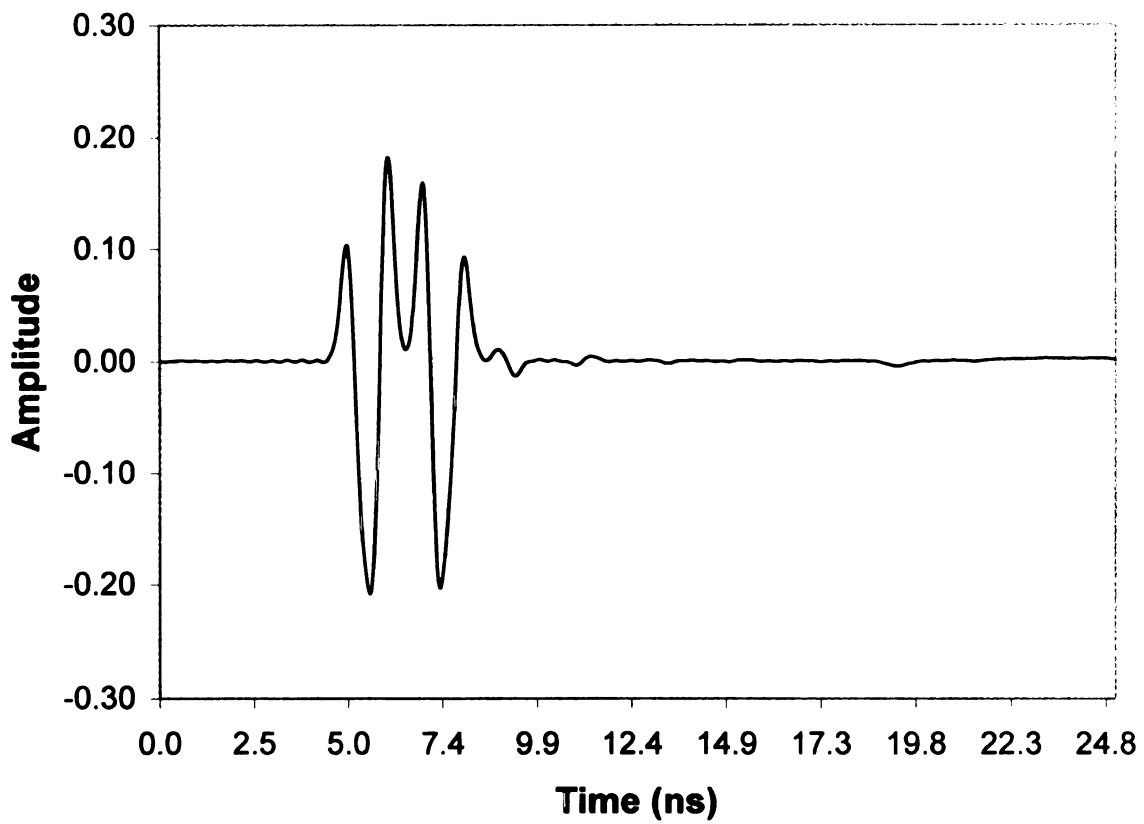


Figure 6.16. TEz subtracted convolved E-pulse vs. time, $a = .9$ m, $a_1 = .8$ m, $a_2 = .7$ m, with x as the major axis.

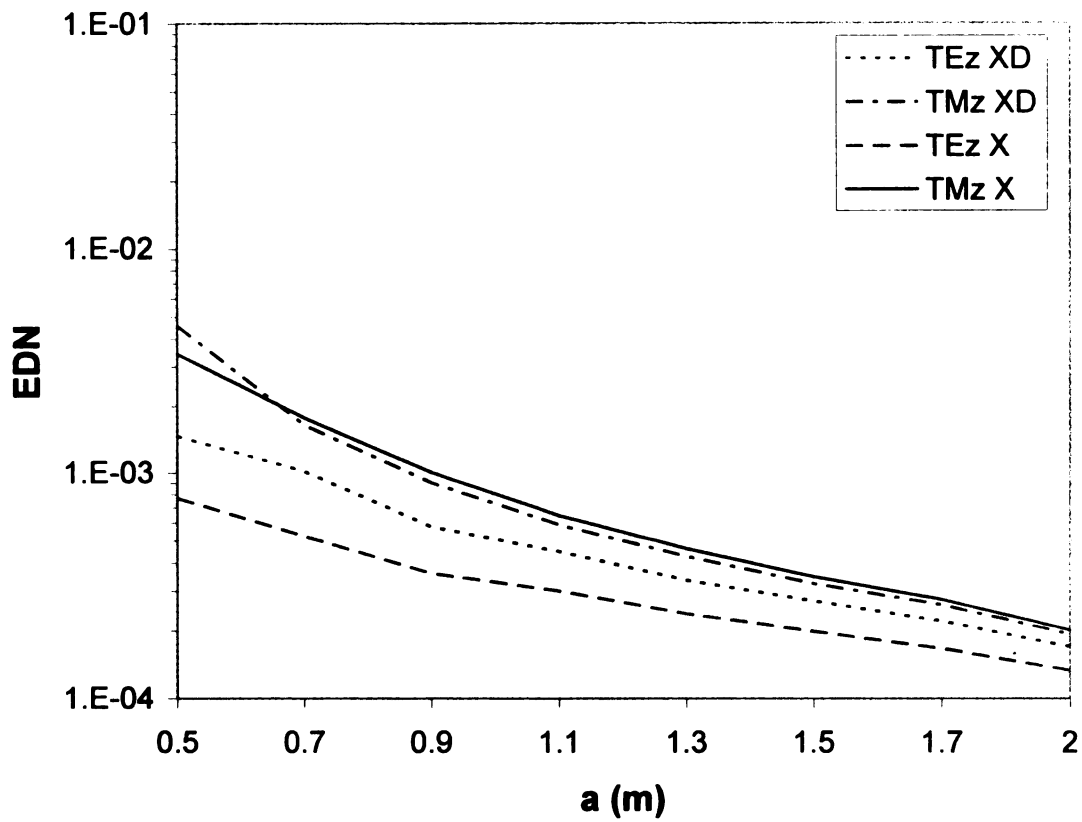


Figure 6.17. EDN vs outer radii, subtracted vs non-subtracted, x as major axis. XD indicates that it is the subtracted case with x as the major axis. X indicates that it is the non-subtracted case with x as the major axis.

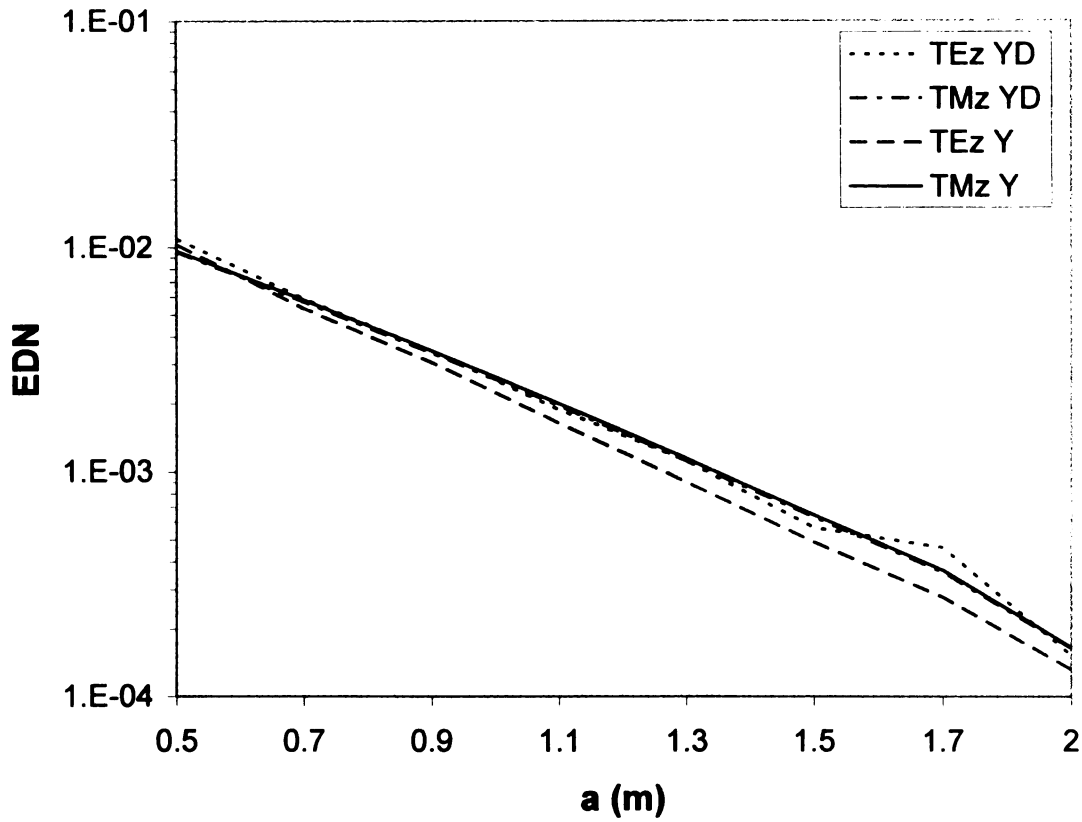


Figure 6.18. EDN vs outer radii, subtracted vs non-subtracted, y as major axis. YD indicates that it is the subtracted case with y as the major axis. Y indicates that it is the non-subtracted case with y as the major axis.

Table 6.1. EDN values calculated for flat case and for cylinders of various radii in meters

a=	Flat	TMz X	TMz Y	TEz X	TEz Y
	9.71E-07				
0.5		3.42E-03	9.64E-03	7.69E-04	1.03E-02
0.7		1.77E-03	5.83E-03	5.23E-04	5.33E-03
0.9		1.00E-03	3.44E-03	3.59E-04	3.05E-03
1.1		6.45E-04	1.99E-03	3.00E-04	1.62E-03
1.3		4.61E-04	1.14E-03	2.38E-04	8.96E-04
1.5		3.46E-04	6.40E-04	1.98E-04	4.86E-04
1.7		2.74E-04	3.65E-04	1.67E-04	2.77E-04
2		2.01E-04	1.65E-04	1.33E-04	1.31E-04
a=		TMz XD	TMz YD	TEz XD	TEz YD
0.5		4.56E-03	9.50E-03	1.47E-03	1.09E-02
0.7		1.65E-03	5.70E-03	1.02E-03	5.88E-03
0.9		9.04E-04	3.37E-03	5.76E-04	3.44E-03
1.1		5.87E-04	1.94E-03	4.48E-04	1.86E-03
1.3		4.26E-04	1.11E-03	3.34E-04	1.11E-03
1.5		3.23E-04	6.26E-04	2.71E-04	5.64E-04
1.7		2.60E-04	3.58E-04	2.20E-04	4.60E-04
2		1.93E-04	1.63E-04	1.70E-04	1.52E-04

CHAPTER 7

Conclusion

This thesis has demonstrated that the E-pulse technique can be successfully applied to a coated curve surface with a varying thickness and curvature using the E-pulse of the coated planar surface. The E-pulse technique is applied to various size radii of coated elliptic cylinders and the reflection from the surface is shown to be a summation of damped sinusoids, which is the early-time natural response for the coated curved surface. As the radius of the cylinder increases, the EDN value from the cylinder become closer to the value of the coated planar surface. Another aspect of the increasing radius of the cylinder is the reduction of the effect of changing the placement of the major axis or which polarization applied, TE_z or TM_z; for the largest cylinder radius, the EDN values are similar for the four different combinations of the polarization and placement of the major axis, since the largest radius cylinders are closet to the planar case.

The variation of the scattered electric field for the various configurations of polarization and the placement of the major axis has the largest effect in the frequency domain when the placement of the major axis is changed. In the time domain data, changing y as the major axis produces larger multiple reflections than in the planar case, while choosing x as the major axis produces smaller multiple reflections. Thus, whether the thickness increases or decreases away from the

contact point has a large effect on the time domain response. EDN values for the various configurations of polarization and major axis placement are larger for smaller cylinder radii and become smaller as the cylinder radius increases. This is because larger radius cylinders have surface curvature closer to the flat case.

The methods that check whether the scattered electric field equations have been derived correctly, are matching of the expansion coefficients of the elliptical case to the circular case and computing the echo width of the elliptical metallic core. The matching of the TE_z and TM_z expansion coefficients of the elliptical case to the circular case shows that for the major and minor axes being equal, the derived equations match a known equation. The echo width calculation shows that the point matching technique is valid.

Future work in applying the E-pulse technique to various surfaces includes changing the shapes of the metallic core and the dielectric coating. Shapes may be chosen that will be more realistic than the coated planar surface, a constant coated curved surface, or the varying coated curved surface examined in this thesis.

APPENDICES

APPENDIX A

TMz Case Source Code

```
! TMZ.f90
! FUNCTIONS:
! TMZ
!*****
! PROGRAM: TMZ
! PURPOSE: Calculating Scattering Electric Field
!*****

program TMZ

parameter (pi=3.14159265358979,e0=8.85418781762e-12, u0=1.25663706144e-6, &
nsize=10000, nf = 2000, er = 1.01, ur = 1, a = 2., nmax = 275, u1 = 20,nbig=1000)

implicit real*8 (a-h,o-z)

integer ipvt(1:nbig),flag,isecho,nf1,i,m,n,l

real*8 e,n0,phi,phi0,u,n1,n2,en,Xn(0:nmax), Yn(0:nmax),ka1, ka2,k(1:nf)

real*8 k0(1:nf),f(1:nf),Rm(0:nmax),Phim(0:nmax)

complex*16 arg,Fmn,Fpmn,r,e_jk0p,a2, diag(1:nbig),j

complex*16 bjka(0:nsize),byka(0:nsize),bjpka(0:nsize), bypka(0:nsize)

complex*16 bhka(0:nsize),bhpk(0:nsize),bjk0a(0:nsize), byk0a(0:nsize)

complex*16 bjpk0a(0:nsize),bypk0a(0:nsize),bhk0a(0:nsize), bhpk0a(0:nsize)
```

```

complex*16 bjkrm(0:nsize),bykrm(0:nsize),bjpkrm(0:nsize), bypkrm(0:nsize)
complex*16 bhkrm(0:nsize),bhpkrm(0:nsize),A1(1:nbig,1:nbig),B1(1:nbig), Es(1:nf)
complex*16 Cn(1:nbig),W(1:nf)
j = (0.D0,1.D0)
phi = 0
u = ur * u0
e = er * e0
n0 = sqrt(u0/e0)
n1 = sqrt(u/e)
ka1=1.4 !X Axis
ka2=1.3 !Y Axis
r = 1
e.jk0p = 1
n2 = n1 / n0
flag = 1
isecho = 0
!Open the data file
open (u1, FILE='temp10.txt', STATUS='OLD')
!Creates N+1 points on an ellipse with axis lengths ka1, ka2 in rectangular and polar
!forms
dphi = pi/(nmax+1)
do i=0,nmax
    phi0 = i*dphi+dphi/2.
    Xn(i) = ka1 * cos(phi0)
    Yn(i) = ka2 * sin(phi0)
    Rn(i) = sqrt(Xn(i) * Xn(i) + Yn(i) * Yn(i))
    Phim(i) = atan2(Yn(i), Xn(i))

```

```

enddo

if(isecho == 1) then !Number of data
    nf1 = 153
elseif(isecho == 2) then
    nf1 = 191
else
    nf1 = nf
endif !creating the range of frequencies

do i=1,nf1
    if(nf == 500) then
        f(i) = i * 5.e6
    elseif(nf == 1000) then
        f(i) = i * 2.5e6
    elseif(nf == 2000) then
        f(i) = i * 1.25e6
    endif
enddo

!creating the wave numbers
do i=1, nf1
    k(i) = 2 * pi * f(i) * sqrt(u*e)
    k0(i) = 2 * pi * f(i) * sqrt(u0*e0)
enddo

do i=1, nf1
    Es(i) = 0
enddo

!Creating the arguement of the bessel functions and calling the
!function that creates the ln of the bessel function
arg = k(i) * a

```

```

call logbjyh(arg,nmax,bjka,byka,bjpka,bypka,bhka,bhpka)
arg = k0(i) * a
call logbjyh(arg,nmax,bjk0a,byk0a,bjpk0a,bypk0a,bhk0a,bhpk0a)
!Creating the m x n matrix
do m=0, nmax
  if(flag == 4) then
    arg = k0(i) * Rm(m)
  else
    arg = k(i) * Rm(m)
  endif
  call logbjyh(arg,nmax,bjkrm,bykrm,bjprkrm,bypkrm,bhkrm,bhprkrm)
  B1(m+1) = 0
  do n=0, nmax
    if(n == 0) then
      en = 1
    else
      en = 2
    endif
    Fmn = exp(bjka(n) + bykrm(n)) - exp(bjkrm(n) + byka(n))
    Fpmn = exp(bjpka(n) + bykrm(n)) - exp(bypka(n) + bjkrm(n))
    if(flag == 0) then !divide by H2p(n) normalization
      A1(m+1,n+1) = (n2 * Fmn - Fpmn * exp(bhk0a(n) - bhpk0a(n)))
      * cos(Phim(m) * n)
      B1(m+1) = B1(m+1) - en * (j ** (n)) * (n2 * Fmn * exp(bjpk0a(n) &
      - bhpk0a(n)) - Fpmn * exp(bjk0a(n) - bhpk0a(n))) * cos(Phim(m) * n)
    else if(flag == 1) then ! Factor H2p(n) Normalization
      A1(m+1,n+1) = (n2 * Fmn - Fpmn * exp(bhk0a(n) - bhpk0a(n)))

```

```

* cos(Phim(m) * n)
B1(m+1) = B1(m+1) - en * (j ** (n)) * (n2 * Fmn * &
exp(bjpk0a(n)) - Fpmn * exp(bjk0a(n))) * cos(Phim(m) * n)
else if(flag == 2) then !divide by H2p(nmax) normalization
A1(m+1,n+1) = (n2 * Fmn * exp(bhpk0a(n) - bhpk0a(nmax)) - Fpmn * &
exp(bhk0a(n) - bhpk0a(nmax))) * cos(Phim(m) * n)
B1(m+1) = B1(m+1) - en * (j ** (n)) * (n2 * Fmn * exp(bjpk0a(n) &
- bhpk0a(nmax)) - Fpmn * exp(bjk0a(n) - bhpk0a(nmax))) * &
cos(Phim(m) * n)
else if(flag == 3) then !no normalization
A1(m+1,n+1) = (n2 * Fmn * exp(bhpk0a(n)) - Fpmn * exp(bhk0a(n))) &
* cos(Phim(m) * n)
B1(m+1) = B1(m+1) - en * (j ** (n)) * (n2 * Fmn * exp(bjpk0a(n)) &
- Fpmn * exp(bjk0a(n))) * cos(Phim(m) * n)
else if(flag == 4) then !no normalization, no dielectric
A1(m+1,n+1) = exp(bhkrm(n)) * cos(Phim(m) * n)
B1(m+1) = B1(m) - en * (j ** (n)) * exp(bjkrm(n))
* cos(Phim(m) * n)
endif
enddo
enddo
do l=1, nmax+1
Cn(l) = B1(l)
end do
call DCOMPC (nbig,nmax+1,A1,IPVT,DIAG)
call SOLVEC (nbig,nmax+1,A1,IPVT,Cn)
a2 = sqrt(2/(pi * k0(i) * r)) * e_jk0p * exp(pi * j / 4)

```

```

do l=0, nmax
  if(flag == 1) then
    Es(i) = Es(i) + Cn(l+1) * exp(0 - bhp0a(l)) * cos (l * phi) * &
    exp(l * j * pi / 2)
  else
    Es(i) = Es(i) + Cn(l+1) * cos (l * phi) * exp(l * j * pi / 2)
  endif
enddo

Es(i) = Es(i) * a2

if(isecho == 1) then
  W(i) = 2 * pi * Es(i) * conjg(Es(i))
  write(u1,*) real(k0(i)),real(W(i)),aimag(W(i))
  write(*,*) i,real(W(i)),aimag(W(i))
elseif(isecho == 2) then
  W(i) = 2 * pi * Es(i) * conjg(Es(i)) / (pi * Rm(1))
  write(u1,*) real(k0(i) * Rm(1)),real(W(i)),aimag(W(i))
  write(*,*) i,real(W(i)),aimag(W(i))
else
  !write(u1,*) f(i)*1.d-9,real(Es(i)),aimag(Es(i))
  write(u1,*) real(Es(i)),aimag(Es(i))
  write(*,*) i,real(Es(i)),aimag(Es(i))
endif

enddo

!prints out the points on the ellipse
!do i=0,nmax
!write(u1,*) Xn(i),Yn(i),Rm(i), Phim(i)
!write(*,*) Xn(i),Yn(i)

```

```

!end do
close(u1)
end program TMZ
!Calculating the ln of the bessel functions subroutine
logbjyh(arg,n,logj,blogy,logjp,logyp,blogh,bloghp)
implicit real*8 (a-h,o-z)
parameter (nsize=10000,test=1.d-10,gamma=0.57721566490153, &
pi=3.14159265358979)
complex*16 arg,resn,res,prod,zsum,zsum1,zj0,zy0
complex*16 logj(0:nsize),blogy(0:nsize),ratio(0:nsize)
complex*16 logjp(0:nsize),blogyp(0:nsize)
complex*16 blogh(0:nsize),bloghp(0:nsize)
complex*16 ysum,ysum1
complex*16 zj,yj1,yj
!computes the log of J0-Jn for complex arguments
!first compute J0 using ratios Jn-1/Jn and
!equation 9.1.44 from Abramowitz
!also compute Y0 using ratios Jn-1/Jn and
!equation 9.1.89 from Abramowitz
zj = dcplx(0.d0,1.d0)
zsum = 1.d0
ysum = 2.d0*(zlog(arg)+dlog(0.5d0)+gamma)/pi
prod = 1.d0
iyflag = 1
izflag = 1 i = 0
10 i = i + 2
zsum1 = zsum

```

```

ysum1 = ysum
call bratio(arg,i-1,res)
prod = prod*res
ratio(i-1) = res
call bratio(arg,i,res)
prod = prod*res
ratio(i) = res
j = i/2
if (izflag .eq. 1) then
    zsum = zsum + 2.d0*(-1)**j/prod
    if (abs(zsum1-zsum)/abs(zsum1) .lt. test) then
        izflag=0
    end if
end if
if (iyflag .eq. 1) then
    ysum = ysum - 4.d0*(-1)**j/(prod*pi*j)
    if (abs(ysum1-ysum)/abs(ysum1) .lt. test) then
        iyflag=0
    end if
end if
if ((izflag .eq. 0) .and. (iyflag .eq. 0)) go to 20
zsum1 = zsum
ysum1 = ysum
go to 10
20 zj0 = cos(arg)/zsum
zy0 = ysum*zj0
! finish computing ratios

```

```

if (i .lt. n) then
  do j=i+1,n
    call bratio(arg,j,res)
    ratio(j) = res
  end do
end if

! now compute log(Jn)
blogj(0) = zlog(zj0)
do i=1,n
  blogj(i) = blogj(i-1)-zlog(ratio(i))
end do

! now compute JnYn and then log(Yn)
! using Wronskian 9.1.16 from Abramowitz
yj1 = zj0*zy0
blogy(0) = zlog(zy0)
do i=1,n
  yj = yj1/(ratio(i)*ratio(i))-(2.d0/(pi*arg))/ratio(i)
  blogy(i) = zlog(yj)-blogj(i)
  yj1 = yj
end do

! next compute log(Jn') from recursion formula
blogjp(0) = dcplx(0.d0,pi)+blogj(1)
do i=1,n
  blogjp(i) = blogj(i)+zlog(ratio(i)-i/arg)
end do

! next compute log(Yn') from recursion formula
blogyp(0) = dcplx(0.d0,pi)+blogy(1)

```

```

do i=1,n
  blogyp(i) = -blogj(i)+zlog(exp(blogy(i-1)+ &
  blogj(i))-(i/arg)*exp(blogj(i)+blogy(i)))
end do
! next compute log(Hn(2)) from cross product
blogh(0) = zlog(zj0-zj*zy0)
do i=1,n
  blogh(i) = zlog(exp(blogj(i)+blogh(i-1))- &
  2.d0/(zj*pi*arg)) - blogj(i-1)
end do
! lastly compute log(Hn(2)') from cross product
bloghp(0) = zlog(exp(blogjp(0))-zj*exp(blogyp(0)))
do i=1,n
  bloghp(i) = zlog(exp(blogjp(i)+blogh(i))- &
  (2.d0*zj)/(pi*arg)) - blogj(i)
end do
! reduce phase by increments of 2pi
do i=0,n
  call reducepi(blogj(i))
  call reducepi(blogy(i))
  call reducepi(blogjp(i))
  call reducepi(blogyp(i))
  call reducepi(blogh(i))
  call reducepi(bloghp(i))
end do
return
end

```

```

subroutine bratio(arg,n,res)
! computes the ratio of  $J_{n-1}(\arg)/J_n(\arg)$ 
! to relative accuracy of test using
! continued fraction expansion of Lentz
! Reference: IEEE Trans on AP, vol. 48,
! no. 10, pp. 1528-1532, October 2000
! parameter (nmax=10000,test=1.d-14)
implicit real*8 (a-h,o-z)
complex*16 arg,res,res1,zvec(nmax)

nterms = 2
ii = -2
do i=1,nterms
    ii = -ii
    zvec(i) = ii*(n+i-1)/arg
end do

res = zvec(nterms)
do j=nterms-1,1,-1
    res = 1.d0/res + zvec(j)
end do

res1 = res
do k=nterms+1,nmax
    ii = -ii
    zvec(k) = ii*(n+k-1)/arg
    res = zvec(k)
    do j=k-1,1,-1
        res = 1.d0/res + zvec(j)
    end do
end do

```

```

    diff = abs(res-res1)/abs(res1)
    if (diff .lt. test) go to 100
    res1 = res
end do
write (*,*) 'ERROR*** maximum number of terms exceeded'
write (*,*) ' in subroutine bratio'
100 return
end
subroutine reducepi(z)
! reduces imaginary part of complex number
implicit real*8 (a-h,o-z)
parameter (tpi=6.283185307179586477)
complex*16 z
x = dreal(z)
y = dimag(z)
10 if (y .gt. tpi) then
    y=y-tpi
    go to 10
end if
20 if (y .lt. -tpi) then
    y=y+tpi
    go to 20
end if
z=dcmplx(x,y)
return
end
subroutine DCOMPC (nbig,N,A,IPVT,DIAG)

```

```

! Decomposes matrix a to triangular form
! **** COMPLEX VERSION ****
! FROM: LINEAR ALGEBRA BY GILBERT STRANG
! parameter(nbig=101)
integer N,IPVT(nbig)
integer NM1,I,J,K,KP1,M
complex*16 A(nbig,nbig),DIAG(nbig)
complex*16 P,T
IPVT(N) = 1
if (N == 1) GO TO 70
NM1 = N-1
do 60 K=1,NM1
    KP1 = K+1
! find pivot p
    M = K
do 10 I=KP1,N
10 if (abs(A(I,K)) < abs(A(M,K))) M=I
IPVT(K) = M
if (M /= K) IPVT(N) = -IPVT(N)
P = A(M,K)
A(M,K) = A(K,K)
A(K,K) = P
DIAG(K) = P
if (P == 0.D0) go to 60
! compute multipliers
20 do 30 I=KP1,N 30 A(I,K) = -A(I,K)/P
! interchange rows and columns

```

```

do 50 J=KP1,N
T = A(M,J)
A(M,J) = A(K,J)
A(K,J) = T
if (T == 0.D0) go to 50
do 40 I=KP1,N
A(I,J) = A(I,J) + A(I,K)*T
40 continue
50 continue
60 continue
70 DIAG(N) = A(N,N)*IPVT(N)
return end

subroutine SOLVEC (nbig,N,A,IPVT,B)
! Solves matrix eqn AX=B with a decomposed by dcompc
! parameter(nbig=101)
integer N,IPVT(nbig)
integer NM1,K,KB,KP1,KM1,M,I
complex*16 A(nbig,nbig),B(nbig)
complex*16 S
! forward elimination
if (N == 1) go to 30
NM1 = N-1
do 10 K=1,NM1
KP1 = K+1
M = IPVT(K)
S = B(M)
B(M) = B(K)

```

```
B(K) = S
do 10 I=KP1,N
10 B(I) = B(I) + A(I,K)*S
! back substitution
do 20 KB=1,NM1
KM1 = N-KB
K = KM1+1
B(K) = B(K)/A(K,K)
S = -B(K)
do 20 I=1,KM1
20 B(I) = B(I) + A(I,K)*S
30 B(1) = B(1)/A(1,1)
return
end
```

APPENDIX B

TEz Case Source Code

```
! TEZ.f90
!*****
! PROGRAM: TEZ
! PURPOSE: Calculating the scattered electric field of TEz case
!*****

program TEZ
parameter (pi=3.14159265358979,e0=8.85418781762e-12, u0=1.25663706144e-6, &
nsize=10000, nf = 2000, er = 9., ur = 1, a = 2., nmax = 275, u1 = 20,nbig=1000)
implicit real*8 (a-h,o-z)
integer ipvt(1:nbig),flag,isecho,nf1,i,m,n,l
real*8 e,n0,phi,phi0,u,n1,n2,en,Xn(0:nmax),Yn(0:nmax),ka1,ka2,k(1:nf)
real*8 k0(1:nf),f(1:nf),Rm(0:nmax),Phim(0:nmax)
complex*16 arg,Fmn,Fpmn,r,e_jk0p,a2,diag(1:nbig),j,W(1:nf)
complex*16 bjka(0:nsize),byka(0:nsize),bjpka(0:nsize),bypka(0:nsize)
complex*16 bhka(0:nsize),bhpk(0:nsize),bjk0a(0:nsize), byk0a(0:nsize)
complex*16 bjpk0a(0:nsize),bypk0a(0:nsize),bhk0a(0:nsize), bhpk0a(0:nsize)
complex*16 bjkrm(0:nsize),bykrm(0:nsize),bjpkrm(0:nsize), bypkrm(0:nsize)
complex*16 bhkrm(0:nsize),bhpkrm(0:nsize),A1(1:nbig,1:nbig), B1(1:nbig),Es(1:nf)
```

```

complex*16 F1mn,F1pmn,G,Gp, one, two, three, four,Cn(1:nbig)
j = (0.D0.1.D0)
phi = 0
u = ur * u0
e = er * e0
n0 = sqrt(u0/e0)
n1 = sqrt(u/e)
ka1=1.9 !X Axis
ka2=1.95 !Y Axis
r = 1
e_jk0p = 1
n2 = n0 / n1
flag = 1
isecho = 0
! Open the data file
open (u1, FILE='temp10.txt', STATUS='OLD')
!Creates N+1 points on an ellipse with axis lengths ka1, ka2 in rectangular and polar
!forms
dphi = pi/(nmax+1)
do i=0,nmax
    phi0 = i*dphi+dphi/2.
    Xn(i) = ka1 * cos(phi0)
    Yn(i) = ka2 * sin(phi0)
    Rm(i) = sqrt(Xn(i) * Xn(i) + Yn(i) * Yn(i))
    Phim(i) = atan2(Yn(i), Xn(i))
enddo
if(isecho == 1) then !Number of data

```

```

    nf1 = 153
elseif(isecho == 2) then
    nf1 = 191
else
    nf1 = nf
endif !creating the range of frequencies
do i=1,nf1
    if(nf == 500) then
        f(i) = i * 5.e6
    elseif(nf == 1000) then
        f(i) = i * 2.5e6
    elseif(nf == 2000) then
        f(i) = i * 1.25e6
    endif
enddo ! creating the wave numbers
do i=1, nf1
    k(i) = 2 * pi * f(i) * sqrt(u*e)
    k0(i) = 2 * pi * f(i) * sqrt(u0*e0)
enddo
do i=1, nf1
    Es(i) = 0
! Creating the argument of the bessel functions and calling the
! function that creates the ln of the bessel function
    arg = k(i) * a
    call logbjyh(arg,nmax,bjka,byka,bjpka,bypka,bhka,bhpka)
    arg = k0(i) * a
    call logbjyh(arg,nmax,bjk0a,byk0a,bjpk0a,bypk0a,bhk0a,bhpk0a)

```

! Creating the m x n matrix

do m=0, nmax

if(flag == 4) then

arg = k0(i) * Rm(m)

else

arg = k(i) * Rm(m)

endif

call logbjyh(arg,nmax,bjkrm,bykrm,bjpkrm,bypkrm,bhkrm,bhpkrm)

B1(m+1) = 0

do n=0, nmax

if(n == 0) then

en = 1

else

en = 2

endif

Fmn = exp(bjka(n) + bykrm(n)) - exp(bjkrm(n) + byka(n))

Fpmn = exp(bjpka(n) + bykrm(n)) - exp(bypka(n) + bjkrm(n))

F1mn = exp(bjka(n) + bypkrm(n)) - exp(bjpkrm(n) + byka(n))

F1pmn = exp(bjpka(n) + bypkrm(n)) - exp(bjpkrm(n) + bypka(n))

G = (ka2-ka1) * cos(Phim(m)) * sin(Phim(m)) / sqrt(ka1**2 * &
(sin(Phim(m)))**2 + ka2**2 * (cos(Phim(m)))**2)

Gp = (ka1 * sin(Phim(m))*sin(Phim(m)) + ka2 * cos(Phim(m))* &
cos(Phim(m))) / sqrt(ka1**2 * (sin(Phim(m)))**2 + ka2**2 * &
(cos(Phim(m)))**2)

if(flag == 0) then !divide by H2p(n) normalization

!Not done because the TMz version did not work.

else if(flag == 1) then ! Factor H2p(n) Normalization

```

one = (G/r)*(n2*Fmn - Fpmn*exp(bhk0a(n) - bhpk0a(n)))*n*
sin(n*Phim(m))
two = Gp*k(i)*(n2*F1mn - F1pmn*exp(bhk0a(n) - bhpk0a(n)))*
cos(n*Phim(m))
three = (G/r)*(n2*Fmn*exp(bjpk0a(n)) - Fpmn*exp(bjk0a(n)))*n*
sin(Phim(m)*n)
four = Gp*k(i)*(n2*F1mn*exp(bjpk0a(n)) - F1pmn*exp(bjk0a(n)))*
cos(Phim(m)*n)
A1(m+1,n+1) = one + two
B1(m+1) = B1(m+1) - en * (j ** (n)) * (four + three)
else if(flag == 2) then !divide by H2p(nmax) normalization
    !Not done because the TMz version did not work.
else if(flag == 3) then !no normalization
    one = (G/r)*(n2*Fmn*exp(bhpk0a(n)) - Fpmn*exp(bhk0a(n)))*n*
    sin(n*Phim(m))
    two = Gp*k(i)*(n2*F1mn*exp(bhpk0a(n)) - F1pmn*exp(bhk0a(n)))*
    cos(n*Phim(m))
    three = (G/r)*(n2*Fmn*exp(bjpk0a(n)) - Fpmn*exp(bjk0a(n)))*n*
    sin(Phim(m)*n)
    four = Gp*k(i)*(n2*F1mn*exp(bjpk0a(n)) - F1pmn*exp(bjk0a(n)))*
    cos(Phim(m)*n)
    A1(m+1,n+1) = one + two
    B1(m+1) = B1(m+1) - en * (j ** (n)) * (four + three)
else if(flag == 4) then !no normalization, no dielectric
    !Not done because comparison was not needed.
endif
enddo

```

```

enddo
do l=1, nmax+1
    Cn(l) = B1(l)
end do
call DCOMPC (nbig,nmax+1,A1,IPVT,DIAG)
call SOLVEC (nbig,nmax+1,A1,IPVT,Cn)
a2 = sqrt(2/(pi * k0(i) * r)) * e_jk0p * exp(pi * j / 4)
do l=0, nmax
    if(flag == 1) then
        Es(i) = Es(i) + Cn(l+1) * exp(0 - bhpk0a(l)) * cos (l * phi) * exp(l*j*pi/2)
    else
        Es(i) = Es(i) + Cn(l+1) * cos (l * phi) * exp(l * j * pi / 2)
    endif
end do
Es(i) = Es(i) * a2
if(isecho == 1) then
    W(i) = 2 * pi * Es(i) * conjg(Es(i))
    write(u1,*) real(k0(i)),real(W(i)),aimag(W(i))
    write(*,*) i,real(W(i)),aimag(W(i))
elseif(isecho == 2) then
    W(i) = 2 * pi * Es(i) * conjg(Es(i)) / (pi * Rm(1))
    write(u1,*) real(k0(i) * Rm(1)),real(W(i)),aimag(W(i))
    write(*,*) i,real(W(i)),aimag(W(i))
else
    !write(u1,*) f(i)*1.d-9,real(Es(i)),aimag(Es(i))
    write(u1,*) real(Es(i)),aimag(Es(i))
    write(*,*) i,real(Es(i)),aimag(Es(i))

```

```

        endif
    enddo

!prints out the points on the ellipse
!do i=0,nmax
! write(u1,*) Xn(i),Yn(i),Rm(i), Phim(i)
! write(*,*) Xn(i),Yn(i)
!end do

close(u1)

end program TEZ

! Calculating the ln of the bessel functions
subroutine logbjyh(arg,n,logj,blogy,logjp,logyp,blogh,bloghp)
implicit real*8 (a-h,o-z)
parameter (nsize=10000,test=1.d-10,gamma=0.57721566490153, &
pi=3.14159265358979)
complex*16 arg,resn,res,prod,zsum,zsum1,zj0,zy0
complex*16 logj(0:nsize),blogy(0:nsize),ratio(0:nsize)
complex*16 logjp(0:nsize),logyp(0:nsize)
complex*16 blogh(0:nsize),bloghp(0:nsize)
complex*16 ysum,ysum1
complex*16 zj,yj1,yj

!computes the log of J0-Jn for complex arguments
!first compute J0 using ratios Jn-1/Jn and
!equation 9.1.44 from Abramowitz
!also compute Y0 using ratios Jn-1/Jn and
!equation 9.1.89 from Abramowitz
zj = dcplx(0.d0,1.d0)
zsum = 1.d0

```

```

ysum = 2.d0*(zlog(arg)+dlog(0.5d0)+gamma)/pi
prod = 1.d0
iyflag = 1
izflag = 1
i = 0
10 i = i + 2
zsum1 = zsum
ysum1 = ysum
call bratio(arg,i-1,res)
prod = prod*res
ratio(i-1) = res
call bratio(arg,i,res)
prod = prod*res
ratio(i) = res
j = i/2
if (izflag .eq. 1) then
    zsum = zsum + 2.d0*(-1)**j/prod
    if (abs(zsum1-zsum)/abs(zsum1) .lt. test) then
        izflag=0
    end if
end if
if (iyflag .eq. 1) then
    ysum = ysum - 4.d0*(-1)**j/(prod*pi*j)
    if (abs(ysum1-ysum)/abs(ysum1) .lt. test) then
        iyflag=0
    end if
end if

```

```

if ((izflag .eq. 0) .and. (izflag .eq. 0)) go to 20
zsum1 = zsum
ysum1 = ysum
go to 10
20 zj0 = cos(arg)/zsum
zy0 = ysum*zj0
! finish computing ratios
if (i .lt. n) then
  do j=i+1,n
    call bratio(arg,j,res)
    ratio(j) = res
  end do
end if
! now compute log(Jn)
blogj(0) = zlog(zj0)
do i=1,n
  blogj(i) = blogj(i-1)-zlog(ratio(i))
end do
! now compute JnYn and then log(Yn)
! using Wronskian 9.1.16 from Abramowitz
yj1 = zj0*zy0
blogy(0) = zlog(zy0)
do i=1,n
  yj = yj1/(ratio(i)*ratio(i))-(2.d0/(pi*arg))/ratio(i)
  blogy(i) = zlog(yj)-blogj(i)
  yj1 = yj
end do

```

```

! next compute log(Jn') from recursion formula
blogjp(0) = dcplx(0.d0,pi)+blogj(1)
do i=1,n
  blogjp(i) = blogj(i)+zlog(ratio(i)-i/arg)
end do
! next compute log(Yn') from recursion formula
blogyp(0) = dcplx(0.d0,pi)+blogy(1)
do i=1,n
  blogyp(i) = -blogj(i)+zlog(exp(blogy(i-1)+ &
  blogj(i))-(i/arg)*exp(blogj(i)+blogy(i)))
end do
! next compute log(Hn(2)) from cross product
blogh(0) = zlog(zj0-zj*zy0)
do i=1,n
  blogh(i) = zlog(exp(blogj(i)+blogh(i-1))- &
  2.d0/(zj*pi*arg)) - blogj(i-1)
end do
! lastly compute log(Hn(2)') from cross product
bloghp(0) = zlog(exp(blogjp(0))-zj*exp(blogyp(0)))
do i=1,n
  bloghp(i) = zlog(exp(blogjp(i)+blogh(i))- &
  (2.d0*zj)/(pi*arg)) - blogj(i)
end do
! reduce phase by increments of 2pi
do i=0,n
  call reducepi(blogj(i))
  call reducepi(blogy(i))

```

```

    call reducepi(blogjp(i))
    call reducepi(blogyp(i))
    call reducepi(blogh(i))
    call reducepi(bloghp(i))
end do
return
end
subroutine bratio(arg,n,res)
! computes the ratio of  $J_{n-1}(\arg)/J_n(\arg)$ 
! to relative accuracy of test using
! continued fraction expansion of Lentz
! Reference: IEEE Trans on AP, vol. 48,
! no. 10, pp. 1528-1532, October 2000
parameter (nmax=10000,test=1.d-14)
implicit real*8 (a-h,o-z)
complex*16 arg,res,res1,zvec(nmax)
nterms = 2
ii = -2
do i=1,nterms
    ii = -ii
    zvec(i) = ii*(n+i-1)/arg
end do
res = zvec(nterms)
do j=nterms-1,1,-1
    res = 1.d0/res + zvec(j)
end do
res1 = res

```

```

do k=nterms+1,nmax
  ii = -ii
  zvec(k) = ii*(n+k-1)/arg
  res = zvec(k)
  do j=k-1,1,-1
    res = 1.d0/res + zvec(j)
  end do
  diff = abs(res-res1)/abs(res1)
  if (diff .lt. test) go to 100
  res1 = res
end do
write (*,*) 'ERROR*** maximum number of terms exceeded'
write (*,*) ' in subroutine bratio'
100 return
end
subroutine reducepi(z)
! reduces imaginary part of complex number
implicit real*8 (a-h,o-z)
parameter (tpi=6.283185307179586477)
complex*16 z
x = dreal(z)
y = dimag(z)
10 if (y .gt. tpi) then y=y-tpi go to 10 end if 20 if (y .lt. -tpi) then
  y=y+tpi
  go to 20
end if
z=dcmplx(x,y)

```

```

return
end
subroutine DCOMPC (nbig,N,A,IPVT,DIAG)
!Decomposes matrix a to triangular form
!**** COMPLEX VERSION ****
!FROM: LINEAR ALGEBRA BY GILBERT STRANG
!parameter(nbig=101)
integer N,IPVT(nbig)
integer NM1,I,J,K,KP1,M
complex*16 A(nbig,nbig),DIAG(nbig)
complex*16 P,T
IPVT(N) = 1
if (N == 1) GO TO 70
NM1 = N-1
do 60 K=1,NM1
    KP1 = K+1
    ! find pivot p
    M = K
do 10 I=KP1,N
10 if (abs(A(I,K)) > abs(A(M,K))) M=I
    IPVT(K) = M
    if (M /= K) IPVT(N) = -IPVT(N)
    P = A(M,K)
    A(M,K) = A(K,K)
    A(K,K) = P
    DIAG(K) = P
    if (P == 0.D0) go to 60

```

```

! compute multipliers
20 do 30 I=KP1,N
30 A(I,K) = -A(I,K)/P
! interchange rows and columns
do 50 J=KP1,N
    T = A(M,J)
    A(M,J) = A(K,J)
    A(K,J) = T
    if (T == 0.D0) go to 50
do 40 I=KP1,N
    A(I,J) = A(I,J) + A(I,K)*T
40 continue
50 continue
60 continue
70 DIAG(N) = A(N,N)*IPVT(N)
return
end
subroutine SOLVEC (nbig,N,A,IPVT,B)
!Solves matrix eqn AX=B with a decomposed by dcompe
!parameter(nbig=101)
integer N,IPVT(nbig)
integer NM1,K,KB,KP1,KM1,M,I
complex*16 A(nbig,nbig),B(nbig)
complex*16 S
!forward elimination
if (N == 1) go to 30
NM1 = N-1

```

```

do 10 K=1,NM1
  KP1 = K+1
  M = IPVT(K)
  S = B(M)
  B(M) = B(K)
  B(K) = S
  do 10 I=KP1,N
10 B(I) = B(I) + A(I,K)*S
!back substitution
do 20 KB=1,NM1
  KM1 = N-KB
  K = KM1+1
  B(K) = B(K)/A(K,K)
  S = -B(K)
do 20 I=1,KM1
20 B(I) = B(I) + A(I,K)*S
30 B(1) = B(1)/A(1,1)
return
end

```

APPENDIX C

Flat Case Source Code

```
! FLAT.f90
! FUNCTIONS:
! FLAT
!*****
! PROGRAM: FLAT ! PURPOSE: Calculate the scattering field of the flat case
!*****
program FLAT
parameter (pi=3.14159265358979, e0=8.85418781762e-12, u0=1.25663706144e-6, &
nsize=10000, nf = 2000, er = 9., ur = 1, a = 1.1, nmax = 275, u1 = 20,nbig=1000)
complex*16 P, R(1:nf), j, Gamma
real*8 e,u, d, f(1:nf), k(1:nf),n0,n1
d = .1
j = (0.D0,1.D0)
u = ur * u0
e = er * e0
n0 = sqrt(u0/e0) n1 = sqrt(u/e)
!Open the data file open (u1, FILE='temp10.txt', STATUS='OLD')
nf1 = nf
```

```

!creating the range of frequencies
do i=1,nf1
  if(nf == 500) then
    f(i) = i * 5.e6
  elseif(nf == 2000) then
    f(i) = i * 1.25e6
  elseif(nf == 2500) then
    f(i) = i * 1.e6
  endif
enddo

!creating the wave numbers do i=1, nf1
  k(i) = 2 * pi * f(i) * sqrt(u*e)
enddo

do i=1, nf1
  P = exp(-j*k(i)*d)
  Gamma = (n1 - n0) / (n1 + n0)
  R(i) = (Gamma - P ** 2)/(1 - Gamma * (P) ** 2)
  write(u1,*) f(i)*1.d-9,real(R(i)),aimag(R(i))
  !write(u1,*) real(R(i)),aimag(R(i))
  write(*,*) i,real(R(i)),aimag(R(i))
enddo

close(u1)

end program FLAT

```

BIBLIOGRAPHY

BIBLIOGRAPHY

- [1] Milton Abramowitz and Irene A. Stegun. *Handbook of Mathematical Functions*. Dover Publications, Inc, 1964.
- [2] Constantine A. Balanis. *Advanced Engineering Electromagnetics*. John Wiley and Sons, Inc., 1989.
- [3] P. Ilavarasan, J.E. Ross, Edward Rothwell, Dennis P. Nyquist, and K. M. Chen. Performance of an Automated Target Discrimination Scheme using E pulses and S pulses. *IEEE Transactions on Antennas and Propagation*, 41:582-588, May 1993.
- [4] Jerrold E. Marsden and Anthony J. Tromba. *Vector Calculus*. W. H. Freeman and Company, 1976.
- [5] C. R. Mullin, R. Sandburg, and C. O. Velline. A Numerical Technique for the Determination of Scattering Cross Sections of Infinite Cylinders of Arbitrary Geometrical Cross Section. *IEEE Transactions on Antennas and Propagation*, 13:141-149, January 1965.
- [6] Edward Rothwell, Dennis P. Nyquist, K. M. Chen, and B. Drachman. Radar Target Discrimination using the Extinction Pulse Technique. *IEEE Transactions on Antennas and Propagation*, 33:929-937, September 1985.
- [7] Edward J. Rothwell and Micheal J. Cloud. *Electromagnetics*. CRC Press LLC, 2001.
- [8] Garrett J. Stenholm. Nondestructive Evaluation of Layer Materials Using the E-pulse Technique. Master Thesis, Michigan State University, 2002.
- [9] Garrett J. Stenholm, Edward Rothwell, Dennis P. Nyquist, Leo C. Kempel, and Lydell L. Frasch. E-pulse Diagnostics of Simple Layered Materials. *IEEE Transactions on Antennas and Propagation*, 51:3221-3227, December 2003.

- [10] Heike Vollmer. Natural Mode Analysis of the Early-Time Response of a Dielectric Coated Cylinder. Junior Thesis, Michigan State University and University of Kaiserslautern, 2003.
- [11] Heike Vollmer and Edward J. Rothwell. Resonance Series Representation of the Early-Time Field Scattered by a Coated Cylinder. *IEEE Transactions on Antennas and Propagation*, 52:2186–2190, August 2004.
- [12] Eric W. Weisstein. Radius of Curvature. From MathWorld – A Wolfram Web Resource. <http://mathworld.wolfram.com/RadiusofCurvature.html>.
- [13] H. Y. Yee. Scattering of Electromagnetic Waves by Circular Dielectric-Coated Conducting Cylinders with Arbitrary Cross Section. *IEEE Transactions on Antennas and Propagation*, 13:822–823, September 1965.

MICHIGAN STATE UNIVERSITY LIBRARIES



3 1293 02736 3229